SPACECRAFT DEMAND TASKING AND SKIP ENTRY RESPONSIVE MANEUVERS

THESIS

Robert A. Bettinger, Captain, USAF

AFIT/GA/ENY/11-J03

DEPARTMENT OF THE AIR FORCE
AIR UNIVERSITY

AIR FORCE INSTITUTE OF TECHNOLOGY

Wright-Patterson Air Force Base, Ohio

AFIT/GA/ENY/11-J03

SPACECRAFT DEMAND TASKING AND SKIP ENTRY RESPONSIVE MANEUVERS

THESIS

Presented to the Faculty

Department of Aeronautics and Astronautics

Graduate School of Engineering and Management

Air Force Institute of Technology

Air University

Air Education and Training Command

In Partial Fulfillment of the Requirements for the

Degree of Master of Science in Astronautical Engineering

Robert A. Bettinger, BS

Captain, USAF

June 2011

AFIT/GA/ENY/11-J03

SPACECRAFT DEMAND TASKING AND SKIP ENTRY RESPONSIVE MANEUVERS

Robert A. Bettinger, BS

Captain, USAF

Approved:

_____	_____
Jonathan T. Black, Ph.D, USAF (Chairman)	Date
_____	_____
Kerry D. Hicks, Ph.D (Member)	Date
_____	_____
William E. Wiesel, Ph.D, USAF (Member)	Date

AFIT/GA/ENY/11-J03

Abstract

The purpose of this research was to parametrically investigate the viability of skip entry maneuvers as an alternative to vacuum-only maneuvers, and to identify whether skip entry maneuvers can extend spacecraft mission lifetime by limiting propellant expenditure through the exploitation of the aerodynamic interaction between the upper atmosphere and an example entry vehicle and remote-sensing orbital platform. Employing the X-37B Orbital Test Vehicle (OTV) and a notional satellite design as the example entry vehicles, the entry profile dynamics of a skip entry maneuver were characterized with varying trajectory initial conditions such as entry altitude, entry flight-path angle, and vehicle aerodynamics. In addition, the requirements of skip entry maneuvers were characterized, specifically the required to complete one or more successive skip entry trajectories as well as to execute a desired change in orbit inclination angle.

Acknowledgments

I would like to acknowledge and express my sincere gratitude to my research advisor, Dr. Jonathan Black, and all of the professors and instructors at the Air Force Institute of Technology (AFIT) for their invaluable academic guidance and mentorship with not only the engineering courses comprising my degree program, but also the composition of this thesis. I would also like to thank my family, specifically my wife and parents, for without their steadfast encouragement and unwavering support my aspirations of attaining my graduate degree in Astronautical Engineering would not have come to fruition.

Robert A. Bettinger

Table of Contents

Page

List of Figures

Page

List of Tables

Page

SPACECRAFT DEMAND TASKING AND SKIP ENTRY RESPONSIVE MANEUVERS

I. Introduction

General Issue

Growing in prominence within the policy decisions of the U.S. Department of Defense, the term "responsive space" represents a shift from a solution-oriented to a capabilities-oriented approach to space acquisition and space system design, in which the performance of a new system is "intended to respond to new taskings within days, hours or minutes without proscribing how it is done" (Newberry, 2005:46). Although dominated by the development of spacecraft and launch vehicles, an aspect of the responsive space initiative that has garnered increased attention within the defense space community is the exploration of new and novel orbits and maneuvers that can enhance the ability for a space system to be operationally responsive to demand taskings and short-duration missions. Not limited by the vacuum environment of space, responsive orbits and maneuvers can also utilize the aerodynamic re-entry environment of the Earth's upper atmosphere. Identified as a type of aeroassisted maneuver, a responsive maneuver which operates within and exploits the aerodynamic re-entry environment is that of skip entry.

Defined as a special case of lifting entry, a skip maneuver occurs when an entry vehicle generates and "intentionally uses lift" to pull back out of the atmosphere rather than landing on the Earth following re-entry (Hicks, 2009:108). For the purposes of this thesis, an entry vehicle is defined as a spacecraft that is designed to either (1) operate at

hypersonic velocities within the upper atmosphere for short durations by using lift devices to complete a specified skip entry maneuver, or (2) complete a specified re-entry profile with the intent of landing on the Earth. Traditionally, skip entry maneuvers have been utilized by space mission planners as a means of ensuring that spacecraft can meet specified time and geographic windows for landing on the Earth following atmospheric re-entry. As an example, skip entry maneuvers are proposed to increase the mission flexibility of the NASA Crew Exploration Vehicle (CEV) upon re-entry from either low-Earth or lunar orbit. With the former, skip entry maneuvers will permit the extension of the CEV's in-track range, whereas with the latter, a skip entry maneuver followed by a partial Keplerian orbit provides the CEV the freedom to "leave the moon at any time and still land at any point on the Earth" (Hicks, 2009:280-281).

Beyond the context of traditional re-entry profiles, the implementation of skip entry as a responsive maneuver in order to fulfill various mission demand taskings and/or orbital experiments normally assigned to low-Earth orbit (LEO) space assets represents the broad scope of this thesis and associated research.

Problem Statement

Without skip entry maneuvers, mission demand taskings and/or experiments require the completion of vacuum-only maneuvers to alter a spacecraft's classical orbital elements (COEs) via simple plane changes, combined changes to inclination and right ascension of the ascending node (RAAN), or coplanar and non-coplanar phasing rendezvous maneuvers. Expensive in terms of propellant usage, the aforementioned vacuum-only maneuvers have the propensity of negatively impacting LEO spacecraft by

limiting the potential available for subsequent orbital maneuvers, both in- and out-of-plane, and shortening overall mission lifetime. Consequently, the viability of skip entry and other alternative maneuvers needs to be investigated and analyzed so as to provide the spacecraft user several maneuver options, both aerodynamic and vacuum-only in nature – to enable the efficient completion of LEO orbital maneuvers in response to short-duration demand taskings.

Research Objectives

It is the intent of this research to analyze the viability of skip entry maneuvers as an alternative to vacuum-only maneuvers, and to identify whether skip entry maneuvers can extend mission lifetime by limiting propellant expenditure through the exploitation of the aerodynamic interaction between the upper atmosphere and a specified entry vehicle and remote-sensing orbital platform. Fundamentally, the analysis will consist of parametric studies to be conducted with *Matlab* that will fulfill the following research objectives:

- Characterize the entry profile dynamics of a skip entry maneuver with varying trajectory initial conditions such as entry altitude, entry flight-path angle, and entry vehicle aerodynamics.
- Characterize the requirements of skip entry maneuvers, specifically the required to complete one or multiple skip entry trajectory with varying trajectory initial conditions.
- Formulate conclusions regarding the viability of skip entry maneuvers when compared with the performance of vacuum-only maneuvers.

Research Focus

The research and associated parametric studies will analyze the skip entry performance of two example entry vehicles: (1) the unmanned Boeing X-37B Orbital Test Vehicle (OTV), and (2) a notional satellite modeled to reflect the aerodynamic characteristics of the X-37B as well as be compliant with the launch requirements of the scaled version of the Evolved-Expendable Launch Vehicle (EELV) Secondary Payload Adaptor (ESPA) ring for small launch vehicles. In addition, both the skip entry and vacuum-only maneuvers will only be analyzed within LEO since spacecraft that will perform such maneuvers predominantly operate within this altitude regime in order to fulfill remote-sensing missions.

Investigative Questions

The parametric studies will seek to answer the following investigative questions:

- What is the impact of flight-path angle and entry vehicle aerodynamics, specifically coefficients of drag and lift, on skip entry trajectory dynamical parameters such as drag and lift force, deceleration, stagnation heat flux, and entry vehicle velocity?
- What is the relationship between entry altitude and the minimum altitude that can be reached for a skip entry maneuver? Also, what is the relationship between the coefficient of lift and flight-path angle of an entry vehicle and the minimum skip entry trajectory altitude?
- What is the relationship between entry altitude and the required to complete a single skip entry maneuver?

- What is the requirement to complete two successive skip entry maneuvers?
- What is the required to complete a user-specified change in orbit inclination angle for a skip entry maneuver compared with that of a vacuum-only maneuver?

Methodology

Illustrated in Figure 1, a general skip entry is comprised of an atmospheric entry and exit condition, with the former denoted by the subscript *e* and the latter by the subscript *f*. While an entry vehicle at skip exit achieves an orbital radius and flight-path angle that are approximately equal in magnitude to the entry conditions, the exit velocity

is less than its entry counterpart due to losses in kinetic energy stemming from aerodynamic drag and friction-induced heating effects.

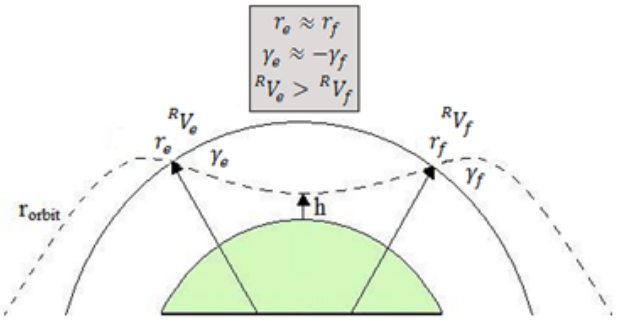

Figure 1. General Skip Entry Profile

As a consequence of the decreased velocity upon skip exit, must be expended in order to force an immediate re-orientation of an entry vehicle by conducting thruster burns to not only re-circularize to remain in orbit at the exit radius, but also alter the exit flight-path angle so as to either execute a subsequent skip entry maneuver, or complete a non-skip re-entry profile.

Foundational definitions for skip entry maneuvers aside, the preceding investigative questions characterize the scope of the thesis and provide a framework for the parametric studies which individually as well as comparatively evaluate the performance of skip entry and vacuum-only maneuvers. For both types of maneuvers, the parametric studies are comprised of the following test cases and initial conditions:

Table 1. Skip Entry Maneuver Performance Parametric Studies

Case	**Initial Altitude**	**Entry Flight-Path Angle**	**Lift-to-Drag Ratio**
Variable Coefficient of Lift	120, 400 km		0.9, 1.0, 1.5, 2.0
Variable Entry Flight-Path Angle	120, 400 km		1.0
Minimum Altitude of Skip Entry	120, 200, 400 km		1.0, 1.5, 2.0
Required for Skip Entry	120, 200, 400 km		1.0, 1.5, 2.0

Table 2. Vacuum-Only Maneuver Performance Parametric Studies

Case	**Initial Altitude**	**Initial Inclination**	**Orbit Angle**	**Orbit Angle**
Required for Simple Plane Change	200, 300, 400, 500, 750,1000 km			N/A
Required for Combined Change to and	400 km			
Required for Coplanar Phasing Rendezvous	200, 300, 400, 500, 750,1000 km	or		N/A
Required for Non-coplanar Phasing Rendezvous	400 km			

Not explicitly defined in Table 2, the angular variables and represent rendezvous phasing angle and argument of latitude, respectively.

All of the parametric studies were simulated in *Matlab* utilizing a series of program scripts given in the Appendix, specifically the scripts for skip entry maneuvers in Appendix A and the scripts for vacuum-only maneuvers in Appendix B. For the skip entry maneuver parametric studies, entry vehicle performance data arises from the numerical integration of the kinematic and force equations of motion for atmospheric re-entry subsequently outlined in Chapter III. Based on user-defined initial conditions that include not only the entry altitude, latitude, and longitude of the maneuver, but also the orientation angles and model parameters of the specified entry vehicle, the equations of motion propagate the entry vehicle states and yield maneuver position and time vectors from which various trajectory performance parameters are obtained. In addition to determining the trajectory time and altitude values associated with flight below the ionosphere, the minimum skip entry altitude, and the exit altitude of the maneuver, the program script also calculates the required to enter a single as well as a successive skip entry trajectory following a period of Keplerian orbital flight.

Besides skip entry maneuvers, the vacuum-only maneuver parametric studies also leverage the initial COEs defined by the user for the spacecraft to calculate the required to perform a simple plane change, a combined change to inclination and RAAN, and both a coplanar and non-coplanar phasing rendezvous. In order to directly compare with the performance of the skip entry maneuvers, the vacuum-only maneuvers were simulated within the LEO altitude regime and restricted to altering only the spacecraft's orbit inclination and RAAN for the non-rendezvous cases. In terms of coplanar and non-

coplanar rendezvous however, the program script calculates the geometry of the phasing orbit required for the spacecraft to intercept the space-based location which corresponds to a nadir ground-based target.

For all maneuver performance parametric studies the X-37B and notional satellite were employed as the primary example entry vehicles and spacecraft. Due to the scope of the research, the design of the notional satellite became restricted to accounting for only the parameters of spacecraft mass, volume, and aerodynamic characteristics such as coefficient of drag and planform area. As a result, the design for each spacecraft subsystem was considered negligible and deemed superfluous to the investigation of skip entry maneuver performance.

In terms of reference frames, all skip entry trajectory parameters were calculated with respect to a non-inertial vehicle-pointing frame , while all vacuum-only maneuvers as well as the orbit inclination angle at skip exit were calculated with respect to the Earth-Centered Inertial (ECI) frame . The following figures depict not only the ECI and vehicle-pointing frames, but also the graphical relationship between these frames and the planet-fixed reference frame (Hicks, 2009:28, 31).

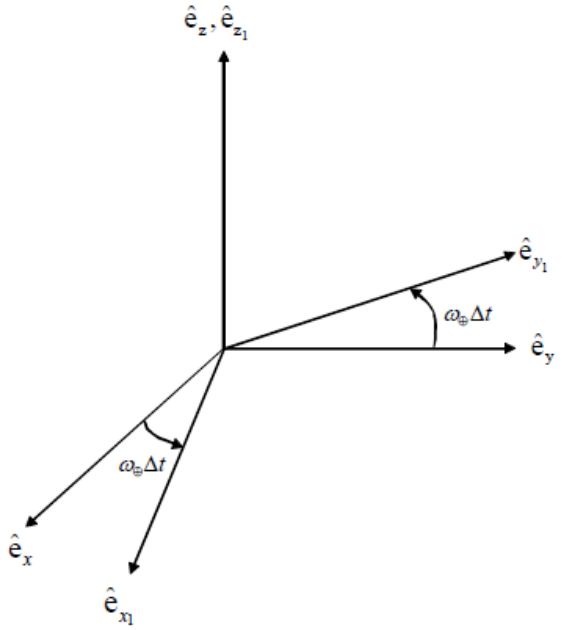

Figure 2. ECI and Planet-Fixed Reference Frames (Hicks, 2009:28)

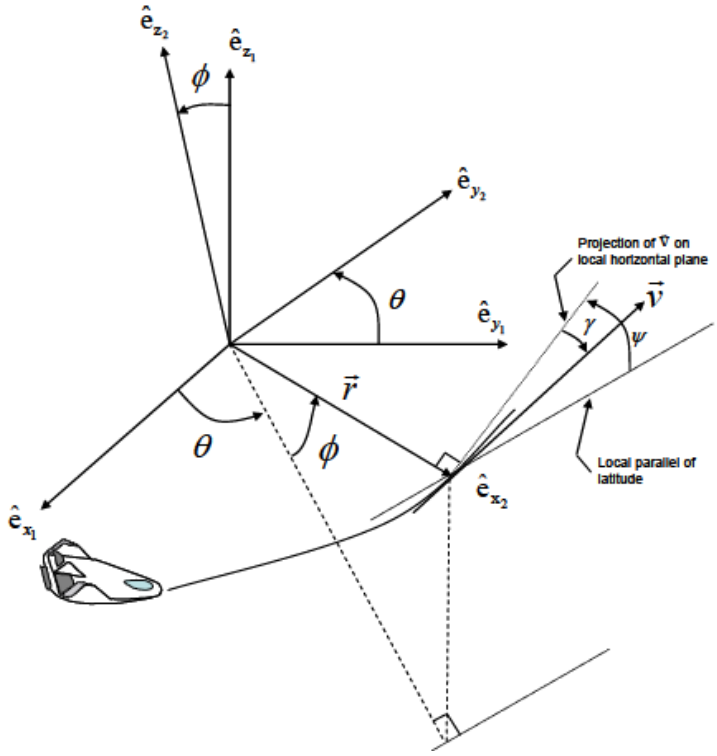

Figure 3. Planet-Fixed and Vehicle Pointing Reference Frames (Hicks, 2009:31)

Assumptions/Limitations

As a means of simplifying the numerical simulation of the skip entry and vacuum-only maneuvers, the following assumptions were formulated concerning the example entry vehicles – specifically the X-37B and a notional satellite – and the atmospheric entry environment of Earth. Note that both the assumption and, where applicable, a description of the reality that the assumption seeks to simplify are provided below.

- The entry vehicle is modeled as a point mass, with the gravity force directed along a vector from the point mass to the center of mass of a spherical Earth (Hicks, 2009:27, 48).
  - Reality: The mass of the X-37B and the notional satellite is distributed throughout the three-dimensional shape of the respective vehicle, with such a distribution expressed as a mass moment of inertia calculated about the principal axes of the vehicle body-fixed coordinate frame. Although a more accurate representation of the entry vehicle mass, the calculation of mass moment of inertia values is contingent on the implicit assumption that the example entry vehicles are rigid bodies, which are bodies that do not deform nor change shape (Bedford and Fowler, 2005:280, 398). Such an assumption is permissible since the X-37B and the notional satellite are operating within the envelope of their intended mission geometric configuration with any shape changes – such as the opening of payload bay doors for the X-37B or any required articulation of the solar arrays for the notional satellite – occurring prior to and/or following the maneuver being analyzed.

- The entry vehicle maintains a constant mass throughout the skip entry maneuver; propellant is only expended prior to and/or following a maneuver and a non-ablative thermal control subsystem is employed.
  - Reality: Although a non-ablative thermal control subsystem is employed for the example entry vehicles, the possibility of ablation still exists due to the high-temperature gas dynamics and the associated high-temperature molecular interactions between the surface of the example entry vehicles and the various gaseous species which comprise the "chemically reacting boundary layer" produced in hypersonic flow environment encountered during skip entry (Anderson, 2006:17).
- The entry vehicle maintains a hypersonic velocity throughout the skip entry maneuver; the hypersonic flow regime of the upper atmosphere is characterized as inviscid and steady, where viscous effects are considered negligible and , , and within the governing conservation equations for fluid flow (Bertin, 2002:23).
  - Reality: The viscosity coefficient increases with temperature within a high-velocity, hypersonic flow over a body such as the X-37B or the notional satellite. Such an increase in viscosity, in conjunction with a decrease in flow density, leads to an increase in the thickness of the boundary layer thus spurring the onset of viscous interactions with the inviscid free-stream flow outside the boundary layer. Overall, viscous interactions not only effect the surface-pressure distribution which impact the lift, drag, and stability characteristics of a hypersonic vehicle, but also increase both skin friction and

heat transfer between the vehicle and the hypersonic flow environment (Anderson, 2006:15-16).

- The coefficient of drag for the entry vehicle is modeled as a constant value.
  - Reality: Defined as , the coefficient of drag is a dynamic quantity within the hypersonic flow environment due to viscous interactions and the decrease in density arising from increases in temperature.
- The drag force acts in a direction opposite to the entry vehicle velocity vector, while the lift force acts perpendicular to the velocity vector; see Figure 2 for the X-37B and Figure 3 for the notional satellite (Hicks, 2009:43-44).

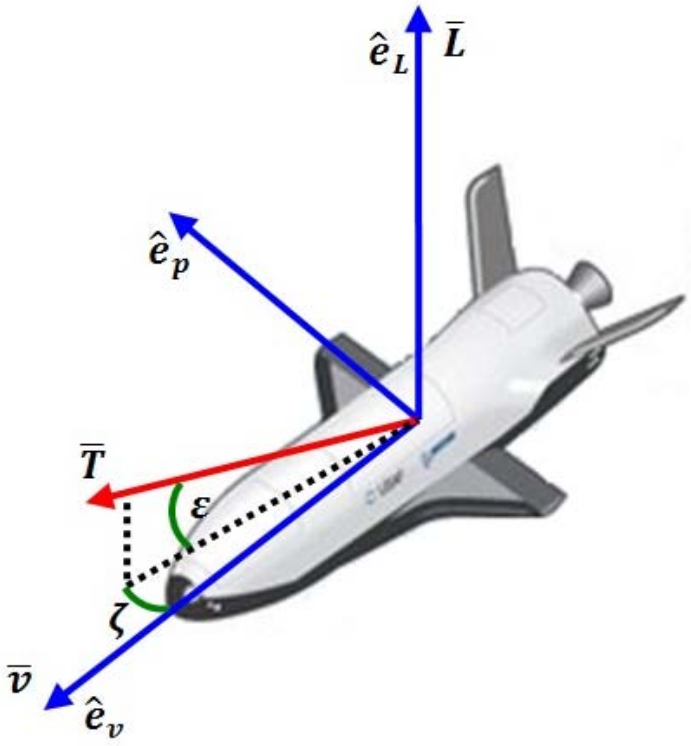

Figure 4. Body-Fixed Coordinate Frame and Vector Definition for X-37B

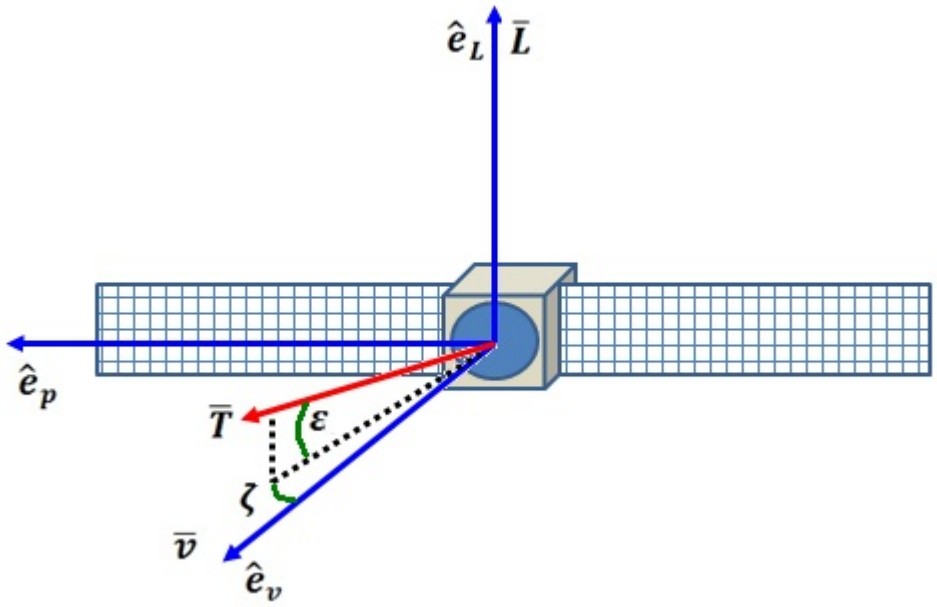

Figure 5. Body-Fixed Coordinate Frame and Vector Definition for Notional Satellite

- In addition to being instantaneous and impulsive in nature, all thrusting and corrections are conducted prior to and/or following a skip entry maneuver.
  - Reality: The force produced by a thruster is not instantaneous but rather transient since time is required for not only the transmission of the electrical signal to activate and de-activate the thruster, but also the actuation of flow valves and the passage of propellant through the feed-system, and the chemical interaction between the species of the bipropellant system and the resultant production of a desired thrust level.
- At skip exit, correction burns are impulsive in nature and applied instantaneously in order to re-circularize the entry vehicle orbit at the exit radius (Vinh, 1981:382).

- Reality: Instantaneous burns are infeasible since a thruster burn profile is not analogous to a Heaviside function. Instead, a burn profile is comprised of a rise time required for thrust to increase from zero to a nominal operating level following the opening of the propellant valve, as well as a settling time for thrust to decrease from a nominal operating level back to zero after the propellant valve is closed.

- All skip entry and vacuum-only maneuvers commence from circular orbits (eccentricity, $e = 0.0$).
- Vacuum-only maneuvers are simulated within the framework of two-body dynamics. In other words, orbital perturbations induced by effects such as atmospheric drag, planetary oblateness, solar radiation pressure, and variable gravitational field strength are considered negligible for the analysis of vacuum-only maneuvers.
  - Reality: Spacecraft orbiting the Earth in all altitude regimes are impacted by orbital perturbations. Although the assumption of two-body dynamics simplifies the calculation of vacuum-only maneuvers, the absence of perturbation analysis produces an underestimation of required .
- The atmospheric density of Earth is modeled as an exponential function:

(1)

Where:

= Atmospheric density at sea-level
= Radius of Earth
= Radial distance of entry vehicle from the center of Earth defined in terms of the altitude above sea-level as:

  - Reality: In addition to altitude/radius, atmospheric density is also a function of time, specifically local time and date, which indicates an approximate level of solar activity and the resultant interaction between such activity and the upper atmosphere.

- The planetary rotation rate of Earth is constant about the inertial -axis, an axis of the ECI frame that is aligned with the planet's geographic North Pole. For the purposes of the following parametric studies however, the planetary rotation rate is deemed negligible due to the relatively short spatial and temporal duration of atmospheric re-entry maneuvers.
- Various planetary and entry environment parameters are modeled as constant values; see Table 3 (Vallado, 2001:138).

Table 3. Planetary and Entry Environment Constants

Constant	Symbol	Value
Atmospheric Density at Sea-Level		
Atmospheric Scale Height		
Gravitational Acceleration at Sea-Level		
Gravitational Parameter		
Planetary Radius		
Planetary Rotation Rate		

In addition to assumptions regarding aspects of the entry vehicle model and entry environment, the simulation also accounts for specific constraints for the X-37B and notional satellite. Outlined in Table 4, the constraints identify arbitrary deceleration and stagnation heat flux limits for the example entry vehicles, as well as the maximum

capability. Absent from the table, a constraint for maximum wall (average) heat flux is not provided since maximum stagnation heat flux occurs at a higher altitude with a greater relative magnitude.

Table 4. Entry Vehicle Constraints

Maneuver Constraints	—	
Velocity Constraints	(X-37B)	(Notional Satellite)

Pivotal to the selection of the final skip maneuver profile, the vehicle entry constraints provide limits on entry vehicle performance which, if surpassed, jeopardize ultimate mission success due to deceleration- and heating-induced failure of the entry vehicle's structure and subsystems such as remote sensing payload(s). Overall, it is recognized that deceleration can be minimized by maintaining a shallow flight-path angle, while heat flux can be minimized by maintaining a steep flight-path angle in order to reduce the time-of-flight of re-entry. In light of such dissonance between flight-path angle requirements, a skip entry trajectory must be pursued that strives to complete a specified demand tasking while ensuring that deceleration and heat flux remain within the design limits of a given entry vehicle.

Preview

Having defined the research objectives, outlined the analysis methodology, and described research assumptions and constraints in Chapter I, a review of relevant literature related to atmospheric maneuvers, specifically skip entry maneuvers is provided in Chapter II. The analysis methodology is further developed in Chapter III, with

algorithms for the calculation of skip entry and vacuum-only maneuvers, to include simple plane changes, combined changes to inclination and RAAN, and coplanar and non-coplanar phasing rendezvous, provided in detail. In addition, the vehicle properties for the X-37B are explored and the design methodology for the notional satellite is described in Chapter III.

With the analysis space and methodology defined in the previous chapters, Chapter IV examines the performance of skip entry and vacuum-only maneuvers for a set of parametric studies outlined in the Methodology section of Chapter I for the X-37B and notional satellite. Furthermore, Chapter IV provides an analysis of required to perform two sequential skip entry maneuvers as well as a comparison of the required for a skip entry and vacuum-only maneuver to execute a given change of orbit inclination angle. In the final chapter, the results of the preceding analysis are summarized and interpreted so as to provide conclusions regarding the viability of skip entry maneuvers compared with vacuum-only maneuvers. Recommendations for action and future study are also given to further assess skip entry maneuver performance and the application of such maneuvers to future LEO missions. In terms of the appendices, the *Matlab* scripts and functions employed to conduct the skip entry and vacuum-only maneuver parametric studies are provided in Appendix A and B, respectively.

As a final note, all values and figures depicted within this document are expressed in SI units. In limited cases, specifically the discussion regarding to minimum altitude reached during skip entry, English units of feet (ft) for distance are utilized as a alternative mode of describing the values given in units of kilometers (km).

II. Literature Review

Chapter Overview

The purpose of this chapter is to provide an overview of the relevant research pertaining to skip entry maneuvers and their utilization as an alternative to traditional vacuum-only maneuvers. Besides analyzing the viability of leveraging atmospheric maneuvers as a means to alter the orbital elements of a given spacecraft in low-Earth orbit (LEO), preceding studies have also focused on modeling the flow environment of the upper atmosphere, specifically the ionosphere, and spacecraft aerodynamics.

Relevant Research

Analyzed within a series of theses published by the United States Naval Postgraduate School in the early 1990s, atmospheric maneuvers conducted by LEO spacecraft were identified as being synergistic in nature since the maneuvers utilized both atmospheric forces, in the form of aerodynamic lift and drag, and propulsive forces. In his thesis "Effects of Thrust Vector Control on the Performance of the Aerobang Orbital Plane Change Maneuver," Richard E. Johnson divided synergistic maneuvers into three categories, or subtypes: aerobang, aerocruise, and aeroglide. Representing one extreme of the continuum of synergistic maneuvers, Johnson indicates that aerobang maneuvers consist of an upper atmospheric flight trajectory augmented by continuously thrusting "set at the maximum" (Johnson, 1993:4). Employed to not only vary the spacecraft's angle-of-attack, maximum thrust also reduces the duration of atmospheric flight, thereby reducing heat effects produced by re-entry. Similar to aerobang maneuvers, aerocruise also utilizes propulsive force during the atmospheric trajectory, but at a throttle condition

sufficient to only counteract aerodynamic drag forces. In addition, Johnson states that any orbit inclination change incurred by an aerocruise maneuver is a function of the generated aerodynamic lift and angle-of-attack of the spacecraft. The final maneuver, aeroglide, is directly equivalent to what is identified in works such as *Introduction to Astrodynamic Re-Entry*, by Dr. Kerry Hicks as a skip entry maneuver. Relying primarily on aerodynamic forces, aeroglide maneuvers produce a gliding, unpowered trajectory which employs propulsive forces to only deorbit prior to and re-circularize at the end of the maneuver (Johnson, 1993:3-4).

Expanding on Johnson's maneuver definitions, John C. Nicholson in "Numerical Optimization of Synergistic Maneuvers" observes that despite greater heating rates stemming from prolonged flight at lower, denser regions of the atmosphere, aeroglide maneuvers are the least expensive in terms of propellant consumption compared with purely propulsive maneuvers both within and without the atmosphere. In terms of aerocruise, Nicholson states previous studies have shown that such maneuvers are "more efficient," with the metric of efficiency being change in orbit inclination per amount of fuel expended, as the bank angle increases during the atmospheric trajectory (Nicholson, 1994:5). Besides using the moniker of aeroassisted rather than synergistic, Christopher Darby and Anil V. Rao, in their study of minimum-fuel LEO aeroassisted orbital transfer, further categorized atmospheric maneuvers by identifying aerobrake, aerocapture, and aerogravity assist. Darby and Rao describe that an aerobrake maneuver is purely aerodynamic and is employed to reduce orbit semi-major axis. Not applicable for LEO spacecraft, aerocapture maneuvers exploit atmospheric drag to reduce orbital energy thereby changing an orbit from hyperbolic to elliptic, while aerogravity assist "combines

the atmosphere with propulsion and [planetary] gravity" to modify the orbital elements of a hyperbolic trajectory (Darby and Rao, 2010:3).

Underpinning all trajectory analyses and simulations for atmospheric entry and LEO spacecraft is the method by which the atmosphere is modeled. Due to the short time scales involved with atmospheric entry scenarios, various atmospheric dynamics can be deemed negligible, primarily any geomagnetic-induced variations in density and temperature arising due to the solar cycle and related space weather phenomena. As a result, the atmospheric model employed depicts density as both decaying exponentially as altitude increases from sea-level, and independent of any functional relation to time and geographic location. Such a model, as defined in David A. Vallado's text *Fundamentals of Astrodynamics and Applications*, was employed by Michael L. Gargasz in his thesis "Optimal Spacecraft Attitude Control using Aerodynamic Torques," and Blake B. Hajovsky in his thesis "Satellite Formation Control using Atmospheric Drag."

In addition to depicting the macroscopic atmospheric environment as a function of altitude, atmospheric re-entry maneuver simulations have also sought to garner increased model fidelity by capturing the flow characteristics of the upper atmosphere and their relation to entry vehicle aerodynamics. In his study of the viability of achieving three-axis attitude control using only aerodynamic torques, Gargasz divided atmospheric particle-body interactions in two categories: specular and diffuse collisions. David B. Guettler, in his thesis "Satellite Attitude Control using Atmospheric Drag," echoes Gargasz and defines specular collisions as a transfer of momentum in which the air "molecules are perfectly elastic…the tangential velocity is constant and the normal velocity is reversed," whereas diffuse collusions are composed of air molecules which are

reflected from the body in a “diffuse manner [with] no memory of previous velocities” (Guettler, 2007:23). The flow environment for atmospheric re-entry maneuvers can also be expressed in terms of flow regime rather than momentum exchange. In his thesis “Investigation of Atmospheric Re-Entry for the Space Maneuver Vehicle,” Dennis J. McNabb describes that for a given re-entry trajectory, an entry vehicle will operate in the rarefied (free molecular), transition, and continuum flow regimes. Defined by the Knudsen number (Kn), or the ratio of the particle mean free path to characteristic length, with the latter “typically chosen [to be] the mean aerodynamic cord” of the entry vehicle, McNabb identified rarefied flow as Kn >10, transitional flow as , and continuum flow as Kn < 0.01 (McNabb, 2004:14-15). In terms of the density-defined atmospheric model, flow transitions from rarefied to continuum as density increases with decreasing altitude.

With the flow characteristics established for flight in the upper atmosphere, the aerodynamics of entry vehicles within such flow can be determined through either assuming or directly calculating values for the coefficients of drag and lift. Consulting a Douglas Aircraft Company technical report entitled “Surface-Particle-Interaction Measurements using Paddlewheel Satellites,” Guettler assumes a constant value for coefficient of drag of 2.2 for his analysis of satellite attitude control authority arising from aerodynamic torques produced by deployable drag panels (Guettler, 2007:24). A coefficient of drag of 2.2 is also given by Vallado, who states that such a value is derived by modeling a satellite operating within the upper atmosphere as a flat plate (Vallado, 2001:525). Although greater in magnitude than that utilized by Guettler, Timothy S. Hall in his thesis “Orbit Maneuver for Responsive Coverage using Electric Propulsion”

assumed the coefficient of drag for his model satellite as 3.0, which was viewed as one of many "commonly achievable design parameters based upon existing satellite designs" (Hall, 2010:18).

As for direct calculation, Nicholson computes values for the coefficients of drag and lift as a function of angle-of-attack from empirically-derived equations arising from linearly-interpolated wind tunnel data from tests performed on the Entry Research Vehicle (ERV) within the supersonic velocity range up to Mach 10. Debuted in the conference paper "Performance Evaluation of an Entry Research Vehicle" by R.W. Powell, J.C. Naftel, and M.J. Cunningham, the ERV was a lifting entry test platform with an initial mass of 7725 kg designed to investigate maneuvers involving "long downrange, wide crossrange, and synergistic plane changes" (Nicholson, 1994:34-35, 144). Similarly, Michael S. Parish II in his thesis "Optimality of Aeroassisted Orbital Plane Changes" also computes values for coefficients of drag and lift from interpolated transonic and supersonic wind tunnel data, but for the Maneuverable Re-Entry Research Vehicle (MRRV) with an initial mass of 4899 kg, rather than the ERV. Over the angle-of-attack range of 0 to 40 , the coefficient of drag varies from 0.1 to approximately 1.2 for the ERV, while it varies from 0.03 to approximately 0.6 for the MRRV (Nicholson, 1994:36; Parish, 1995:11-12). Such values for the coefficient of drag for a lifting entry vehicle as depicted by Nicholson and Parish are consistent with the research of Anil V. Rao and Arthur E. Scherich who, in their conference paper "A Concept for Operationally Responsive Space Mission Planning using Aeroassisted Orbital Transfer," utilized a coefficient of drag of approximately 0.49 in their research of aerodynamically maneuverable entry vehicle dynamics (Rao and Scherich, 2008:3-5).

Aside from his discussion of atmospheric and entry vehicle models, an evaluation of aerodynamic re-entry maneuver performance is provided by Nicholson. Comparing the synergistic maneuver subtypes of aerobang, aerocruise, and aeroglide (skip entry), Nicholson concluded that the aeroglide maneuver produces the greatest change in orbit inclination angle for percent propellant expended. From his analysis, Nicholson illustrated that an expenditure of 20% of available propellant can produce an inclination change of approximately 7 for the aeroglide maneuver, while an inclination change of approximately 5 and 6 can be achieved for the aerocruise and aerobang maneuvers, respectively. For a propellant expenditure of 40%, Nicholson stated that the inclination change increased to about 18 for an aeroglide maneuver. With the aerobang and aerocruise maneuvers, Nicholson analyzed the effect of imposing heat constraints on the trajectory and concluded that efforts to maintain a low-heat transfer trajectory result in lower achieved change in inclination for a given level of percent propellant expended. In terms of numerical values, this trend is shown an inclination change of 16 for an aerobang maneuver and 14 for an aerocruise maneuver, with both operating within a low heat transfer trajectory constraint for a propellant expenditure of 40% (Nicholson 1994:68). Heating constraints aside, Nicholson also observed that the all synergistic maneuver subtypes outperformed a purely propulsive, vacuum-only inclination change, with the latter achieving an inclination change of 5 and 11 for the 20% and 40% propellant expenditure levels, respectively (Nicholson, 1994:69).

Confirming Nicholson's comparative analyses, Parish stated that for a given amount of propellant, the aerobang maneuver produced a greater change in inclination angle than the aerocruise maneuver. In addition, Parish concludes that synergistic

maneuvers in general require less propellant than a vacuum-only maneuver to produce a desired change in inclination angle (Parish, 1995:53, 55). Similar to Nicholson, Darby and Rao also utilize various heat transfer constraints when comparing the performance of synergistic, or what the authors identify as “aeroassisted” maneuvers, with that of vacuum-only maneuvers for a vehicle with an initial mass of 818 kg. In the absence of heat transfer constraints, Darby and Rao illustrate that aeroassisted maneuvers require less than vacuum-only maneuvers to complete a desired change in inclination angle.

From their analysis Darby and Rao state that for an inclination change of 20 , an aeroassisted maneuver required a of approximately 1.5 km/s, while a vacuum-only maneuver required about 2.8 km/s. Increasing the inclination change to 40 , Darby and Rao observe that the required increased to about 2 km/s for an aeroassisted maneuver and 5.5 km/s for a vacuum-only alternative (Darby and Rao, 2010:21). When heat transfer constraints were applied, Darby and Rao’s analysis indicated that aeroassisted maneuvers still outperformed vacuum-only maneuvers by requiring less to change inclination angle. To perform an inclination change of 20 with heat transfer rate constraints of and , an aeroassisted maneuver requires 2 km/s and 1.5 km/s of , respectively, compared with 2.8 km/s for a vacuum-only maneuver. For an inclination change 40 at the preceding heat rate constraints, the required increases to approximately 4 km/s and 3 km/s, respectively, for an aeroassisted maneuver compared with 5.5 km/s for a vacuum-only maneuver (Darby and Rao, 2010:24).

Summary

Upon review of the relevant research pertaining to aerodynamic re-entry maneuvers, it can be asserted that despite complexities due to high temperature and varying density gas dynamics, the upper atmosphere provides a useful environment within which maneuvers can be executed to alter a spacecraft's orbital elements, principally inclination angle. Whether performed by small spacecraft, with an initial mass identified by Darby and Rao as being less than 1000 kg, or a large spacecraft with an initial mass greater than 5000 kg, preceding research indicates that skip entry and other aerodynamic re-entry maneuvers require less than a vacuum-only maneuver to produce a desired change in inclination angle.

In a continuance of preceding research, the present thesis seeks to further analyze the viability of aerodynamic re-entry maneuvers, specifically skip entry maneuvers, compared with vacuum-only maneuvers for both large and small spacecraft as embodied by the X-37B and notional satellite. In addition, the analysis will also identify the coupled effects of vehicle aerodynamics and varying initial trajectory conditions, such as altitude and flight-path angle, on not only skip entry profile dynamics, but also the required for a skip entry maneuver to alter inclination angle for large and small spacecraft.

III. Methodology

Chapter Overview

The purpose of this chapter is twofold: (1) Describe the simulation algorithms implemented to perform the skip entry and vacuum-only maneuver parametric studies, and (2) identify the design characteristics of the X-37B and the notional satellite, the example entry vehicle test subjects whose maneuver performance will be ascertained within the parametric studies underpinning this research. Of the plenitude of various spacecraft available, the X-37B was selected as one of two test subjects since it represents a reusable system whose primary missions include LEO experimentation with the prospect of short-duration demand tasking. For the second test subject, the notional satellite was selected since it is an archetype of the non-reusable systems which comprise the majority of national orbital assets operating within the LEO altitude regime.

Skip Entry Maneuver Simulation Algorithm

As illustrated by the *Matlab* program scripts given in Appendix A, the skip entry maneuver profile parametric studies for the X-37B and notional satellite were simulated in accordance with the following:

1. Define the simulation initial conditions for a desired skip entry maneuver:
    a. Numerical integration propagation time step
    b. Initial altitude of skip entry maneuver
    c. Entry vehicle latitude and longitude
    d. Entry vehicle orientation angles, to include the entry flight-path angle and the heading angle

e. Entry vehicle model parameters, to include mass , coefficient of drag , and lift-to-drag ratio

f. Entry vehicle engine parameters, to include the maximum engine thrust and throttle percentage, and the angular orientation of the thrust vector with respect to the body-fixed coordinate frame

2. Numerically integrate the following kinematic and force equations of motion for atmospheric re-entry (Hicks, 2009:42, 52):

(2)

(3)

(4)

(5)

(6)

(7)

Where:

= Force due to aerodynamic drag and lift, respectively
= Gravitational acceleration at a given radial distance from the center of the Earth , defined as the following function:

= Entry vehicle mass
= Radial distance of entry vehicle from center of Earth
= Force due to entry vehicle thrust
= Velocity of entry vehicle with respect to the rotating atmosphere

= Flight-path angle
= Angle between the velocity vector and the projection of the thrust vector onto the , -plane ; see Figures 2 and 3
= Angle between the velocity vector and the projection of the thrust vector onto the , -plane ; see Figures 2 and 3
= Bank angle
= Latitude angle
= Longitude angle
= Heading angle
= Planetary rotation rate ; for the trajectory simulations

3. Calculate the deceleration experienced during the skip entry maneuver by the following (Hicks, 2009:65-66):

(8)

(9)

(10)

Where:

= Tangential deceleration (along velocity vector)
= Normal deceleration (along lift vector)
= Magnitude of deceleration normalized by the gravitational acceleration at sea-level; also expressed as the number of "g's"
= Coefficient of drag and lift, respectively
= Gravitational acceleration at sea-level ; also expressed as
= Entry vehicle mass
= Planetary radius (m); also expressed as
= Radial distance of entry vehicle from center of Earth
= Entry vehicle planform area
= Velocity of entry vehicle with respect to the rotating atmosphere
= Flight-path angle
= Atmospheric density as defined by Equation 1

4. Calculate the non-dimensional stagnation heat flux and the non-dimensional wall heat flux, respectively (Hicks, 2009:177-178):

(11)

(12)

Where:

= Coefficient of drag
= Gravitational acceleration at sea-level ; also expressed as
= Entry vehicle mass
= Planetary radius (m); also expressed as
= Entry vehicle planform area
= Velocity of entry vehicle with respect to the rotating atmosphere
= Atmospheric scale height
= Atmospheric density as defined by Equation 1

5. Extract the trajectory time and altitude values associated with flight below the ionosphere from the skip entry maneuver position and time vectors.
6. Determine the minimum altitude reached during the skip entry maneuver and the associated trajectory time. The minimum altitude is defined as the location where the entry vehicle flight-path angle changes sign from negative to positive.
7. Determine the exit altitude of the skip entry maneuver and the associated trajectory time.
8. Calculate the required to enter the skip entry trajectory from the initial Keplerian orbit by the trigonometric "Law of Cosines":

(13)

Where:

= Skip entry velocity of vehicle
= Entry flight-path angle

9. Calculate the required to enter a second skip entry trajectory in accordance with the following figure and equation:

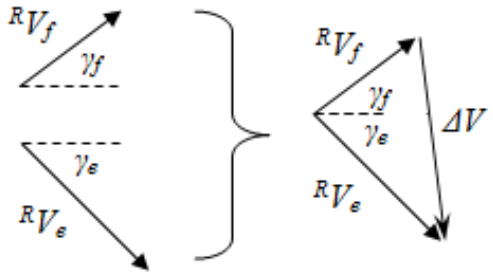

Figure 6. Law of Cosines-Based ΔV Calculation

(14)

Where:

= Entry velocity of vehicle for subsequent skip entry maneuver. Since , then the entry velocity for the subsequent maneuver is defined as:
= Skip exit velocity of vehicle
= Change in flight-path angle , defined as:

10. Calculate the orbit inclination angle at the exit of the skip entry maneuver:

(15)

(16)

(17)

— (18)

Where:

= Unit vector aligned with the planetary polar axis and perpendicular to the orbital plane
= Angular momentum
= Radial distance of entry vehicle from center of Earth
= Radial distance of entry vehicle with respect to the ECI frame
= Velocity of entry vehicle with respect to the ECI frame
= Velocity of entry vehicle with respect to the rotating atmosphere
= Flight-path angle
= Heading angle
= Rotation matrix from inertial to vehicle-pointing reference frame, defined as the following:

In addition to an algorithm, the following depicts the inputs and outputs for the skip entry maneuver *Matlab* scripts in a flow-chart format:

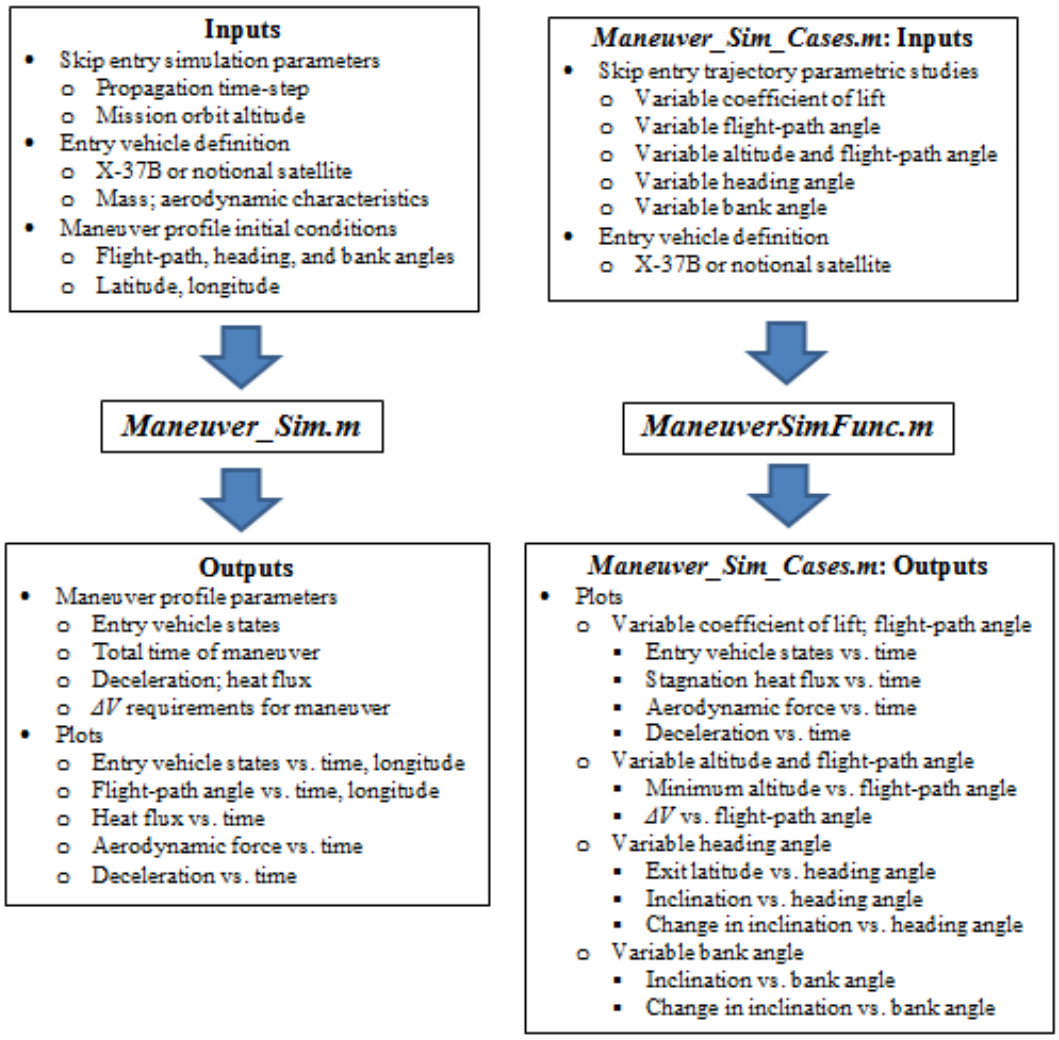

Figure 7. Skip Entry Maneuver *Matlab* Script Flowchart

Vacuum-Only Maneuver Simulation Algorithms

With the performance characteristics of skip entry maneuvers determined by the foregoing algorithm, the viability of such maneuvers must be evaluated against the performance of those which are vacuum-only in nature. Of the various vacuum-only maneuvers available, the only maneuvers whose performance can be directly compared with that of skip entry maneuvers and are applicable to the completion of mission

demand taskings and/or LEO experiments are simple plane changes, combined changes to inclination and RAAN, and coplanar and non-coplanar phasing rendezvous. The *Matlab* program script that simulates the preceding maneuvers is given in Appendix B.

Simple Plane Change

The first vacuum-only maneuver, the simple plane change, alters a spacecraft's inclination while keeping all other COEs constant. From this, the required to complete a simple plane change is influenced by the altitude and associated orbital velocity of the spacecraft as well as the desired change in orbit inclination (Vallado, 2001:332):

– (19)

Where:

= Magnitude of the initial orbital velocity
= Desired change in orbit inclination angle , defined as:
with

Since the initial and final orbits share only two trajectory locations in common, namely the ascending and descending node, the simple plane change must occur at either nodal crossing to minimize the required for the maneuver. Based on the assumption that all orbits are circular for the vacuum-only maneuvers, then the required for the simple plane change will be equal at both nodal crossings.

Combined Change to Inclination and RAAN

The second vacuum-only maneuver is an extension of the simple plane change and explicitly alters both a spacecraft's inclination and node location. In a similar form to

Equation 19, the required for a combined change in orbit inclination and node location is the following for circular orbits (Vallado, 2001:336):

– (20)

with the angle defined by the following spherical trigonometric expression (Vallado, 2001:336):

(21)

Where:

= Orbit inclination angle
= Desired change in orbit ascending node angle , defined as:
and

If the entry vehicle is assumed to be commencing its maneuver from an elliptical rather than a circular orbit however, the complexity of the preceding equations increases since two burns are required to attain the desired argument of perigee for the final orbit.

Coplanar and Non-Coplanar Phasing Rendezvous

The third and final vacuum-only maneuver analyzed is that of orbital rendezvous, specifically coplanar and non-coplanar phasing rendezvous for circular orbits. Whether conducted from coplanar or non-coplanar initial orbits, circular rendezvous is an applicable form of vacuum-only maneuvers available to fulfill a short-duration demand tasking because the remote-sensing spacecraft, or interceptor, must perform phasing maneuvers in order to rendezvous with a space-based location that corresponds to a nadir ground-based target within defined time window. In general, coplanar phasing

rendezvous consists of three basic cases: a leading interceptor and trailing target, a trailing interceptor and leading target, and an interceptor in an initial orbit which is coplanar to the target but differs in semi-major axis. For the purposes of the subsequent analysis the first two cases will be considered because they represent situations in which a spacecraft is either leading or trailing a ground-based target specified within a short-duration demand tasking. The last case, with the interceptor and target in two separate orbits, will not be considered however since it is assumed that the interceptor operates at an orbital altitude compatible with the performance limits of the remote-sensing payload.

Whether leading or trailing the target, the coplanar phasing rendezvous maneuver executed by the interceptor is defined by the following algorithm (Vallado, 2001:349-350):

1. Calculate the mean motion of the space-based location of a nadir ground-based target:

$$\frac{\quad}{\quad} \tag{22}$$

Where:

= Semi-major axis of target
= Gravitational parameter

2. Calculate the phasing time required for rendezvous:

$$\frac{\quad}{\quad} \tag{23}$$

Where:

= Initial phasing angle between the interceptor and target , and is negative in sign if the interceptor trails the target

= User-specified integer number of orbital revolutions allotted to the target in order to complete the phasing maneuver

3. Calculate the semi-major axis of the phasing orbit:

(24)

Where:

= User-specified integer number of phasing orbit revolutions required for the interceptor to ensure that the phasing orbit periapsis is greater than the radius of the Earth

4. Determine the required to complete the coplanar rendezvous:

(25)

Where:

= Semi-major axis of phasing orbit
= Semi-major axis of target

As with the coplanar maneuver case, the non-coplanar phasing rendezvous maneuver assumes circular orbits for both the interceptor and target. In order to simplify the calculation of the maneuver solution the following algorithm, also obtained from Vallado's text, further assumes the use of a Hohmann transfer between the orbits of the interceptor and target, and an equatorial orbit for the target (Vallado, 2001:355-356):

1. Calculate the mean motion of the interceptor and target.
2. Calculate the semi-major axis of the Hohmann transfer ellipse between the interceptor initial orbit and the target orbit:

– (26)

Where:

= Initial semi-major axis of interceptor
= Initial semi-major axis of target

Similar to the coplanar phasing rendezvous, the non-coplanar phasing rendezvous maneuver will assume that the interceptor and target are in orbits with equal values of semi-major axis but differing inclinations and node locations. Consequently, the values for mean motion of the interceptor and target calculated in the preceding step will be equal as well as the semi-major axes of the interceptor, target, and transfer ellipse.

3. Calculate the time required for the interceptor to complete the orbit transfer:

(27)

Where:

= Semi-major axis of transfer orbit

4. Calculate the lead angle between the interceptor and target:

(28)

Where:

= Mean motion of target

5. Find the angle, , the interceptor must traverse between its current orbital angular location and perigee of the transfer orbit. With this angle, the time

required for the interceptor to reach a nodal location is determined by the following:

(29)

Where:

= Mean motion of interceptor

6. Determine the true longitude angular location of the target following :

(30)

Where:

= Initial true longitude of target , defined as:

and if

7. Calculate the new phasing angle by finding the difference in angular distance between the interceptor and target following :

(31)

Where:

= True longitude of interceptor , defined as: , with the auxiliary angle expressed in terms of the interceptor's initial inclination and argument of latitude as:

8. Calculate the new lead angle between the interceptor and target:

(32)

9. Calculate the semi-major axis of the phasing orbit:

(33)

Where:

10. Determine the total required for the interceptor to complete the non-coplanar phasing rendezvous by adding the required to complete phasing and transfer orbits:

(34)

(35)

(36)

(37)

Where:

= Semi-major axis of interceptor
= Semi-major axis of phasing orbit
= Semi-major axis of target
= Semi-major axis of transfer orbit

In addition to an algorithm, the following depicts the inputs and outputs for the skip entry maneuver *Matlab* scripts in a flow-chart format:

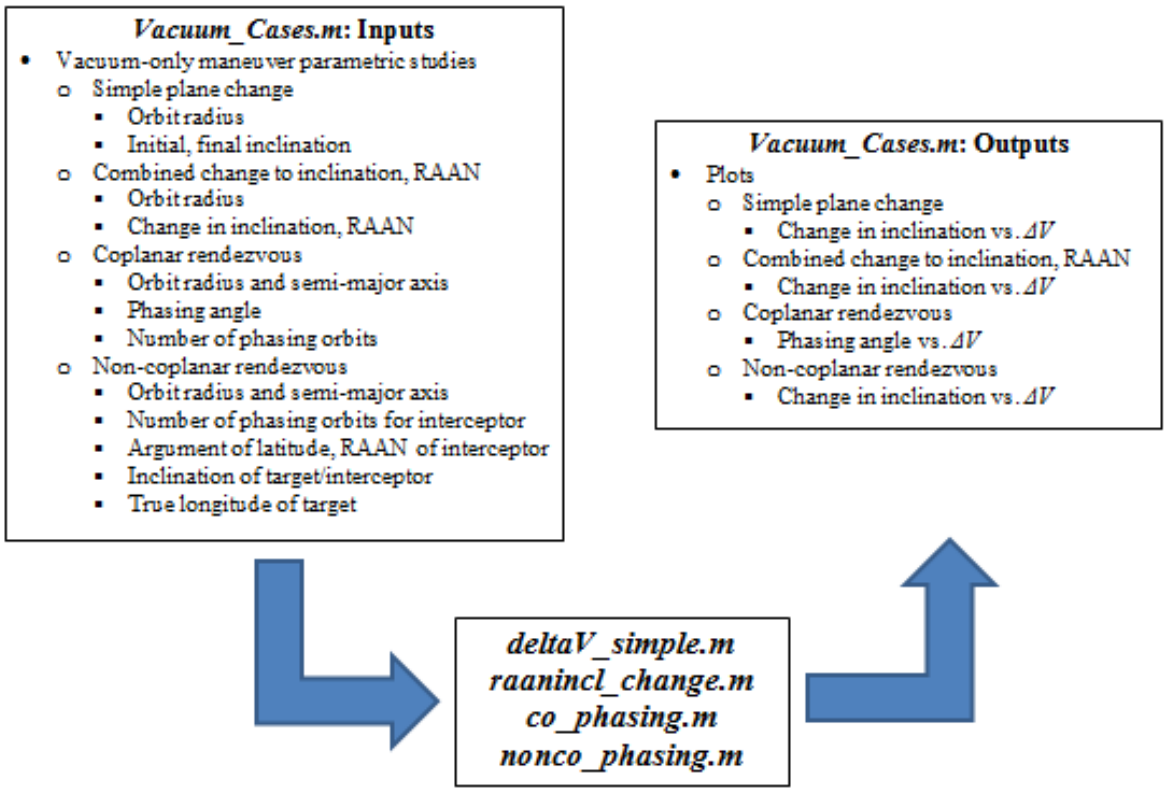

Figure 8. Vacuum-Only Maneuver *Matlab* Script Flowchart

Test Subject: X-37B Orbital Test Vehicle (OTV)

An experimental, unmanned orbital vehicle, the X-37B is intended to serve as a test platform for the U.S. Air Force in a variety of capacities, to include space experimentation, subsystem risk reduction, "concept of operations development" for reusable space vehicles, and "autonomous orbital flight, re-entry, and landing" (SAF/PA, 2010:1). A lifting entry vehicle, the X-37B is provided aerodynamic control by flaperons, ruddervators, and a windward body flap (Erbland, 2004:2). Launched into LEO under the payload shroud of heavy-lift vehicles such as the Lockheed-Martin Atlas V, the X-37B has a total wet mass of 4989.5 kg, a length of 8.915 m, and a wingspan of 4.547 m. When

compared with a payload-configured Space Shuttle orbiter with a mass of 85,230 kg, a length of 32.77 m, and a wingspan of 23.84 m, the X-37B is approximately 94.15% smaller in terms of mass, 72.8% shorter in length, and 80.93% shorter in wingspan (Young and Underwood, 1985:232, 236). Obtained from various sources, Table 5 outlines the vehicle mass properties and geometric dimensions and Figure 5 depicts the internal subsystem configuration of the X-37B as of November 2010.

Based on an estimated payload mass of 226.80 kg (500), a design threshold of 3 km/s (10,000 ft/s), and an estimated specific impulse (*Isp*) of 310 s for a hydrogen peroxide/JP-8 bipropellant propulsion subsystem, values for inert and propellant mass were determined by the following expression (Covault, 2010:36):

— (38)

Where:

= Specific impulse (s)
= Gravitational acceleration at sea-level
= Initial total wet mass (kg)
= Vehicle dry mass (kg), which includes both the vehicle inert and payload mass

The values for both inert and propellant mass are listed along with other vehicle parameters for the X-37B in Table 5 (Covault, 2010:36; Boeing, 2010:1; Bilbey, 2005:28).

Table 5. X-37B Vehicle Parameters

Total Wet Mass	4989.5 kg (11000)
Inert Mass	1633.7 kg (3602)
Propellant Mass	3129.0 kg (6898)
Payload Mass	226.80 kg (500)
Payload Bay Dimensions	2.134 m x 1.219 m (7 ft x 4 ft)
Length	8.915 m (29 ft 3 in)
Height	2.896 m (9 ft 6 in)
Wing Span (b)	4.547 m (14 ft 11 in)
Average Chord Length	4.096 m (13 ft 5.3 in)
Planform Area (S)	18.63 (200.5)

Even though the *Isp* for a hydrogen peroxide/JP-8 propulsion subsystem was utilized in the calculation of the values for vehicle inert and propellant mass, this represents one of two possible configurations for the X-37B as outlined in Table 6. The second configuration maintains a lower value of 230 s for *Isp* if assumed to be mono-propellant in nature (DoD, 2010:8). While both configurations are represented as options for the user when initializing the skip entry simulation program, the former option with hydrogen peroxide as the oxider and JP-8 as the fuel was employed to complete the parametric studies which comprise this thesis (Andrews, 2010:1; Humble et al., 1995:188).

Table 6. X-37B Propulsion Subsystem Options

Propellant	Hydrogen Peroxide/JP-8	Hydrazine
Thrust	13345 N (3000)	9901 N (2226)
Isp	310 s	230 s

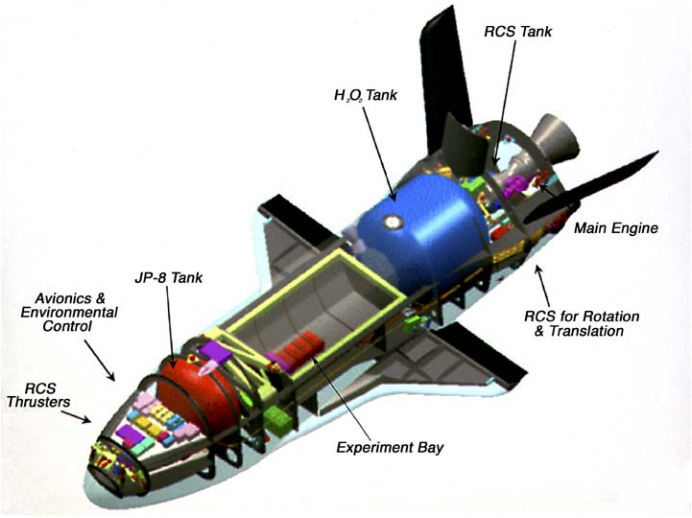

Figure 9. X-37B Internal Subsystem Configuration (Space.com, 2010:1)

With several aspects of the X-37B vehicle design – to include aerodynamic characteristics – currently unavailable, the coefficient of drag was approximated as 0.5. Employing the aerodynamic relation of and values for zero-lift coefficient of drag , coefficient of lift, and drag polar parameter of 0.032, 0.5699, and 1.4, respectively, Rao and Scherich estimated the coefficient of drag to be 0.4867 for an entry vehicle capable of being "aerodynamically maneuverable in hypersonic flight" (Rao and Scherich, 2008:3-5). In terms of lift capability, the coefficient of lift for the X-37B was calculated by dividing the user-defined vehicle lift-to-drag ratio by the aforementioned approximation for coefficient of drag. A function of

vehicle geometry and atmospheric flow characteristics at a given altitude, the values for lift-to-drag ratio available within the skip entry simulation were , which reflect the estimated hypersonic lift-to-drag ratio range of for the X-20A Dynasoar and for the Space Shuttle orbiter (Strom, 2004:1; Young and Underwood, 1985:258).

Test Subject: Notional Satellite

In addition to the X-37B, the skip entry parametric studies were also run with a notional satellite as the entry vehicle. Modeled to both reflect the aerodynamic characteristics of the X-37B and be compliant with the launch requirements of the ESPA program. Overall, the notional satellite represents the second of two vehicle options for the completion of responsive space missions, whether experimental or operational in nature, with the first option being that of re-usable space-plane technology as embodied by the X-37B.

As with the primary version of the ESPA adapter ring, a recently designed scaled version enables a given launch vehicle, such as the Minotaur IV, Falcon 1, and Falcon 1e, to insert a primary payload as well as several secondary payloads into various parking orbits in LEO. Situated below the primary payload, the secondary payloads are attached radially to the adapter ring as illustrated in Figure 6, which depicts the placement of the scaled ESPA adapter ring within the payload fairing of the Minotaur IV, Falcon 1, and Falcon 1e, respectively. Note that the secondary payloads are colored green for the Minotaur IV system and blue for the Falcon 1 and Falcon 1e systems (Maly et al., 2009:3-5).

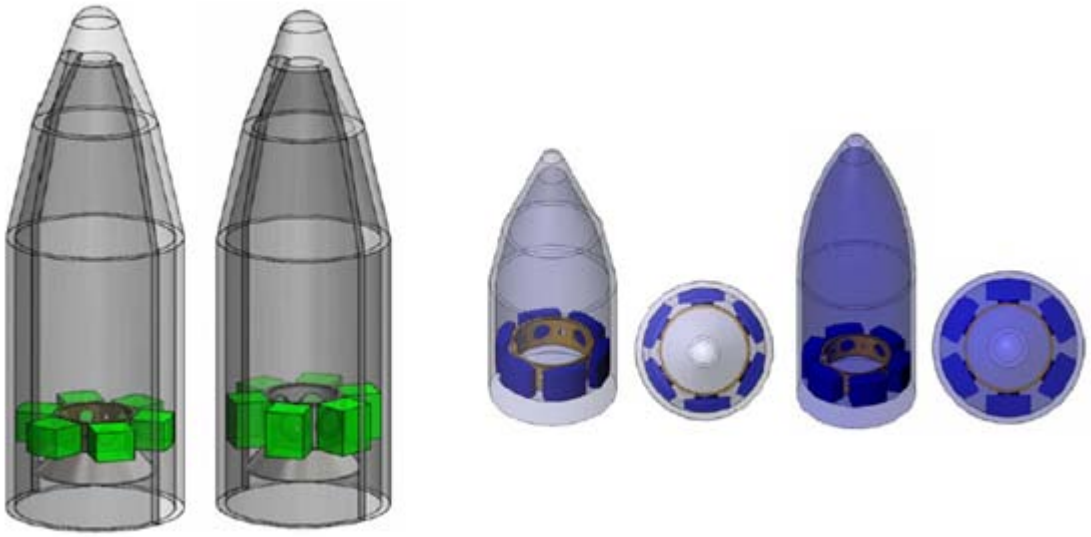

Figure 10. ESPA Payload Configuration Options (Minotaur IV, Falcon 1, Falcon 1e)

In terms of specific dimensions, the Minotaur IV is capable of hosting two different versions of the ESPA adapter ring – the ESPA-15 and ESPA-24. With the ESPA-15 version, the secondary payload envelope has a base 20.0 x 18.75 inches and a height of 15 inches, whereas with the ESPA-24, the payload envelope maintains a height limit of 24 inches (Maly et al., 2009:3-5). Due to sizing constraints within the Falcon 1 and Falcon 1e fairings, only the ESPA-15 version is available.

Constrained by the dimensions of the payload fairing for each small launch vehicle option as well as the allowable secondary payload volume of the ESPA-15 and ESPA-24 adapter ring versions, the notional satellite was sized so as to create a planform area of 18.63 , the same value as the X-37B. Overall, aerodynamic similarity between the X-37B and the notional satellite in terms of planform area was sought in order to retain vehicle mass and the coefficients of drag and lift as the only vehicle design-

influenced dynamic variables within the following acceleration equations for aerodynamic drag and lift :

(39)

(40)

Where:

= Coefficient of drag
= Coefficient of lift
= Local, altitude-dependent estimate of atmospheric density
= Planform area
= Entry vehicle velocity
= Entry vehicle mass

When modeled as a flat plate, the coefficient of drag for satellites operating in the "upper atmosphere" is approximately 2.2 (Vallado, 2001:525). While satellite geometries such as spheres have a coefficient of drag in the range of 2.0 to 2.1 in the upper atmosphere, the value of 2.2 was chosen for the notional satellite since the solar arrays are analogous to flat plates (Vallado, 2001:525). Similar to the X-37B, the coefficient of lift for the notional satellite was calculated by the dividing the user-defined lift-to-drag ratio, chosen from the range , by aforementioned approximation for coefficient of drag.

Designed without wings and/or a lifting-body surface, the notional satellite produces the planform area of 18.63 from the total surface area formed by the solar areas and the largest side of the rectangular bus by area as depicted in Figure 7. Although cylindrical and spherical bus designs were viable options for the notional satellite, a rectangular design was chosen to maximize the surface area of the potential aerodynamic

surface necessary to create the desired planform area in conjunction with the solar arrays. The following tables outline the varying dimensions for the notional satellite required to meet the planform area sizing requirement and either the primary payload fairing diameter constraint , or the secondary payload ESPA volume constraints.

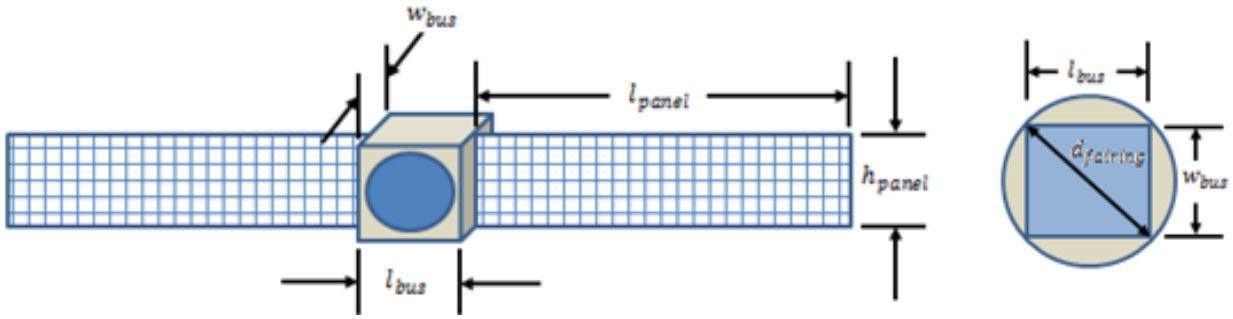

Figure 11. Notional Satellite Design and Illustration of Planform Area

Table 7. Notional Satellite Dimensions for Primary Payload Configuration

Dimension Parameter	Minotaur IV	Falcon 1	Falcon 1e
	2.055 m (80.9 in)	1.372 m (54 in)	1.549 m (61 in)
	1.453 m (57.21 in)	0.9702 m (38.20 in)	1.095 m (43.11 in)
	1.453 m (57.21 in)	0.9702 m (38.20 in)	1.095 m (43.11 in)
	2.0 m (78.74 in)	2.0 m (78.74 in)	2.0 m (78.74 in)
	3.930 m (154.7 in)	4.172 m (164.3 in)	4.110 m (161.8 in)
	2.0 m (78.7 in)	2.0 m (78.7 in)	2.0 m (78.7 in)
Planform Area (S)	18.63 (200.5)	18.63 (200.5)	18.63 (200.5)

Table 8. Notional Satellite Dimensions for Secondary Payload Configuration

Launch Vehicle	**Minotaur IV**		**Falcon 1**	**Falcon 1e**
Payload Configuration	ESPA-15	ESPA-24	ESPA-15	
	0.5080 m (20 in)	0.5080 m (20 in)	0.5080 m (20 in)	
	0.4763 m (18.75 in)	0.4763 m (18.75 in)	0.1290 m (5.08 in)	0.2301 m (9.06 in)
	0.3810 m (15 in)	0.6096 m (24 in)	0.3810 m (15 in)	
	24.20 m (952.8 in)	15.03 m (591.7 in)	24.20 m (952.8 in)	
	0.3810 m (15 in)	0.6096 m (24 in)	0.3810 m (15 in)	
Planform Area (S)	18.63 (200.5)		18.63 (200.5)	

Besides vehicle volume, the notional satellite was also sized to meet the mass constraints imposed by the Minotaur IV, Falcon 1, and Falcon 1e launch vehicles for both primary and secondary payloads. As a primary payload, the notional satellite was assigned an arbitrary mass of 1000 kg whereas being a secondary payload the mass was reduced to 200 kg (SMC, 2006:5). For both payload cases the mass value represents the total vehicle mass, to include inert and propellant mass. Based on the aforementioned values for total mass of the notional satellite and the propellant mass fraction of 0.6271, a value derived from the propellant mass of 3129 kg and total mass of 4989.5 kg for the X-37B, the propellant mass required to produce a of 3 km/s is 627.1 kg for the primary payload configuration of the notional satellite and 125.42 kg for the secondary payload configuration with a hydrazine/JP-10 bipropellant propulsion system and an *Isp* of 310 s.

Summary

The X-37B and notional satellite test subjects represent the current spacecraft available for execution of responsive space missions, short-duration demand taskings, and LEO experimentation. A reusable and non-operational system, the X-37B maintains a lifting-body aerodynamic design that is suitable for skip entry maneuvers, as well as a configurable payload bay capable of adapting to a variety of missions. In comparison, the notional satellite can be chosen as either a primary payload compatible with the fairing dimensions of the Minotaur IV, Falcon 1, and Falcon 1e launch vehicles, or a secondary payload designed to fulfill the mass and volume constraints imposed by the ESPA-15 and ESPA-24-class adapter rings. Despite sharing an equivalent aerodynamic planform area and maximum capability, the X-37B and notional satellite – whether configured as a primary or secondary payload – exhibit differing values for vehicle mass and coefficient of drag which enables the analysis of entry vehicle design on skip entry maneuver performance, in addition to the comparative performance analysis of skip entry and vacuum-only maneuvers.

IV. Analysis and Results

Chapter Overview

The purpose of this chapter is to present the analysis and results of the skip entry and vacuum-only maneuver parametric studies conducted for the X-37B and notional satellite. In order of presentation, the chapter outlines the results of the skip entry maneuver simulations, the vacuum-only maneuver simulations, and the orbit inclination-change analysis for the skip entry and simple plane change maneuvers.

Results of Skip Entry Maneuver Simulations

As an example of the use of skip entry maneuvers, all of the simulations were run in accordance with a hypothetical laser communication experiment between a ground station located at Kirtland AFB, NM and the X-37B. While laser communication is intended between the ground and on-orbit assets, an experiment involving the testing of laser communication between a given ground station and an entry vehicle performing a skip entry maneuver presents several advantages: (1) the laser communication system can be tested while minimizing the potential of negatively impacting existing on-orbit assets if the receiving system fails to collect the beam; (2) the versatility of the laser communication ground-segment can be tested by having the entry vehicle approach the ground station from various azimuth and elevation angles; (3) increased flexibility, since the laser communication receiver hardware and associated software is the payload on a short-duration, reusable entry vehicle like that of the X-37B; and (4) the ability to test the laser communication system without the presence of unintended and/or adverse effects of the ionosphere. A layer of the planet's upper atmosphere between approximately 75 and

2000 km in altitude above sea-level, the ionosphere can impede the transmission of certain signals into space, such as those within the frequency range of 3 kHz (Very Low Frequency/VLF) to 30 MHz (High Frequency/HF) which are reflected by the ionosphere and remain sky waves (Tascione, 1994:89, 117, 122).

Although the X-37B represents the principal example entry vehicle within the aforementioned laser communication experiment, the flight performance of the X-37B is compared with that of the secondary payload version of the notional satellite for all simulations. Underpinned by the laser communication experiment scenario, trajectory simulation parametric studies were devised to theoretically determine the nature in which entry vehicle coefficient of lift, flight-path angle, and initial skip entry altitude impact the dynamics of the skip entry profile.

Since all skip entry trajectories were propagated via a first-order numerical integration scheme, a time step sensitivity analysis was conducted prior to the commencement of the skip entry parametric analysis in order to determine maneuver solution convergence behavior as the temporal step size tends to zero. Due to the wide array of various parameters that comprise the skip entry maneuver solution however, only the minimum trajectory altitude and skip exit velocity were examined for the X-37B and notional satellite. Tables 9-10 below outline the convergence behavior of the aforementioned maneuver parameters for an entry flight-path angle of -10 , a lift-to-drag ratio of 1.0, and skip entry from an initial altitude of either 200 or 400 km.

Table 9. Time Step (Δt) Sensitivity Analysis for X-37B
(h = 200, 400 km, γ = -10°, L/D = 1.0)

Altitude (km)	**Parameter**	**Time Step, (sec)**			
		1.0	0.5	0.1	0.01
200	Minimum Altitude (km)	44.032	44.482	44.823	44.899
	Exit Velocity (km/s)	5.263	5.342	5.398	5.410
400	Minimum Altitude (km)	44.562	45.006	45.342	45.417
	Exit Velocity (km/s)	5.418	5.495	5.550	5.562

Table 10. Time Step (Δt) Sensitivity Analysis for X-37B
(h = 200, 400 km, γ = -10°, L/D = 1.0)

Altitude (km)	**Parameter**	**Time Step, (sec)**			
		1.0	0.5	0.1	0.01
200	Minimum Altitude (km)	77.543	77.994	78.336	78.412
	Exit Velocity (km/s)	5.230	5.308	5.364	5.376
400	Minimum Altitude (km)	77.998	78.442	78.782	78.856
	Exit Velocity (km/s)	5.373	5.450	5.505	5.517

In order to determine the appropriate time step for use within the numerical integration scheme, the percentage change in the minimum trajectory altitude and skip exit velocity was determined as the time step changed from 1.0 to 0.5, 0.5 to 0.1, and 0.1 to 0.01 sec. The results for the second phase of the time step sensitivity analysis are shown below in Tables 9-10:

Table 11. Percentage Change in Trajectory Parameters between Time Steps (Δt)
for X-37B (h = 200, 400 km, γ = -10°, L/D = 1.0)

Altitude (km)	**Parameter**	**Change in Time Step, (sec)**		
200	Minimum Altitude	1.02%	0.767%	0.935%
	Exit Velocity	1.50%	1.05%	0.222%
400	Minimum Altitude	0.996%	0.747%	0.165%
	Exit Velocity	1.42%	1.00%	0.216%

Table 12. Percentage Change in Trajectory Parameters between Time Steps (Δt) for Notional Satellite (h = 200, 400 km, γ = -10°, L/D = 1.0)

Altitude (km)	**Parameter**	**Change in Time Step, (sec)**		
200	Minimum Altitude	0.582%	0.439%	0.097%
	Exit Velocity	1.49%	1.06%	0.224%
400	Minimum Altitude	0.569%	0.433%	0.094%
	Exit Velocity	1.43%	1.01%	0.218%

Based on the preceding parameter convergence behavior and percentage change values, it was assessed that the decrease from a time step of 0.1 to 0.01 sec produced comparatively lower variation in the parameters of minimum trajectory altitude and skip exit velocity than decreases in time step from 1.0 to 0.5 and 0.5 to 0.1 sec. While a time step of 0.01 sec ostensibly achieves the greatest convergence, a time step of 0.1 sec was chosen for all skip entry maneuver analysis due to considerations of not only of parameter convergence behavior, but also computation speed. For an arbitrary simulation period of 1000 sec, the time step of 0.1 sec produces 10,000 time segments while the lower time step of 0.01 sec produces 100,000 time segments. With 100,000 time segments, the time step of 0.01 sec forces the numerical integration scheme to perform 90,000 more calculations per trajectory parameter than the time step of 0.1 sec, which in itself only performs 8000 and 9000 more calculations than the time steps of 0.5 and 1.0 sec, respectively, during a simulation period of 1000 sec. Consequently, the greater computation time required for the time step of 0.01 sec came to outweigh any improved parameter convergence when compared with the time step of 0.1 sec.

Table 13 describes the simulation inputs for the case of variable coefficient of lift for skip entry from an initial altitude of 120 and 400 km above sea-level. As

previously identified, the variability in the entry vehicle coefficient of lift arises from the variability in the user-defined lift-to-drag ratio which, when divided by the vehicle-specific coefficient of drag, yields a value for coefficient of lift.

Table 13. Simulation Inputs for Variable Coefficient of Lift with h = 120, 400 km

Vehicle	Mass	Initial Flight-Path Angle	Aerodynamics	Planform Area
X-37B	4989.5 kg	-10	= 0.5	S = 18.63
Notional Satellite	200 kg	-10	= 2.2	S = 18.63

The simulation results for the variable coefficient of lift case at an entry altitude of 120 km are illustrated by Figures 8-9 for the X-37B and notional satellite, respectively. From these figures and the accompanying simulation data, the minimum altitude, skip entry exit velocity, maximum stagnation heat flux, maximum lift and drag force, and maximum deceleration at lift-to-drag ratios of 0.9 and 2.0 for the two entry vehicles were discerned and compared to yield percent difference values which are outlined in Tables 14-15. For consistency, all percent difference values were calculated in accordance with the following equation:

(41)

Where:

= Arbitrary variable representative of a particular trajectory parameter such as minimum altitude, exit velocity, stagnation heat flux, aerodynamic force, and deceleration

Overall, the above equation conveys the percent difference as a percent deviation from the trajectory parameters calculated at a lift-to-drag ratio of 0.9. Similar results are

depicted in Figures 10-11 and Tables 16-17 for the X-37B and notional satellite at an entry altitude of 400 km.

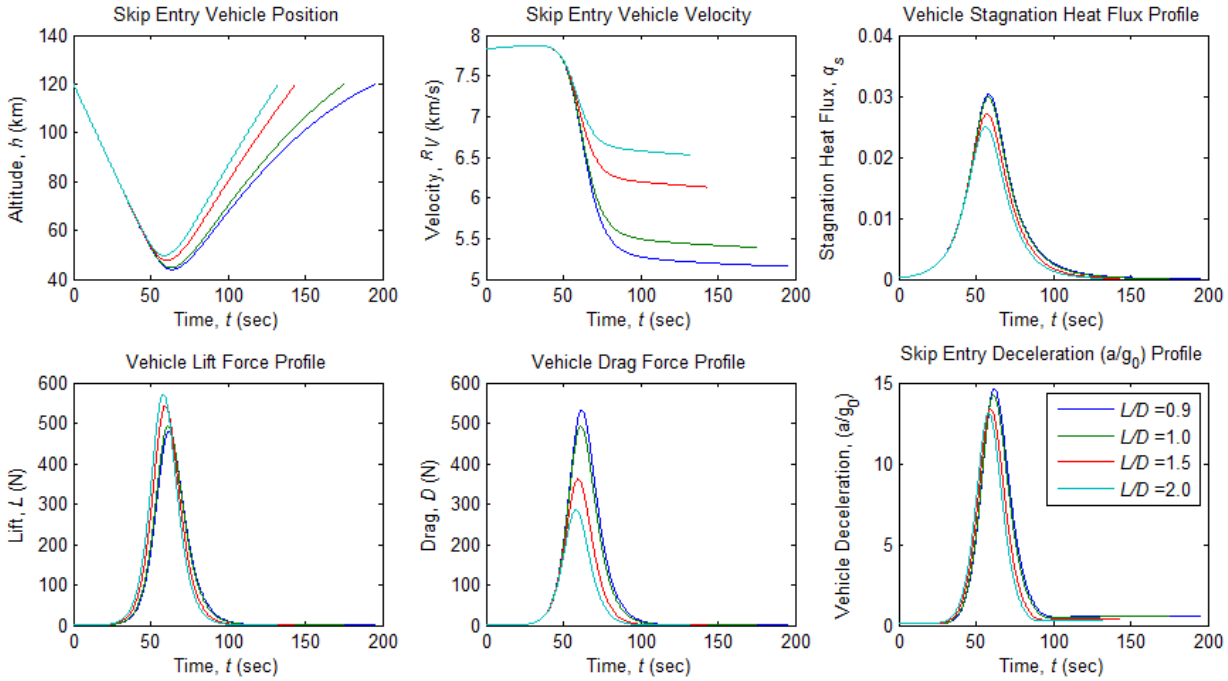

Figure 12. Variable Coefficient of Lift Simulation for X-37B (h = 120 km, γ = -10°)

Table 14. Comparison of X-37B Skip Entry Dynamics Extrema for Variable Coefficient of Lift (h = 120 km, γ = -10°)

Parameter			**Percent Difference**
Minimum Altitude (km)	43.97	49.74	13.13%
Exit Velocity (km/s)	5.158	6.528	26.56%
Max. Stagnation Heat Flux	0.0305	0.0250	18.03%
Maximum Lift Force (N)	478.6	571. 9	19.49%
Maximum Drag Force (N)	531.8	285.9	46.23%
Maximum Deceleration (g)	14.62	13.14	10.15%

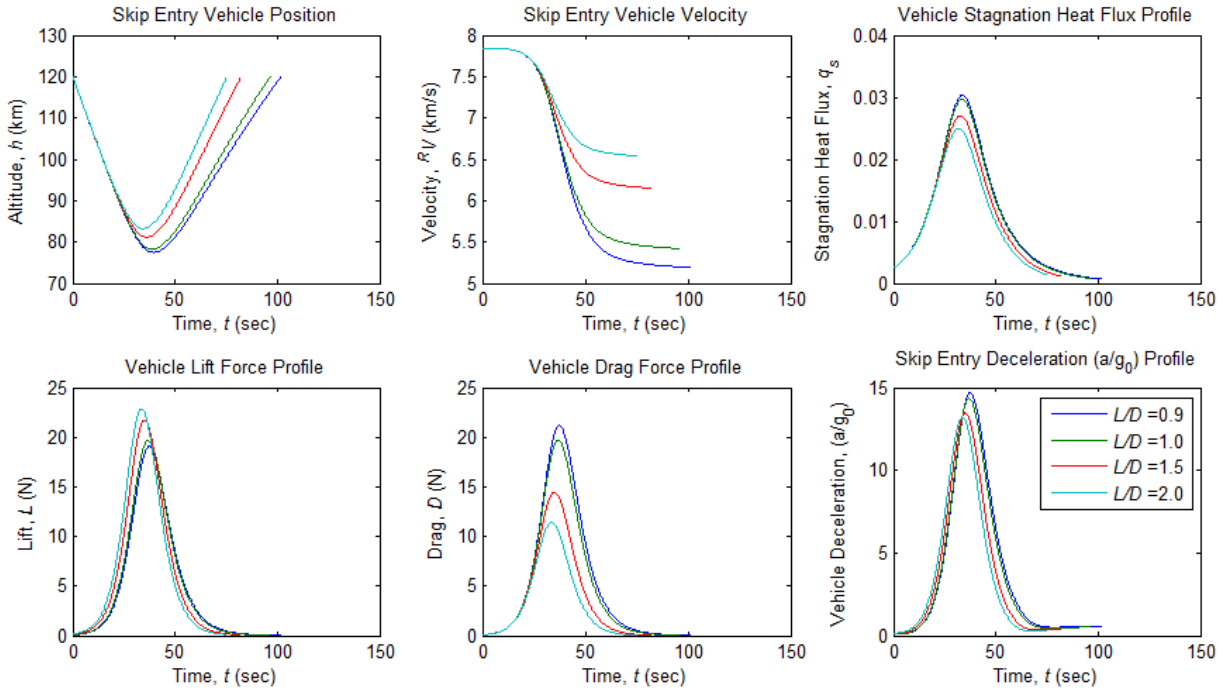

Figure 13. Variable Coefficient of Lift Simulation for Notional Satellite (h = 120 km, γ = -10°)

Table 15. Comparison of Notional Satellite Skip Entry Dynamics Extrema for Variable Coefficient of Lift (h = 120 km, γ = -10°)

Parameter			**Percent Difference**
Minimum Altitude (km)	77.49	83.28	7.48%
Exit Velocity (km/s)	5.190	6.541	26.03%
Max. Stagnation Heat Flux	0.0303	0.0249	17.82%
Maximum Lift Force (N)	19.07	22.86	19.87%
Maximum Drag Force (N)	21.19	11.43	46.06%
Maximum Deceleration (g)	14.69	13.24	9.87%

Tables 14-15 show that with a lower coefficient of drag, the X-37B reached a lower minimum altitude than the notional satellite for skip entry from an altitude of 120 km and a flight-path angle of -10 . By penetrating deeper into the atmosphere during skip

entry, the X-37B experienced a 0.656% greater maximum stagnation heat flux, and a 96.02% greater maximum lift and drag force than the notional satellite at a lift-to-drag ratio of 0.9. For a lift-to-drag ratio of 2.0, the X-37B experienced a 0.400% greater maximum stagnation heat flux and a 96.00% greater maximum lift and drag force than the notional satellite. With a coefficient of drag of 2.2 rather than the value of 0.5 for the X-37B, the notional satellite decelerated at a faster rate despite maintaining a lower maximum drag force and, as a result, produced a 0.456% and 0.756% greater maximum deceleration for lift-to-drag ratios of 0.9 and 2.0, respectively. Producing a greater maximum drag force than the notional satellite for as a result of encountering an exponentially increasing atmospheric density profile during skip entry, the X-37B reached a minimum altitude of 43.97 km and 49.74 km for lift-to-drag ratios of 0.9 and 2.0, whereas the notional satellite only reached a minimum altitude of 77.49 km and 83.28 km.

At the same entry flight-path angle of -10 , a single skip entry maneuver from an entry altitude of 400 km produced similar results to those seen at an entry altitude case of 120 km for the X-37B and the notional satellite, and are depicted in Figures 10-11 and Tables 16-17. For a lift-to-drag ratio of 0.9, the X-37B experienced a 95.98% greater maximum lift and drag force than the notional satellite, while at a lift-to-drag ratio of 2.0 the X-37B experienced a 95.97% greater maximum lift and drag force. In terms of deceleration, the notional satellite experienced a 1.45% and 1.54% greater maximum value than the X-37B for a lift-to-drag ratio of 0.9 and 2.0, respectively.

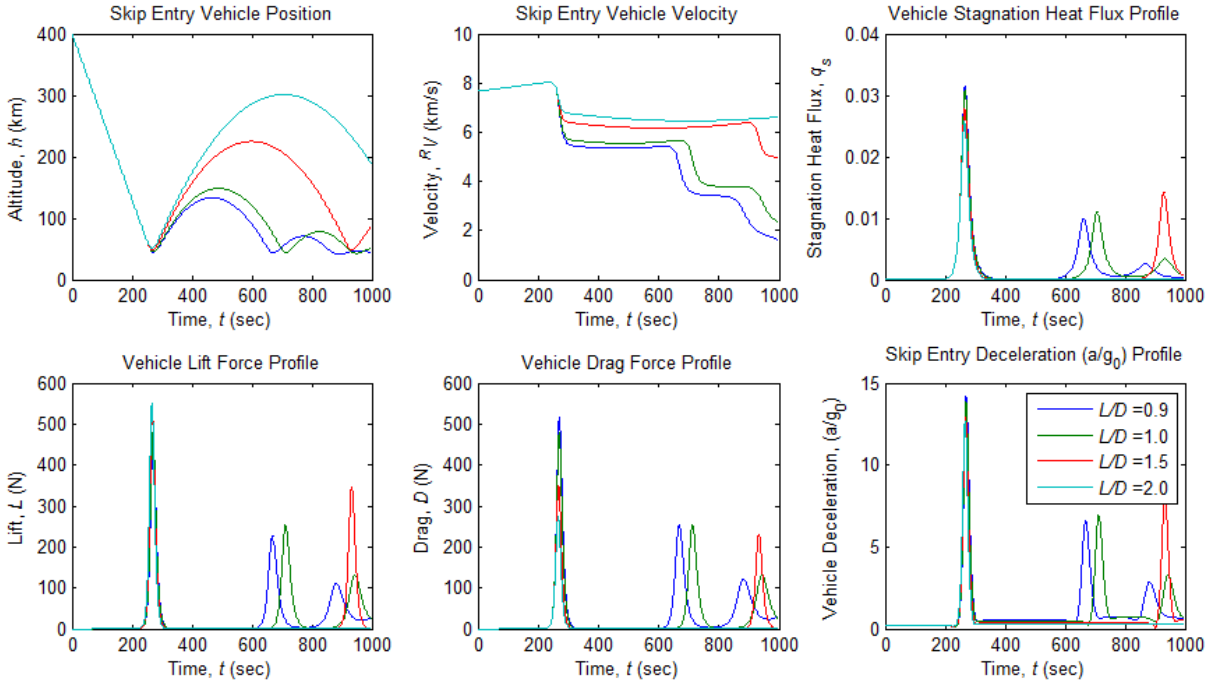

Figure 14. Variable Coefficient of Lift Simulation for X-37B (h = 400 km, γ = -10°)

Table 16. Comparison of X-37B Skip Entry Dynamics Extrema for Variable Coefficient of Lift (h = 400 km, γ = -10°)

Parameter			**Percent Difference**
Minimum Altitude (km)	44.58	50.33	12.91%
Exit Velocity (km/s)	5.345	6.463	20.92%
Max. Stagnation Heat Flux	0.0314	0.0257	18.15%
Maximum Lift Force (N)	463.40	551.06	18.92%
Maximum Drag Force (N)	514.89	275.53	46.489%
Maximum Deceleration (g)	14.178	12.692	10.48%

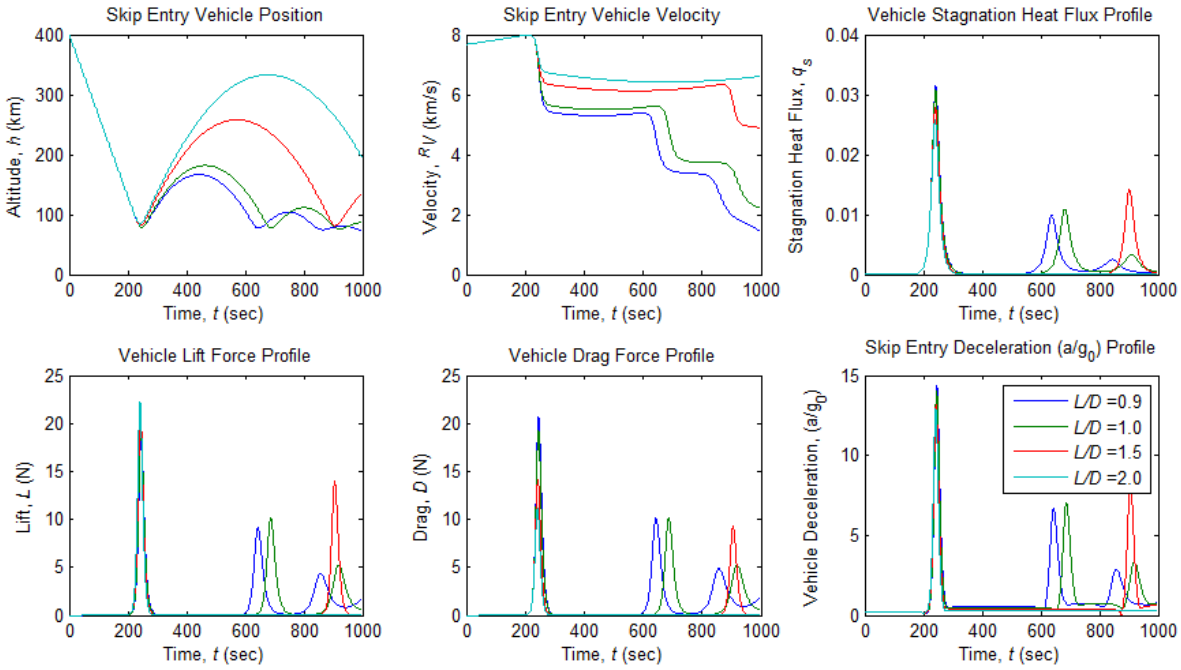

Figure 15. Variable Coefficient of Lift Simulation for Notional Satellite (h = 400 km, γ = -10°)

Table 17. Comparison of Notional Satellite Skip Entry Dynamics Extrema for Variable Coefficient of Lift (h = 400 km, γ = -10°)

Parameter			**Percent Difference**
Minimum Altitude (km)	78.02	83.77	7.38%
Exit Velocity (km/s)	5.299	6.423	21.21%
Max. Stagnation Heat Flux	0.0314	0.0257	18.15%
Maximum Lift Force (N)	18.66	22.21	19.05%
Maximum Drag Force (N)	20.73	11.11	46.43%
Maximum Deceleration (g)	14.39	12.89	10.40%

Even though the results for a single skip entry are given in Tables 15-17, Figures 10-11 depict multiple sequential skip entry maneuvers during the arbitrary simulation period of 1000 sec. Such maneuvers are the product of the dynamics of the first skip entry maneuver in which the entry vehicle – whether the X-37B or notional satellite – was unable to reach an exit orbital altitude that was equivalent in magnitude to the initial entry condition. Coupled with the effects of a lower kinetic energy at skip exit, the entry vehicle continued to re-enter the atmosphere following the initial skip entry to complete a series of subsequent skip entry maneuvers that would ultimately result in the impact of the entry vehicle with the Earth at a time after 1000 sec.

Table 18 outlines the simulation inputs for the case of variable flight-path angle for skip entry from an initial altitude of 120 km and 400 km above sea-level.

Table 18. Simulation Inputs for Variable Flight-Path Angle with h = 120, 400 km

Vehicle	**Mass**	**Initial Flight-Path Angle**	**Aerodynamics**	**Planform Area**
X-37B	4989.5 kg	Variable	L/D = 1.0 = 0.5	S = 18.63
Notional Satellite	200 kg	Variable	L/D = 1.0 = 2.2	S = 18.63

The simulation results for the variable flight-path angle case at an entry altitude of 120 km are illustrated by Figures 12-13 for the X-37B and notional satellite, respectively, with the values for minimum altitude, exit velocity, maximum stagnation heat flux, maximum aerodynamic force, and maximum deceleration compared in Tables 19-20 for flight-path angles of -10 and -25 . Similar results are depicted in Figures 14-15 and Tables 21-22 for the X-37B and notional satellite at an entry altitude of 400 km.

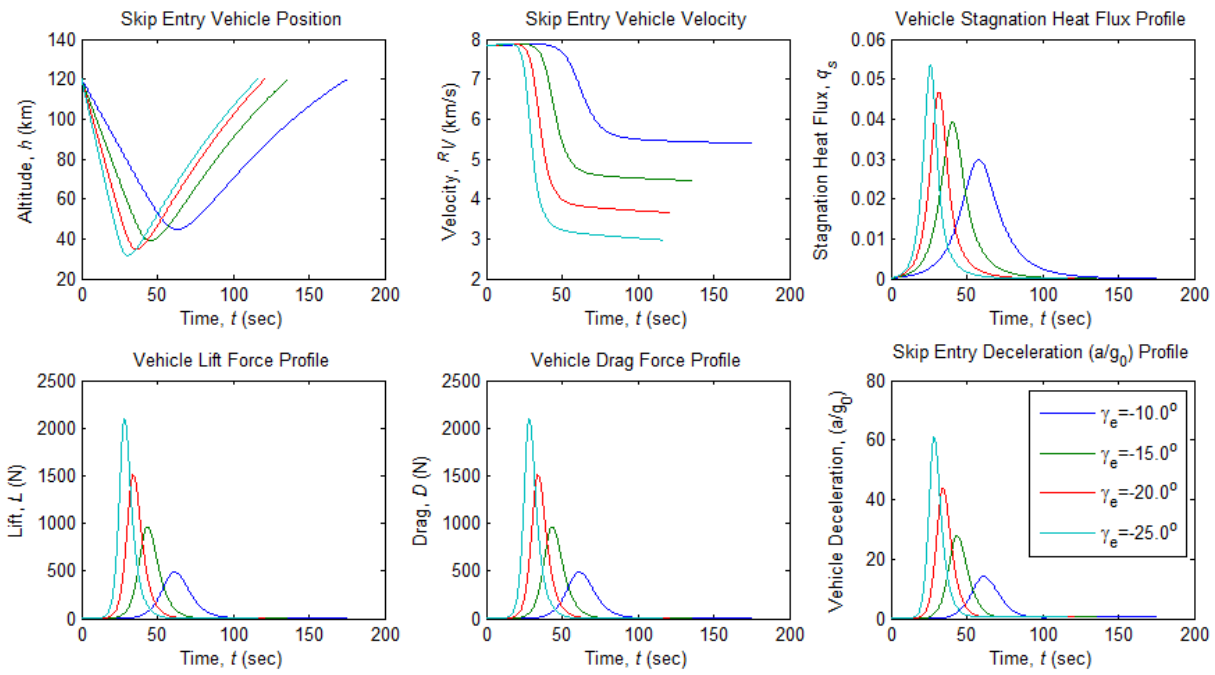

Figure 16. Variable Flight-Path Angle Simulation for X-37B (h = 120 km, L/D = 1.0)

Table 19. Comparison of X-37B Skip Entry Dynamics Extrema
for Variable Flight-Path Angle (h = 120 km, L/D = 1.0)

Parameter			**Percent Difference**
Minimum Altitude (km)	44.73	31.68	29.18%
Exit Velocity (km/s)	5.392	2.972	44.88%
Max. Stagnation Heat Flux	0.0298	0.0536	79.87%
Maximum Lift Force (N)	493.7	210.17	57.43%
Maximum Drag Force (N)	493.7	210.17	57.43%
Maximum Deceleration (g)	14.27	60.94	327.07%

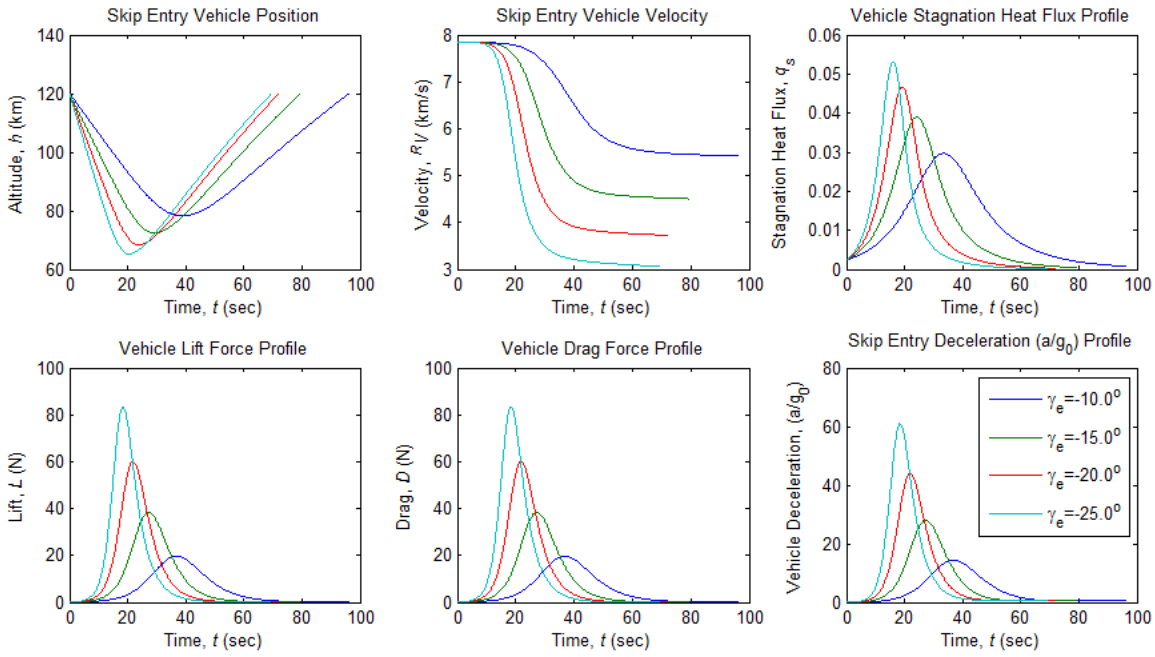

Figure 17. Variable Flight-Path Angle Simulation for Notional Satellite
(h = 120 km, L/D = 1.0)

As depicted in Figures 12-13 and Tables 19-20, both entry vehicles penetrated to a lower altitude as the flight-path angle increased from -10 to -25 , with the X-37B reaching a minimum altitude of 31.68 km and the notional satellite an altitude of 65.23 km from an entry flight-path angle of -25 . In addition to lowering the minimum skip entry altitude, the increase in flight-path angle led to an increase in aerodynamic force and deceleration, with the X-37B experiencing a 57.43% increase in the lift and drag force, and a 327.05% increase in maximum deceleration. With the notional satellite the increase in flight-path angle from -10 to -25 led to an increase of 323.96% and 325.32% for aerodynamic force and deceleration, respectively. Similar results are seen in Figures 14-15 and Tables 21-22 for an entry altitude of 400 km.

Table 20. Comparison of Notional Satellite Skip Entry Dynamics Extrema for Variable Flight-Path Angle (h = 120 km, L/D = 1.0)

Parameter			**Percent Difference**
Minimum Altitude (km)	78.25	65.23	16.64%
Exit Velocity (km/s)	5.420	3.061	43.53%
Max. Stagnation Heat Flux	0.0297	0.0532	79.13%
Maximum Lift Force (N)	19.68	83.44	323.96%
Maximum Drag Force (N)	19.68	83.44	323.96%
Maximum Deceleration (g)	14.34	60.99	325.32%

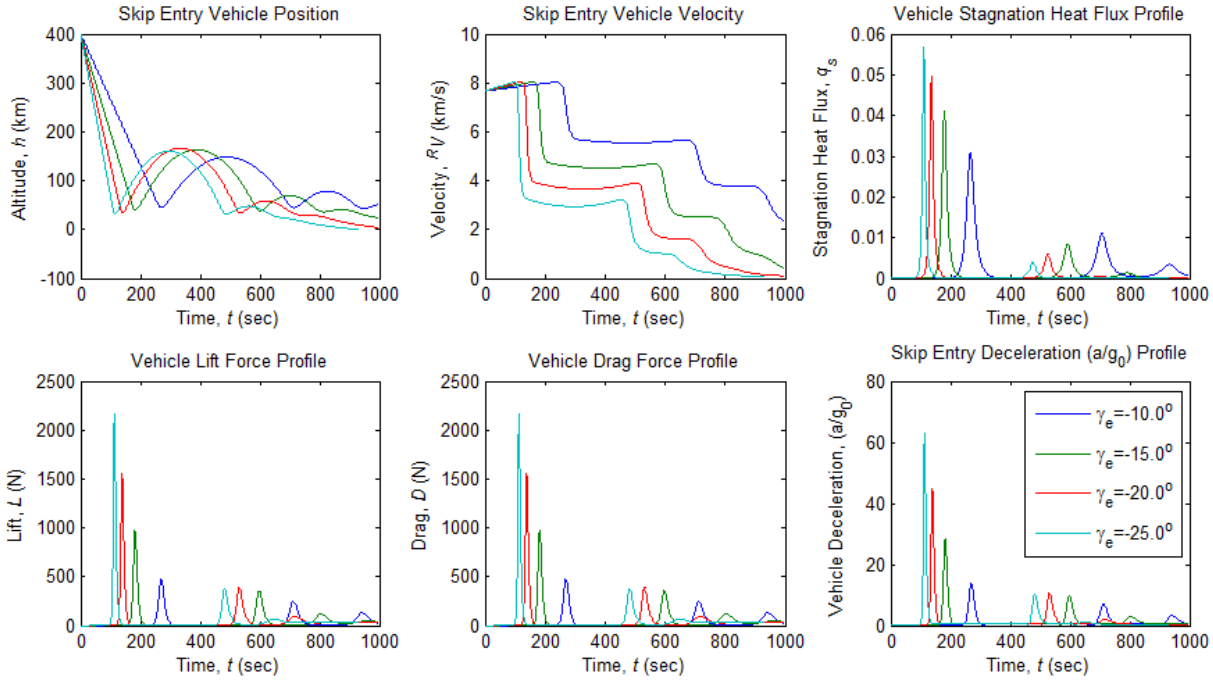

Figure 18. Variable Flight-Path Angle Simulation for X-37B (h = 400 km, L/D = 1.0)

Table 21. Comparison of X-37B Skip Entry Dynamics Extrema
for Variable Flight-Path Angle (h = 400 km, L/D = 1.0)

Parameter			**Percent Difference**
Minimum Altitude (km)	45.34	31.77	29.93%
Exit Velocity (km/s)	5.550	2.940	47.03%
Max. Stagnation Heat Flux	0.0308	0.0566	83.77%
Maximum Lift Force (N)	477.47	2166.74	353.80%
Maximum Drag Force (N)	477.47	2166.74	353.80%
Maximum Deceleration (g)	13.83	62.86	354.53%

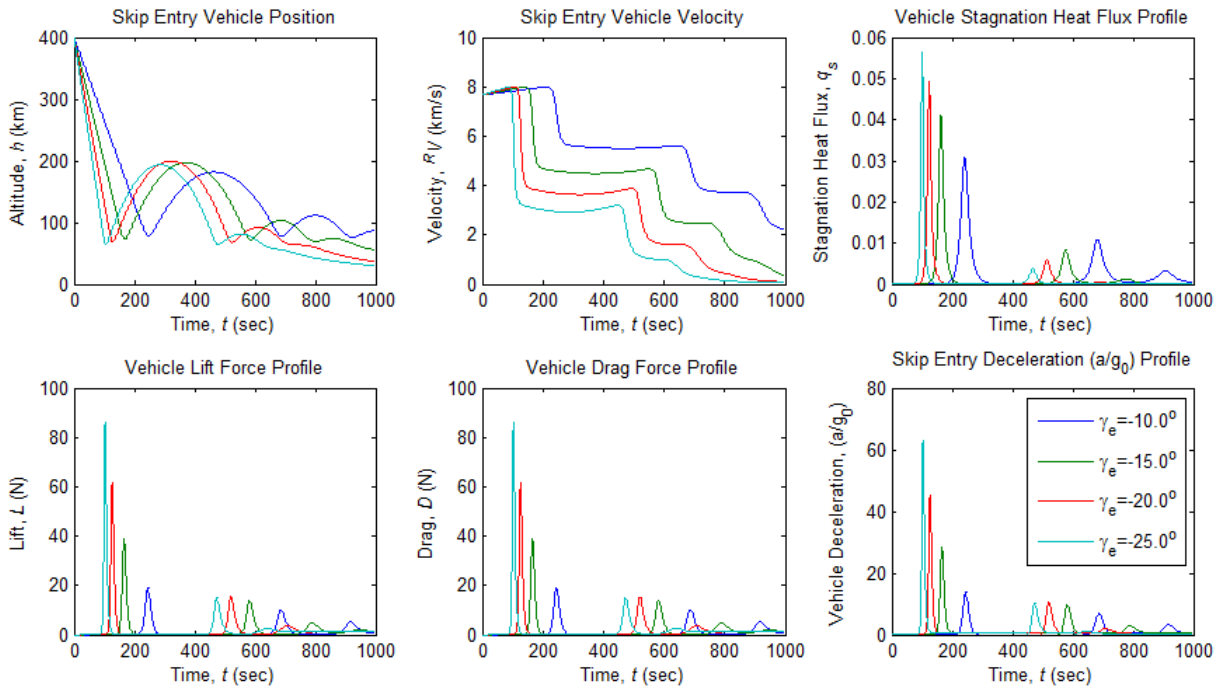

Figure 19. Variable Flight-Path Angle Simulation for Notional Satellite
(h = 400 km, L/D = 1.0)

Table 22. Comparison of Notional Satellite Skip Entry Dynamics Extrema for Variable Flight-Path Angle (h = 400 km, L/D = 1.0)

Parameter			**Percent Difference**
Minimum Altitude (km)	78.78	65.32	17.09%
Exit Velocity (km/s)	5.505	2.922	46.92%
Max. Stagnation Heat Flux	0.0307	0.0563	83.39%
Maximum Lift Force (N)	19.23	86.13	347.94%
Maximum Drag Force (N)	19.23	86.13	347.94%
Maximum Deceleration (g)	14.04	63.00	348.81%

As with Figures 10-11, Figures 14-15 also depict multiple sequential skip entry maneuvers during the arbitrary simulation period of 1000 sec. An artifact of the dynamics of the first skip entry maneuver for both entry vehicles, Figures 14-15 demonstrate the coupled effects of a lower orbital altitude and kinetic energy at skip exit compared with the initial entry condition in the absence of orbit-raising correction burns.

Overall, the aforementioned simulation cases demonstrate that changes in flight-path angle produce a greater impact on the dynamics of a skip entry trajectory than changes in coefficient of lift. While a lower minimum altitude is reached by increasing flight-path angle, the exit velocity also decreases accordingly, thus demanding greater expenditure in order to raise the orbit of the entry vehicle and re-circularize at the entry altitude. In addition, increases in flight-path angle also lead to greater increases in aerodynamic force and deceleration experienced by the entry vehicle when compared with the case of variable coefficient of lift. Although entry vehicle components and subsystems can be designed to withstand decelerations in excess of 50.00 g's, such an operating environment increases not only system design, testing, and manufacturing complexity, but also the risk of system performance degradation or mission failure. Since

the laser communication experiment requires operation below the ionosphere, changes in coefficient of lift are deemed more favorable than those of flight-path angle since the former produces the desired minimum entry altitude allowable for mission completion while reducing the aerodynamic force and deceleration experienced by the entry vehicle.

In addition to characterizing the effect of both variable coefficient of lift and flight-path angle on the trajectory and aerodynamics of a single skip entry maneuver, several simulations were run to identify the minimum altitude reached during skip entry for the X-37B and the notional satellite with a lift-to-drag ratio of 1.0, 1.5, and 2.0 and a flight-path angle defined within the range . As shown in Figure 16 and Table 23, the X-37B – when initiating the skip entry from an altitude of 120 km and a flight-path angle of -5 – reaches a minimum altitude of 54.59 km (179,111 ft) and 59.65 km (195,699 ft) for lift-to-drag ratios of 1.0 and 2.0. When the initial entry altitude is increased to 200 km the minimum skip entry altitude also increases accordingly for the same flight-path angle, with a lift-to-drag ratio of 1.0 producing an altitude of 54.94 km (180,246 ft), and a lift-to-drag ratio of 2.0 producing 59.98 km (196,775 ft).

Initiating the skip entry maneuver from an altitude of 120 km with a flight-path angle of -30 , the X-37B reaches a minimum altitude of 29.10 km (95,482 ft) and 34.05 km (111,719 ft) for a lift-to-drag ratio of 1.0 and 2.0, respectively. Similar to the shallow flight-path angle case of -5 , skip entry from an altitude of 200 km with a steeper flight-path angle of -30 also leads to an increase in the minimum altitude reached by the X-37B, with a lift-to-drag ratio of 1.0 producing an altitude of 29.11 km (95,512 ft), and a lift-to-drag ratio of 2.0 producing 34.06 km (111,749 ft).

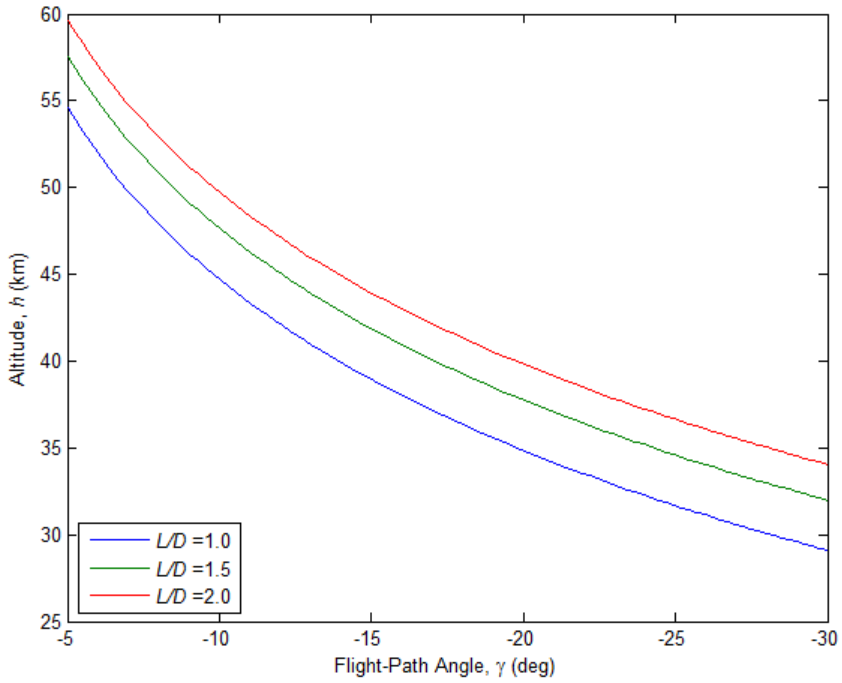

Figure 20. Minimum Altitude of Skip Entry for X-37B (h = 120 km)

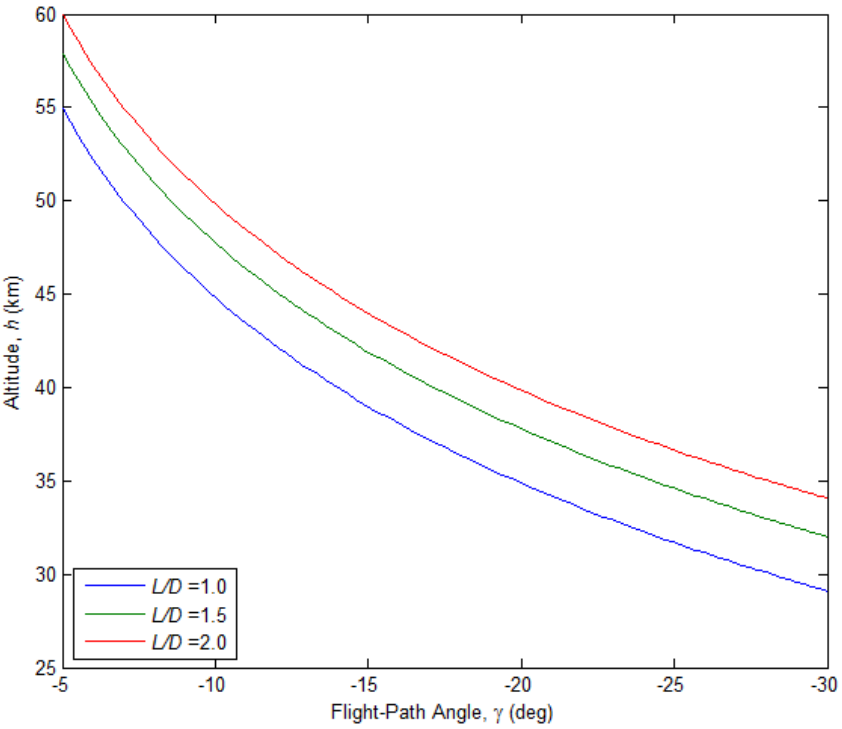

Figure 21. Minimum Altitude of Skip Entry for X-37B (h = 200 km)

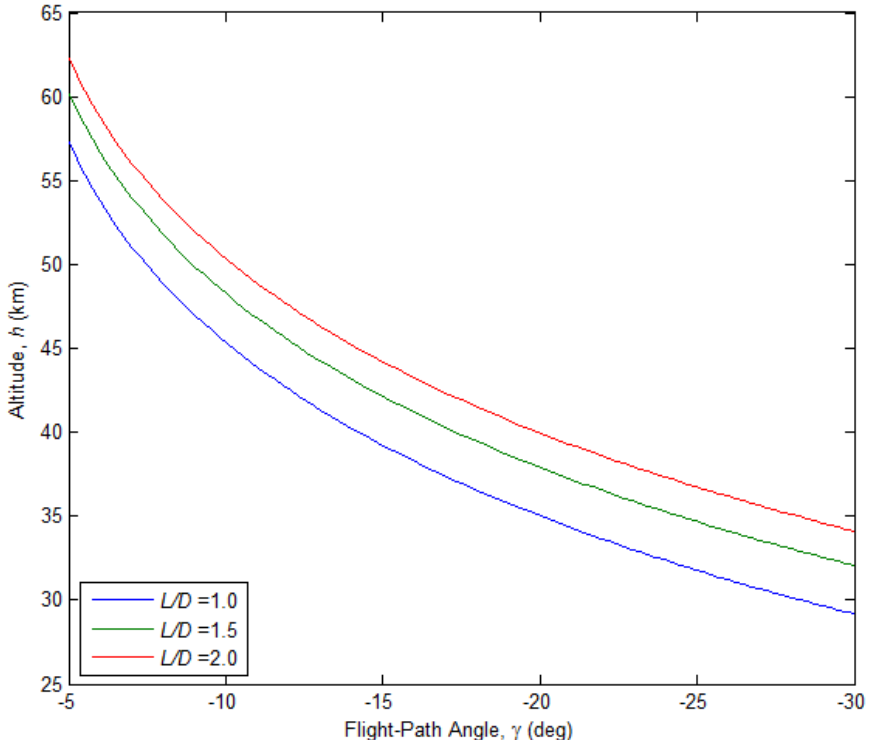

Figure 22. Minimum Altitude of Skip Entry for X-37B (h = 400 km)

Table 23. Minimum Altitude of Skip Entry Trajectory for X-37B with Varying Coefficient of Lift for Variable Flight-Path Angle Extrema

Entry Altitude	**Lift-to-Drag Ratio**		
120 km	1.0	54.59 km	29.10 km
	1.5	57.56 km	32.00 km
	2.0	59.65 km	34.05 km
200 km	1.0	54.94 km	29.11 km
	1.5	57.90 km	32.01 km
	2.0	59.98 km	34.06 km
400 km	1.0	57.25 km	29.16 km
	1.5	60.18 km	32.06 km
	2.0	62.24 km	34.11 km

With the case of , the X-37B reaches a lower minimum altitude for a lift-to-drag ratio of 1.0 than that of 1.5 and 2.0 for the entry altitudes of 120, 200, and 400 km because the vehicle experiences a greater force due to drag stemming from a comparatively lower coefficient of lift. Although a similar trend is seen the case of , the X-37B reaches minimum altitudes that are approximately 45% lower than the case since the steeper flight-path angle produces greater deceleration and drag as a result of the vehicle penetrating deeper into the atmosphere, which is assumed to maintain a density profile which exponentially increases as altitude decreases.

Similar to the X-37B, the notional satellite reaches a comparatively lower minimum altitude during skip entry when starting from an initial altitude of 120 km with a steep flight-path angle and a low lift-to-drag ratio, such as -30 and 1.0, respectively. Despite being evaluated within the same simulation cases of varying entry altitude, flight-path angle, and lift-to-drag ratio, Figures 19-21 and Table 24 illustrate differing values of minimum skip entry altitude for the notional satellite when compared with the X-37B due to a higher drag coefficient and lower vehicle mass with the former. Such differences in minimum altitude stem from the vehicle ballistic coefficient, a parameter defined as , where m is the vehicle mass, is the coefficient of drag, and S is the planform area (Larson and Wertz, 2003:145). With an initial mass of 4989.5 kg and a coefficient of drag of 0.5, the X-37B maintains a maximum ballistic coefficient of 535.641, while the notional satellite, with an initial mass of 200 kg and a coefficient of drag of 2.2, maintains a maximum ballistic coefficient of 4.880. As a result of a greater ballistic coefficient, the X-37B penetrates deeper into the atmosphere than the notional satellite, thus producing skip entry trajectories that reach comparatively lower minimum altitudes.

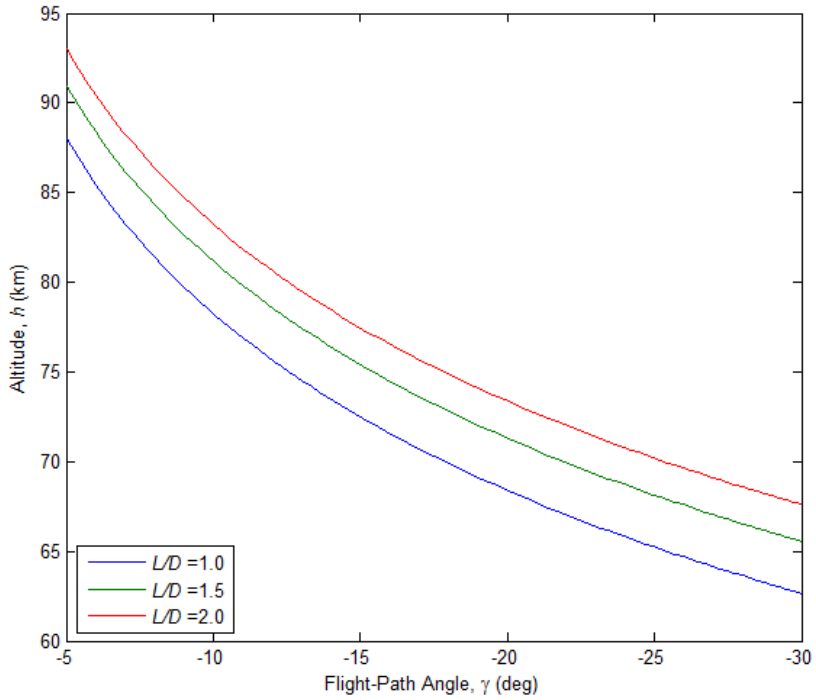

Figure 23. Minimum Altitude of Skip Entry for Notional Satellite (h = 120 km)

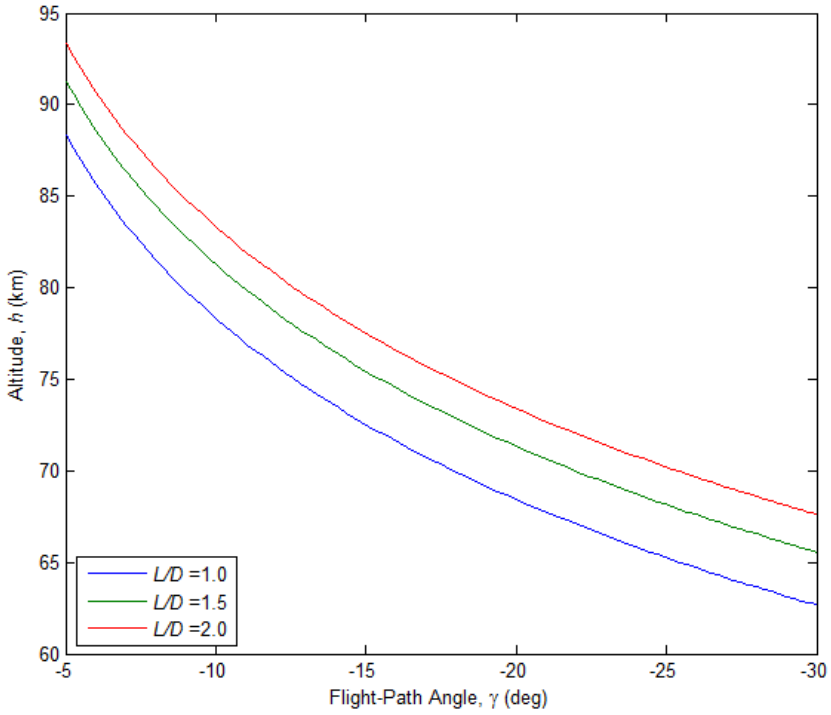

Figure 24. Minimum Altitude of Skip Entry for Notional Satellite (h = 200 km)

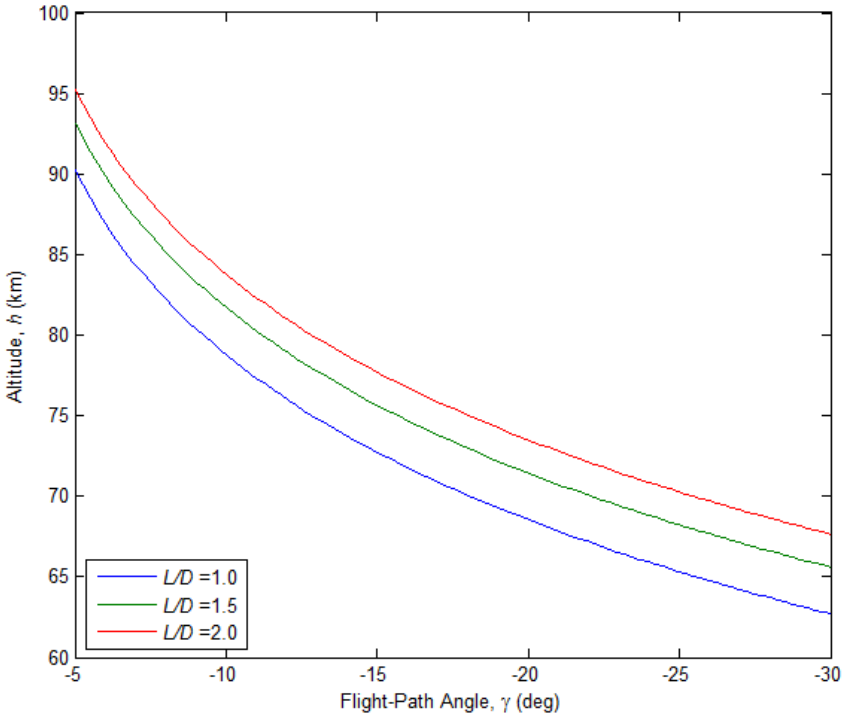

Figure 25. Minimum Altitude of Skip Entry for Notional Satellite (h = 400 km)

Table 24. Minimum Altitude of Skip Entry Trajectory for Notional Satellite with Varying Coefficient of Lift for Variable Flight-Path Angle Extrema

Entry Altitude	**Lift-to-Drag Ratio**		
120 km	1.0	88.02 km	62.66 km
	1.5	90.95 km	65.55 km
	2.0	93.00 km	67.61 km
200 km	1.0	88.32 km	62.67 km
	1.5	91.28 km	65.56 km
	2.0	93.36 km	67.62 km
400 km	1.0	90.22 km	62.71 km
	1.5	93.15 km	65.61 km
	2.0	95.21 km	67.66 km

Beyond minimum achievable trajectory altitude, a series of trajectory simulations were also run for the X-37B and the notional satellite in order to determine the required to commence not only a single skip entry maneuver from either an initial altitude of 120, 200, or 400 km, but also a subsequent skip entry maneuver from the same initial altitude. As shown in Figures 22-24 for the X-37B and Figures 25-27 for the notional satellite, the required to commence a single skip entry is dependent on vehicle flight-path angle and not lift-to-drag ratio since propellant is only expended to alter the entry vehicle angular orientation, specifically the flight-path angle. Alternatively, lift-to-drag ratio influences the required to commence subsequent skip entry maneuvers because altitude and velocity at the exit of a given trajectory is lower than at the entry condition and is directly influenced by entry vehicle aerodynamics. With this, propellant is expended to increase both the entry vehicle's exit altitude and velocity if a subsequent skip entry is desired to commence at the altitude and velocity of the initial maneuver.

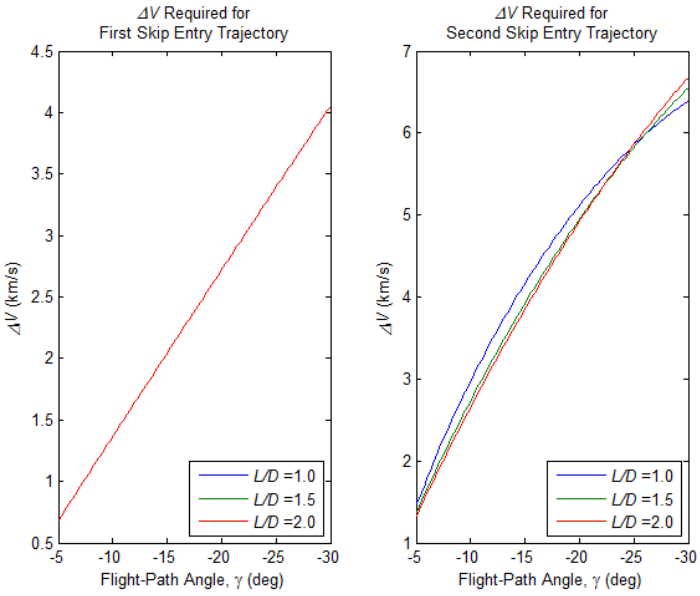

Figure 26. ΔV Required for Skip Entry Maneuver for X-37B (h = 120 km)

Illustrated in Figure 22 and Table 25, the X-37B with a lift-to-drag ratio of 1.0 requires a greater to commence a subsequent skip entry maneuver than the simulated lift-to-drag ratios of 1.5 and 2.0 over the flight-path angle ranges of

and , respectively. For flight-path angles greater in magnitude than -24.8 and -25.9 however, the lift-to-drag ratio cases of 1.5 and 2.0 require a greater despite penetrating to a shallower altitude than the lift-to-drag ratio case of 1.0. Since the figure should depict a continuance of the behavior illustrated between

and for the entire flight-path angle range, then it is surmised that the cross-over of the lift-to-drag ratio curves is due in part to the accuracy of the numerical integration scheme. For the lift-to-drag ratio case of 1.0, the required for a subsequent skip entry maneuver increases from 1.477 km/s to 6.389 km/s, a percentage rise of 332.57%, as the flight-path angle increases in magnitude from -5 to -30 at an entry altitude of 120 km. For the same flight-path angle range and entry altitude, the required increases by 377.33% from 1.372 km/s to 6.549 km/s for the lift-to-drag case of 1.5, and by 401.88% from 1.331 km/s to 6.680 km/s for the lift-to-drag case of 2.0. Results for the required to commence either one or two skip entry maneuvers from an altitude of 200 and 400 km are depicted in Figures 23-24 and Table 25 over

for the aforementioned lift-to-drag ratio cases.

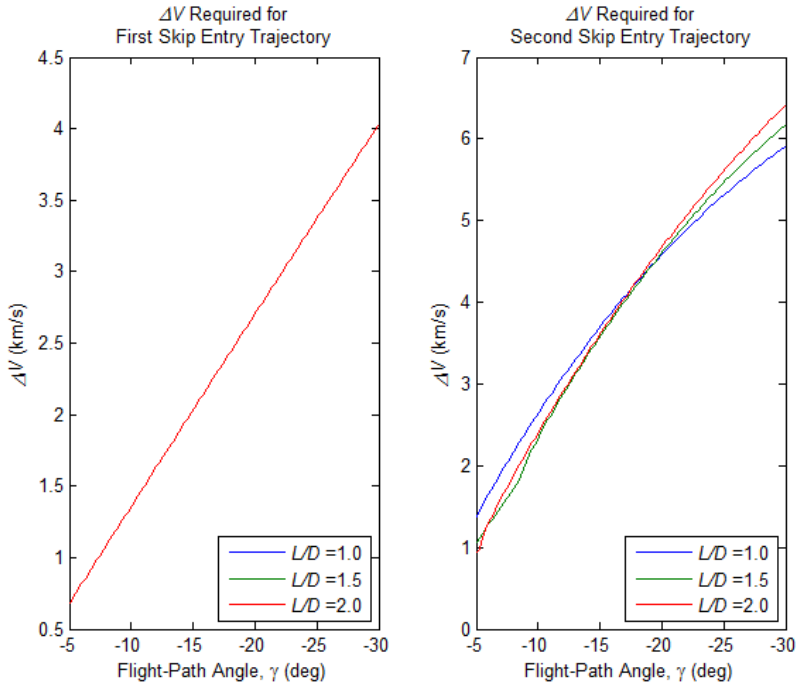

Figure 27. ΔV Required for Skip Entry Maneuver for X-37B (h = 200 km)

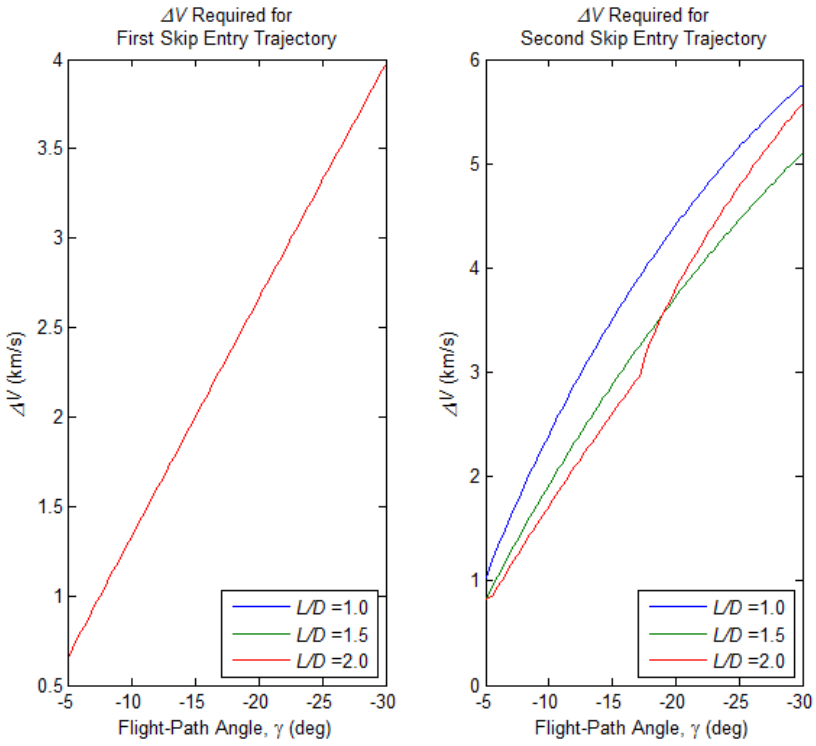

Figure 28. ΔV Required for Skip Entry Maneuver for X-37B (h = 400 km)

Table 25. ΔV Required for Second Skip Entry Maneuver for X-37B with Varying Flight-Path Angle and Entry Altitude

Entry Altitude	**Lift-to-Drag Ratio**				
120 km	1.0	1.477 km/s	2.985 km/s	5.142 km/s	6.389 km/s
	1.5	1.372 km/s	2.744 km/s	4.977 km/s	6.549 km/s
	2.0	1.331 km/s	2.665 km/s	4.950 km/s	6.680 km/s
200 km	1.0	1.372 km/s	2.651 km/s	4.608 km/s	5.908 km/s
	1.5	1.058 km/s	2.351 km/s	4.634 km/s	6.169 km/s
	2.0	0.934 km/s	2.415 km/s	4.704 km/s	6.415 km/s
400 km	1.0	1.038 km/s	2.416 km/s	4.435 km/s	5.761 km/s
	1.5	0.818 km/s	1.929 km/s	3.748 km/s	5.101 km/s
	2.0	0.829 km/s	1.729 km/s	3.828 km/s	5.576 km/s

In terms of the notional satellite, Figure 25 and Table 26 illustrate that a greater is required to commence a subsequent skip entry maneuver for a lift-to-drag ratio of 1.0 than the simulated lift-to-drag ratios of 1.5 and 2.0 over the flight-path angle ranges of and , respectively. Exhibiting similar parametric behavior as the X-37B, the notional satellite requires a greater for the lift-to-drag ratio cases of 1.5 and 2.0 for flight-path angles greater in magnitude than -27.6 and -29.2 . For the lift-to-drag ratio case of 1.0, the required for a subsequent skip entry maneuver increases from 1.709 km/s to 6.647 km/s, a percentage rise of 288.94%, as the flight-path angle increases in magnitude from -5 to -30 at an altitude of 120 km. For the same flight-path angle range and entry altitude, the required increases by 346.59% from 1.494 km/s to 6.672 km/s for the lift-to-drag case of 1.5, and by 376.96% from 1.419 km/s to 6.768 km/s for the lift-to-drag case of 2.0. Results for the required to commence either one or two skip entry maneuvers from altitudes of 200 and 400 km are depicted in Figures 26-27 and Table 26 over for the aforementioned lift-to-drag cases.

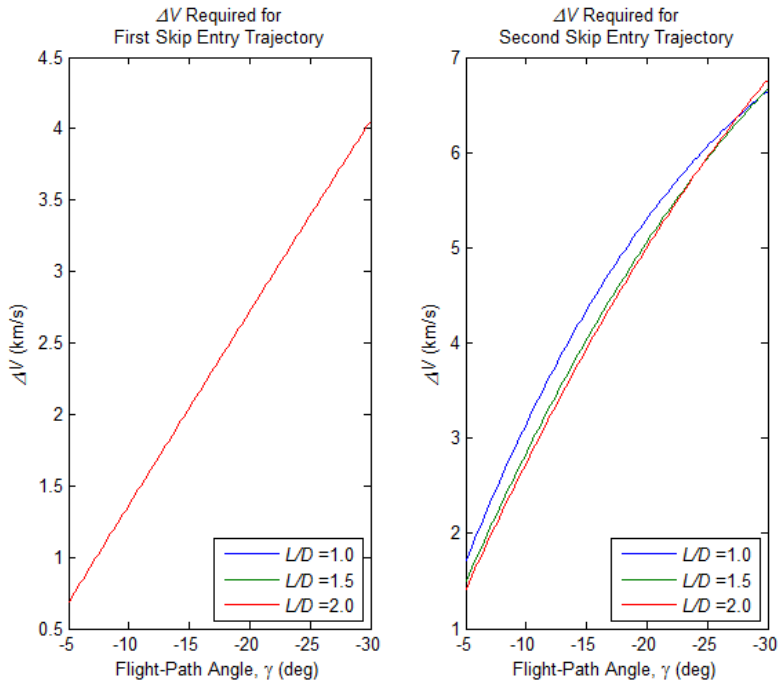

Figure 29. ΔV Required for Skip Entry Maneuver for Notional Satellite (h = 120 km)

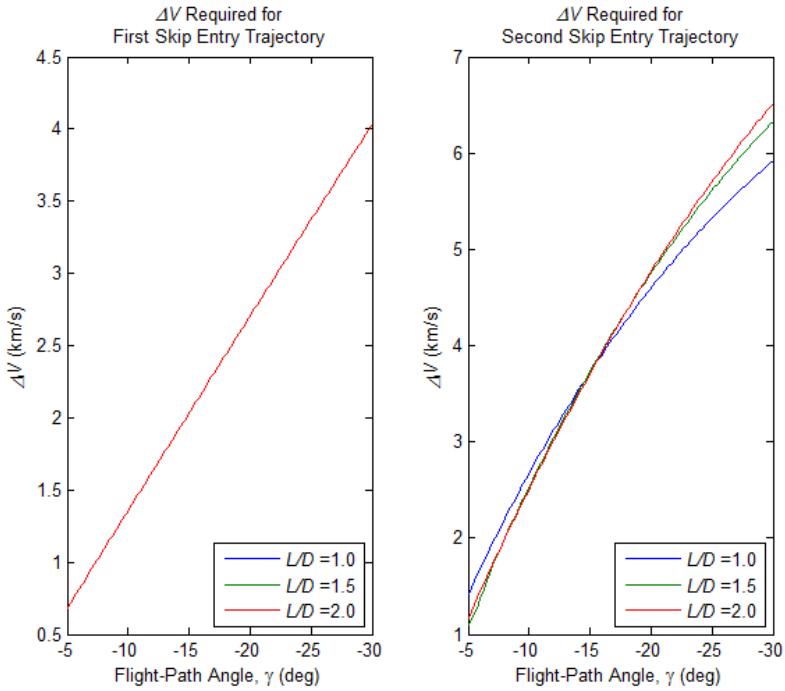

Figure 30. ΔV Required for Skip Entry Maneuver for Notional Satellite (h = 200 km)

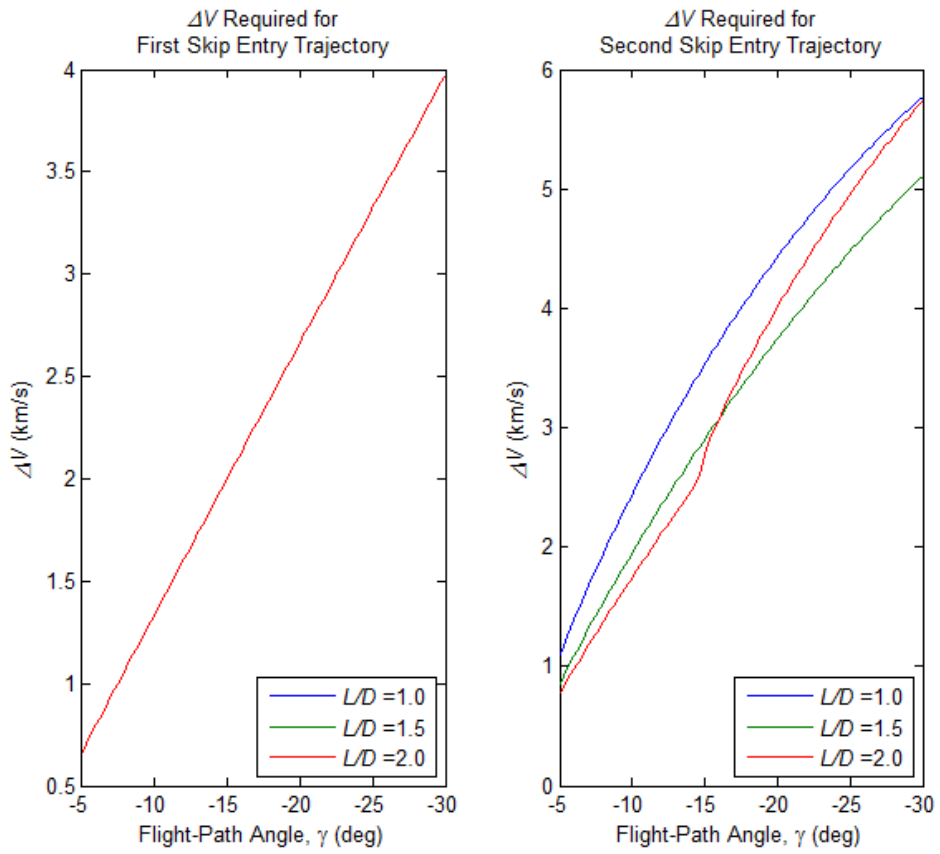

Figure 31. ΔV Required for Skip Entry Maneuver for Notional Satellite (h = 400 km)

Table 26. ΔV Required for Second Skip Entry Maneuver for Notional Satellite with Varying Flight-Path Angle and Entry Altitude

Entry Altitude	**Lift-to-Drag Ratio**				
120 km	1.0	1.709 km/s	3.162 km/s	5.330 km/s	6.647 km/s
	1.5	1.494 km/s	2.855 km/s	5.089 km/s	6.672 km/s
	2.0	1.419 km/s	2.748 km/s	5.033 km/s	6.768 km/s
200 km	1.0	1.415 km/s	2.681 km/s	4.625 km/s	5.917 km/s
	1.5	1.093 km/s	2.545 km/s	4.778 km/s	6.326 km/s
	2.0	1.164 km/s	2.523 km/s	4.800 km/s	6.514 km/s
400 km	1.0	1.101 km/s	2.453 km/s	4.455 km/s	5.772 km/s
	1.5	0.859 km/s	1.959 km/s	3.767 km/s	5.112 km/s
	2.0	0.781 km/s	1.755 km/s	4.038 km/s	5.743 km/s

Leading to a deeper penetration of the atmosphere during skip entry, the maneuver case with a lift-to-drag ratio of 1.0 is expected to require a greater to alter exit altitude and velocity in order to initiate a subsequent maneuver. The preceding parametric analysis illustrate otherwise however, with Figures 25 and 27-28 exhibiting the same lift-to-drag ratio curve cross-over behavior as initially seen in Figure 24, and Figures 26 and 29 depicting the curve corresponding to a lift-to-drag ratio of 2.0 abruptly increasing slope at a flight-path angle greater in magnitude than -15 and crossing-over the 1.0 and 1.5 lift-to-drag ratio curves. Implicit to the trajectory simulation, the occurrence of a greater required for the lift-to-drag ratio cases of 1.5 and 2.0 as the flight-path increases in magnitude is either a product – as mentioned previously – of the accuracy of the numerical integration scheme, the flight-path angle at the exit condition of the skip entry maneuver, or a combination thereof.

Theoretically, the entry and exit flight path angles are equal in magnitude and, as a result, the value of – when considered within the context of the equation for the required to initiate a subsequent skip entry maneuver – is equal to twice the magnitude of either the entry or exit flight-path angle. Given previously as Equation 14, the aforementioned equation for is provided below as a recapitulation:

(42)

From the skip entry parametric analysis however, the exit flight-path angle was shown to be smaller in magnitude than the entry flight-path angle, thus producing a smaller value

for . As an example, the following figure depicts the flight-path angle time history of the X-37B with , , and :

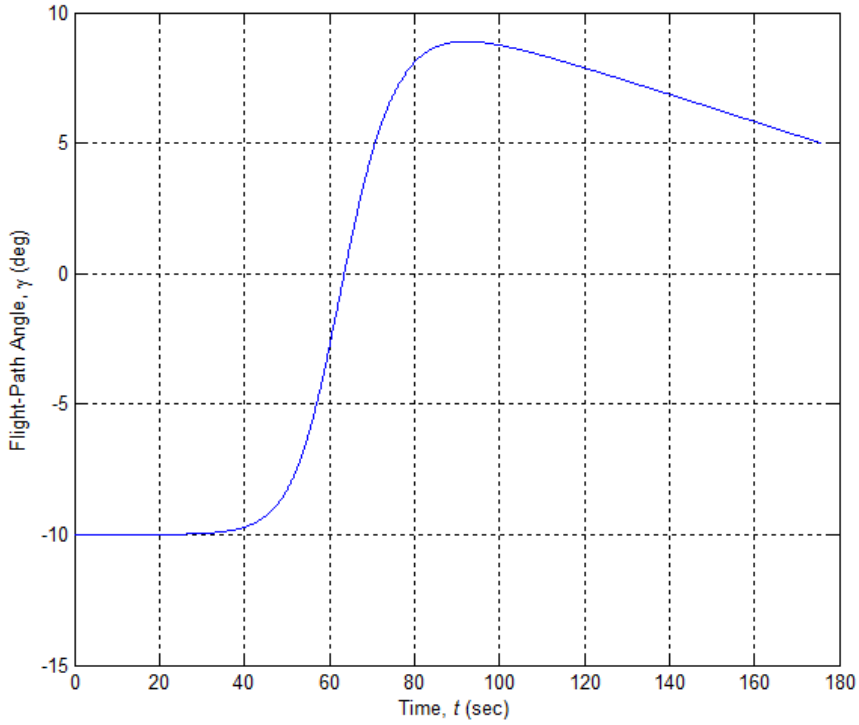

Figure 32. Flight-Path Angle Time History for X-37B
(h = 200 km, γ = -10°, L/D = 1.0)

It can be seen from the figure above that since the exit flight-path angle is equal to and the entry-flight path angle is -10 . In addition to the preceding example, a further series of parametric studies were conducted in order to quantify the difference between exit and entry flight-path angles, or , over for the lift-to-drag cases of 1.0, 1.5, and 2.0. Figures 29-30 graphically depict versus entry flight-path angle for the X-37B and notional satellite, respectively, for an entry altitude of 120 km, while Tables 27-28 outline values of for the X-37B and notional satellite for entry altitudes of 120, 200, and 400 km.

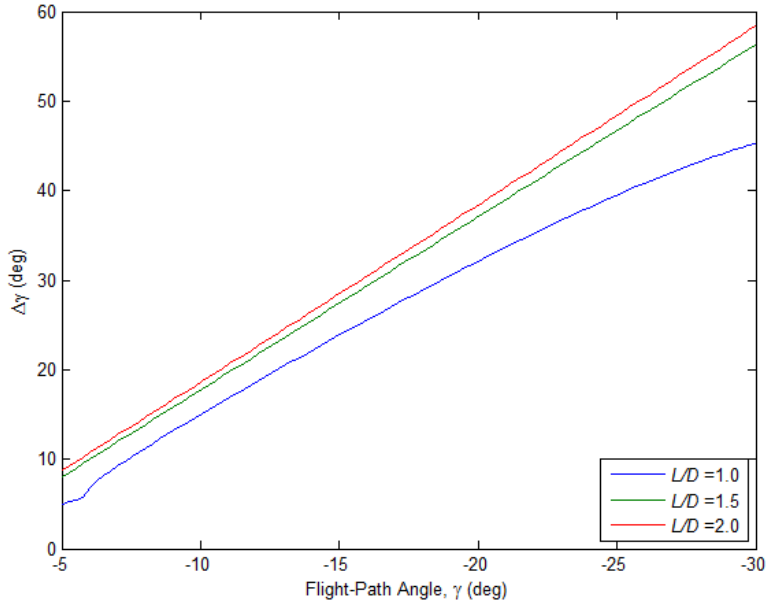

Figure 33. Difference between Exit and Entry Flight-Path Angle for a Single Skip Entry Maneuver for X-37B (h = 120 km)

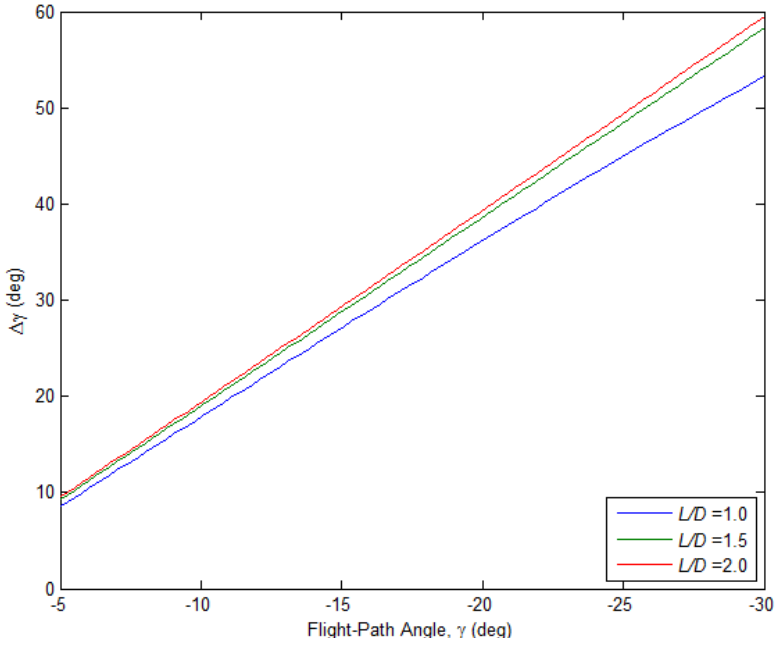

Figure 34. Difference between Exit and Entry Flight-Path Angle for a Single Skip Entry Maneuver for Notional Satellite (h = 120 km)

Table 27. Difference between Exit and Entry Flight-Path Angle ($\Delta\gamma$)
for a Single Skip Entry Maneuver for X-37B

Entry Altitude	**Lift-to-Drag Ratio**				
120 km	1.0	4.995	15.09	32.36	45.28
	1.5	8.803	17.84	37.39	56.28
	2.0	8.758	18.69	38.72	58.39
200 km	1.0	4.995	10.04	20.14	29.97
	1.5	4.997	13.29	32.85	50.28
	2.0	4.998	16.35	36.24	55.49
400 km	1.0	4.997	10.04	20.13	29.96
	1.5	4.999	10.05	20.14	29.98
	2.0	5.701	10.05	26.01	44.52

Table 28. Difference between Exit and Entry Flight-Path Angle ($\Delta\gamma$)
for a Single Skip Entry Maneuver for Notional Satellite

Entry Altitude	**Lift-to-Drag Ratio**				
120 km	1.0	8.564	17.96	36.48	53.21
	1.5	9.290	19.10	38.92	58.27
	2.0	9.554	19.50	39.65	59.47
200 km	1.0	4.996	10.04	20.13	29.96
	1.5	4.997	15.70	34.99	53.13
	2.0	7.284	17.44	37.35	56.79
400 km	1.0	4.997	10.04	20.13	29.97
	1.5	4.998	10.04	20.14	29.97
	2.0	5.027	10.05	28.80	47.13

In Figures 31-33 for the X-37B and Figures 34-36 for the notional satellite, the required to commence a first and second skip entry trajectory was shown for varying initial entry altitudes, flight-path angles, and entry vehicle lift-to-drag ratios. For a more complete depiction of , the following figures illustrate the total required to

commence two sequential skip entry maneuvers as well as the maximum flight-path angle capable for the trajectories constrained by the maximum capability of 3 km/s for the X-37B and notional satellite example entry vehicles.

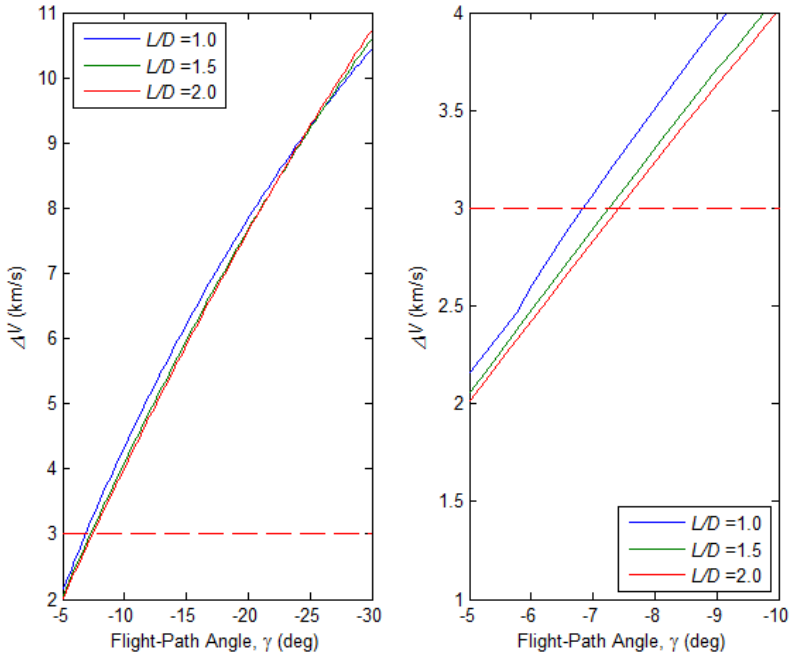

Figure 35. ΔV Required for Initiation of Two Skip Entry Maneuvers for X-37B (h = 120 km)

From Figure 31, it is shown that the required to complete two sequential skip entry maneuvers significantly increases as the magnitude of entry flight-path angle increases from -5 to -30 for the lift-to-drag ratio cases of 1.0, 1.5, and 2.0. When viewed from the perspective of maximum available, the X-37B is capable of commencing two maneuvers, each at an entry flight-path angle of -6.84 for a lift-to-drag ratio of 1.0. As the lift-to-drag ratio increases to 1.5 and 2.0, the entry flight-path angle also increases in magnitude to a value of -7.26 and -7.42 , respectively.

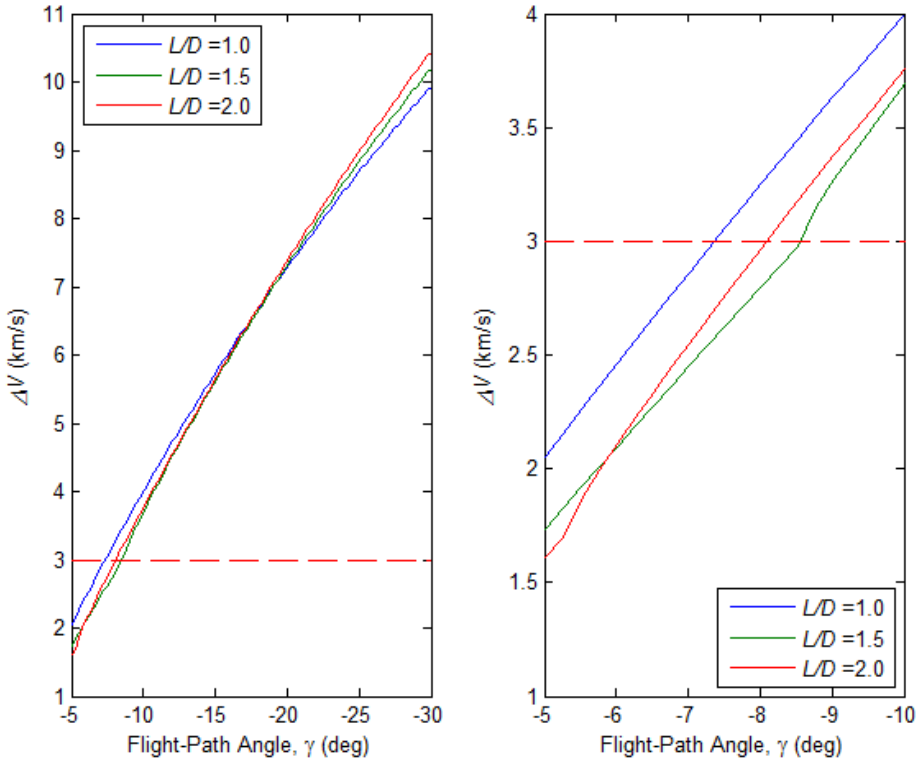

Figure 36. ΔV Required for Initiation of Two Skip Entry Maneuvers for X-37B (h = 200 km)

As the entry altitude increases from 120 km to 200 km, the maximum entry flight-path angle for a given lift-to-drag ratio also increases in relation to the maximum available for the X-37B. In the figure above, two skip entry maneuvers can commence at an entry flight-path angle of -7.38 for a lift-to-drag ratio of 1.0 and -8.10 for a lift-to-drag ratio of 2.0. Similarly, the maximum entry flight-path angle also increases as entry altitude increases from 200 km to 400 km, with a maximum permitting the X-37B to commence two maneuvers at -8.08 for a lift-to-drag ratio of 1.0 and -9.82 for a lift-to-drag ratio of 2.0.

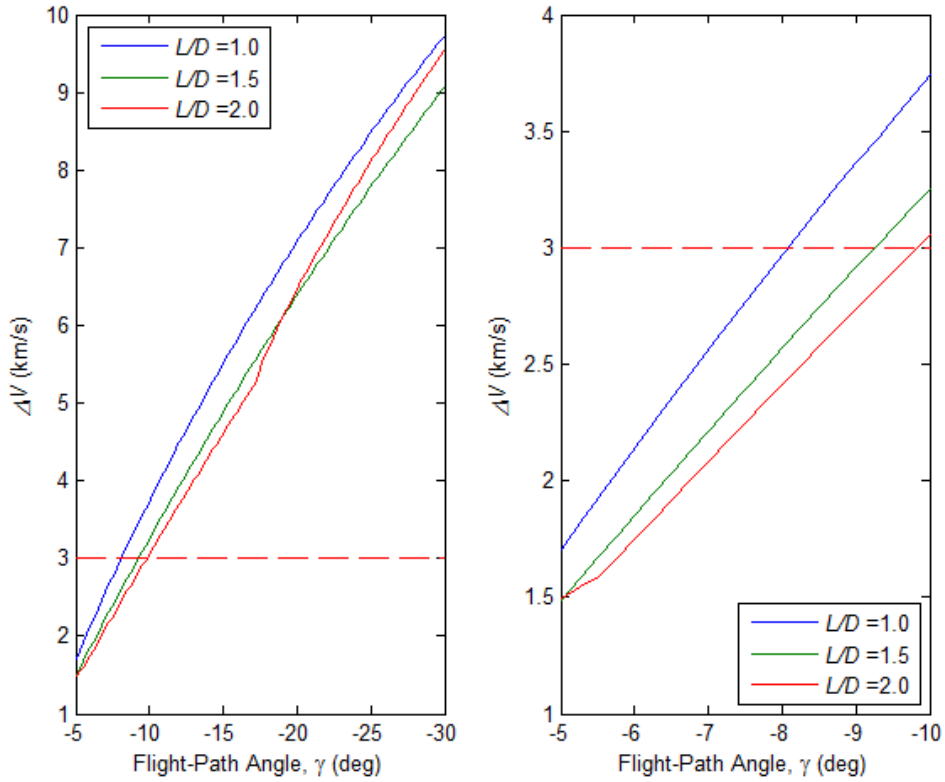

Figure 37. ΔV Required for Initiation of Two Skip Entry Maneuvers for X-37B (h = 400 km)

As with the X-37B, the maximum entry flight-path angle for two skip entry maneuvers permitted by the maximum capability of the notional satellite was also calculated for the preceding lift-to-drag ratios of 1.0, 1.5, and 2.0 and is outlined in the following table. In addition, Figures 34-36 demonstrate not only the total required to commence two sequential skip entry maneuvers for varying lift-to-drag ratios, but also the maximum capability constraint of 3 km/s for the notional satellite..

Table 29. Maximum Flight-Path Angle Permitted for Two Skip Entry Maneuvers for Notional Satellite

Entry Altitude	Lift-to-Drag Ratio	Entry Flight-Path Angle
120 km	1.0	-6.37
	1.5	-6.98
	2.0	-7.21
200 km	1.0	-7.27
	1.5	-7.80
	2.0	-7.81
400 km	1.0	-4.997
	1.5	-4.999
	2.0	-5.701

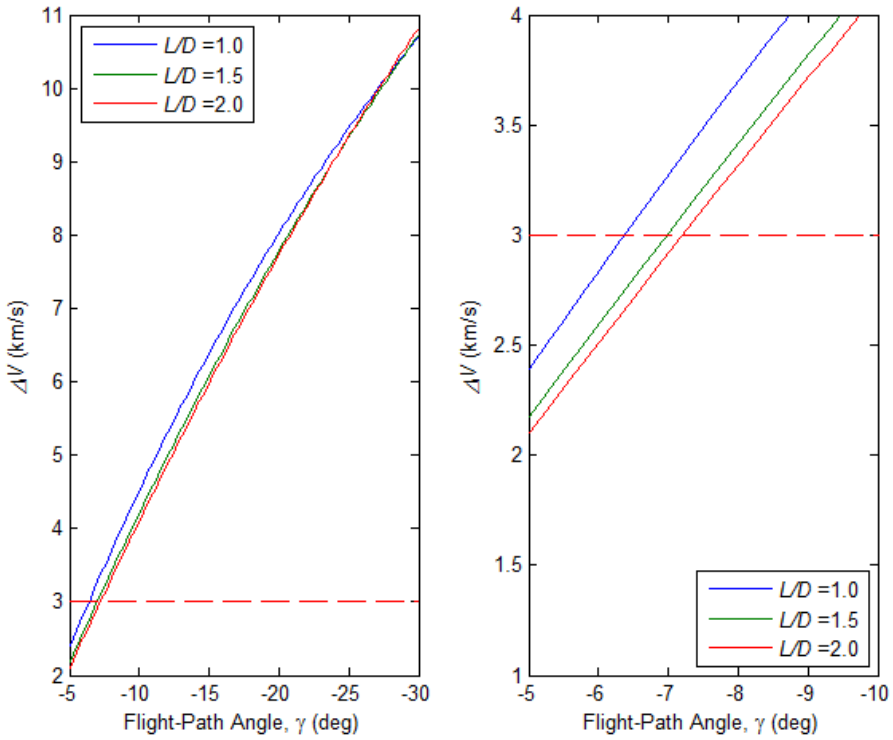

Figure 38. ΔV Required for Initiation of Two Skip Entry Maneuvers for Notional Satellite (h = 120 km)

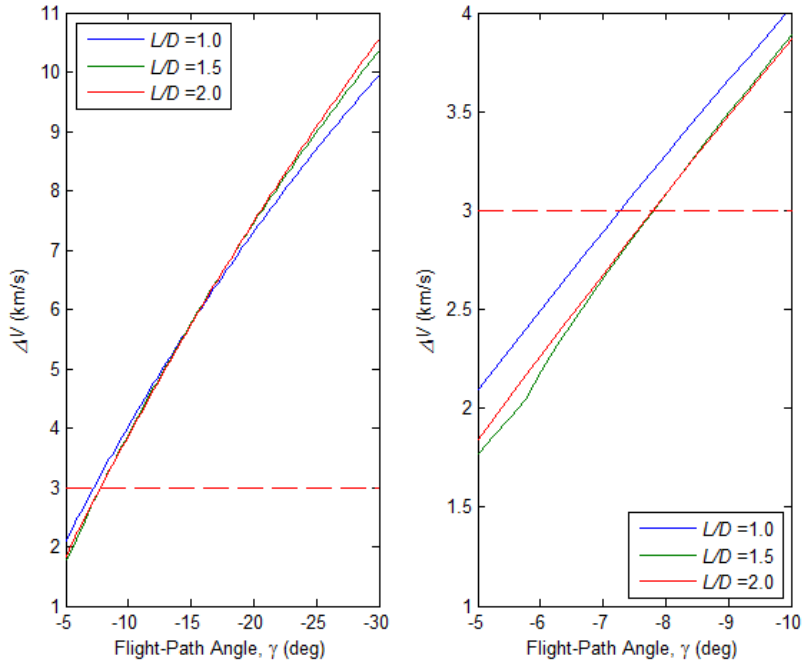

Figure 39. ΔV Required for Initiation of Two Skip Entry Maneuvers for Notional Satellite (h = 200 km)

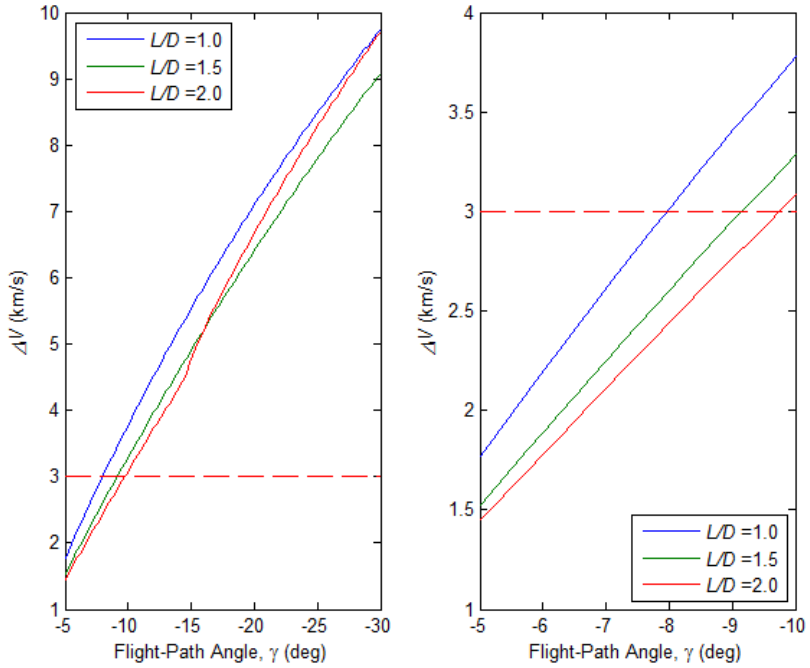

Figure 40. ΔV Required for Initiation of Two Skip Entry Maneuvers for Notional Satellite (h = 400 km)

Results of Vacuum-Only Maneuver Simulations

For all vacuum-only maneuvers simulated and analyzed, the initial orbits were chosen based on the allowable minimum and maximum azimuth values for the two primary launch sites within the United States: Cape Canaveral (Patrick AFB), FL and Vandenberg AFB, CA. Labeled in Figure 24 as the ETR, or Eastern Test Range, Cape Canaveral has an azimuth range of while Vandenberg AFB, labeled WTR, or Western Test Range, has a range of (Brown, 1998:56).

Figure 41. Azimuth Restrictions for Primary US-Based Launch Sites

With these azimuth limits as well as launch site latitude , the available range of initial orbit inclinations was calculated for Cape Canaveral and Vandenberg AFB via the following trigonometric expression and graphically depicted in Figure 38.

(43)

Where:

= Launch site latitude
= Launch azimuth angle

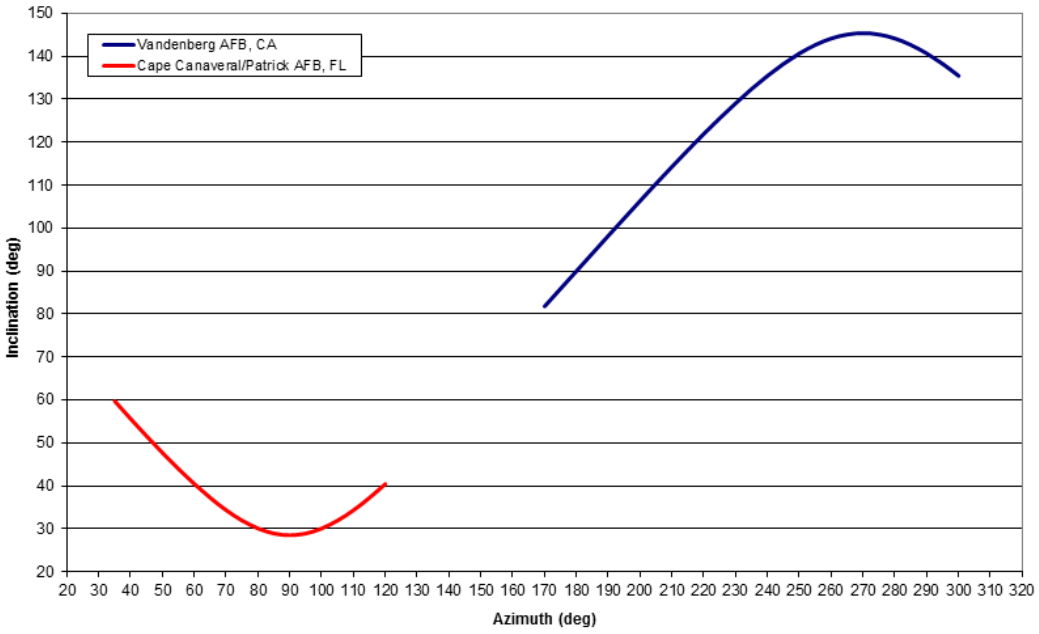

Figure 42. Allowable Orbit Insertion Inclinations from
Primary U.S.-Based Launch Sites

From the preceding figure, initial orbit inclinations of 28.5 and 90 were chosen for launches from Cape Canaveral and Vandenberg AFB, respectively, with the former inclination representing a prograde orbit launched from an azimuth angle of 90 , and the latter a polar orbit launched from an azimuth angle of 180 .

In accordance with the assumption of two-body dynamics, orbital perturbations are considered negligible and, as a result, a distinction is not made between the X-37B or the notional satellite for the analysis of vacuum-only maneuver performance since such analysis is independent of not only vehicle geometry and mass, but also the vehicle itself. With this, vacuum-only maneuver performance becomes purely a function of the spacecraft COEs. For the first vacuum-only maneuver, the required to complete a simple plane change from initial orbit inclinations of 28.5 and 90 was calculated for

orbit altitudes of 200, 300, 400, 500, 750, and 1000 km. As outlined in Table 30 and shown in Figures 39-40, the required to complete a simple plane change increases when not only altitude decreases, which produces an increase in orbital velocity, but also as the desired change in orbit inclination increases. Completing the maneuver from an initial orbit inclination of 28.5 , the spacecraft – at an altitude of 200 km – must produce a of 3.8322 km/s to achieve a prograde equatorial orbit with an inclination of 0 and 15.089 km/s for a retrograde equatorial orbit with an inclination of 180 .

As the altitude increases the required for the simple plane change maneuver decreases, with the spacecraft – at an altitude of 1000 km – producing a of 3.6185 km/s to achieve an inclination of 0 and 14.248 km/s for an inclination of 180 . Similarly, the required decreases as altitude increases for an initial polar inclination of 90 , with a of 11.009 km/s required to achieve an inclination of either 0 or 180 from an altitude of 200 km , and a of 10.395 km/s from an altitude of 1000 km.

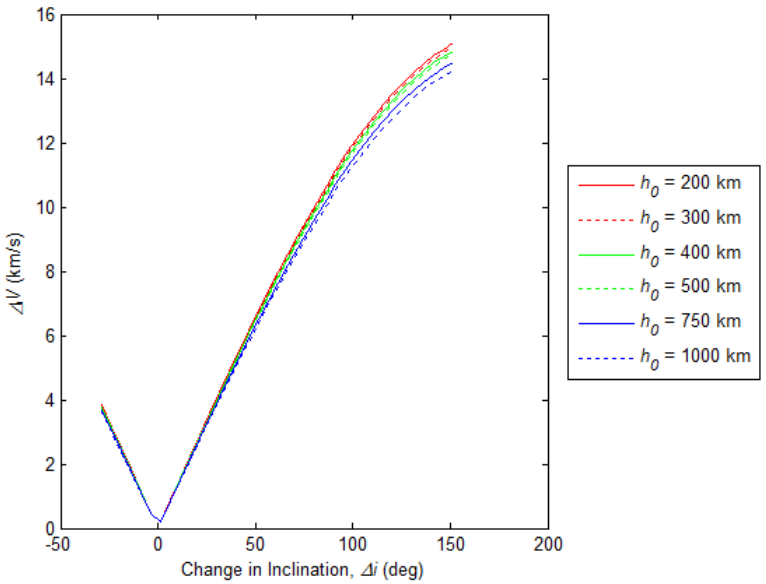

Figure 43. ΔV Required for Simple Plane Change (i = 28.5°)

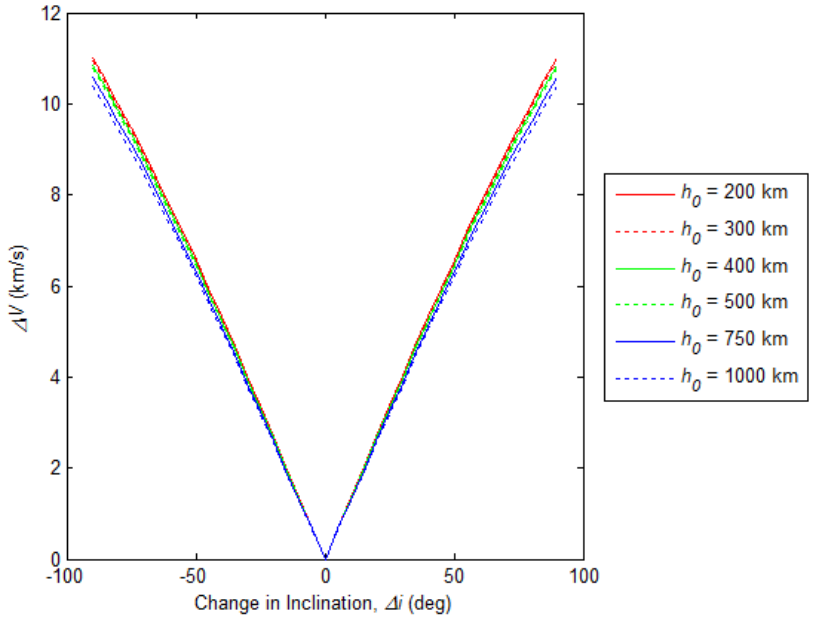

Figure 44. ΔV Required for Simple Plane Change (i = 90°)

Table 30. ΔV Required for Simple Plane Change with Varying Initial Altitude

Altitude			
200 km	3.8322 km/s	15.089 km/s	11.009 km/s
300 km	3.8034 km/s	14.976 km/s	10.926 km/s
400 km	3.7753 km/s	14.865 km/s	10.845 km/s
500 km	3.7477 km/s	14.757 km/s	10.766 km/s
750 km	3.6814 km/s	14.496 km/s	10.575 km/s
1000 km	3.6185 km/s	14.248 km/s	10.395 km/s

Inducing a change to both orbit inclination and RAAN, the second vacuum-only maneuver requires a greater than the preceding maneuver which altered only the spacecraft's inclination. Shown below in Figures 41-42 and Table 31, the required to complete the second vacuum-only maneuver increases as the desired change in both inclination and RAAN also increase. From an altitude of 400 km and , the

required increases from 0.6378 km/s to 14.865 km/s as the change in inclination angle increases from 0 to 151.5 for a change in RAAN of 10 . As the change in RAAN increases from 10 to 150 at the preceding values of altitude and initial inclination, the increases from 7.0689 km/s to 14.865 km/s for .

Following a similar trend as the foregoing case, the required increases from 1.3367 km/s to 10.845 km/s at an altitude of 400 km and an initial inclination of 90 as increases from 0 to 90 for . At a change in RAAN of 90 however, the required a maneuver from an altitude of 400 km and an initial inclination of 90 is 10.845 km/s, a value that is equal for both and . As the change in RAAN increases beyond 90 to 150 , the required increases to 14.815 km/s for while it remains at 10.845 km/s for .

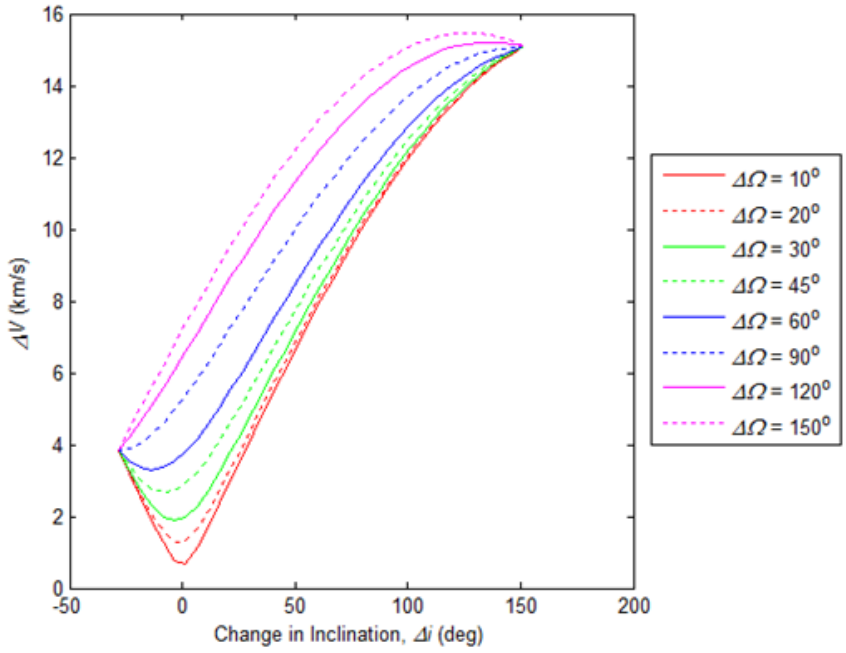

Figure 45. ΔV Required for Combined Change to Inclination and RAAN (i = 28.5°, h = 400 km)

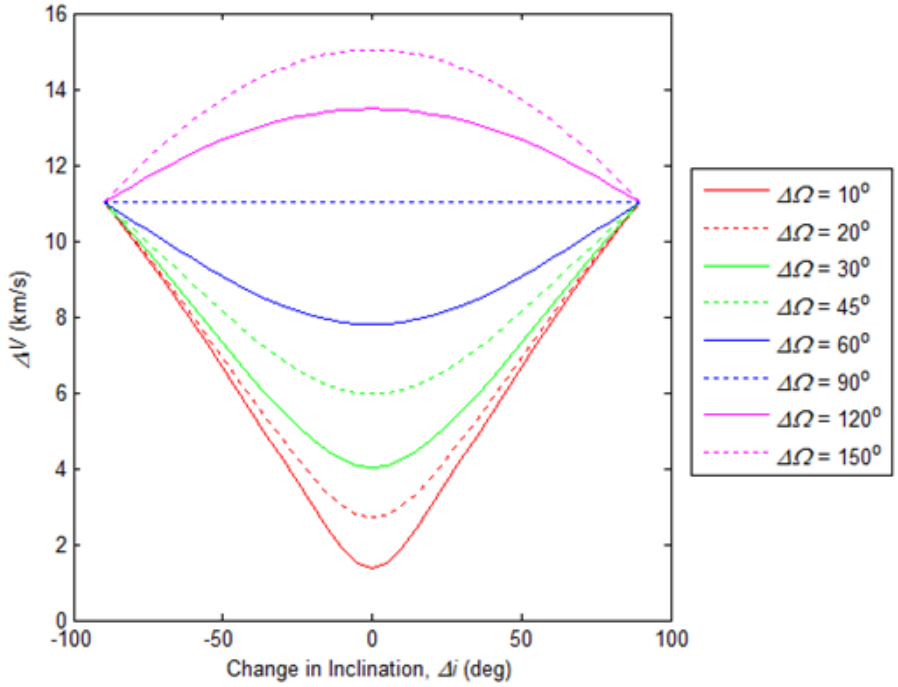

Figure 46. ΔV Required for Combined Change to Inclination and RAAN
(i = 90°, h = 400 km)

Table 31. ΔV Required for Combined Change to Inclination and RAAN for h = 400 km

	0.6378 km/s	3.7753 km/s	13.709 km/s	14.865 km/s	1.3367 km/s	10.845 km/s
	1.2708 km/s	3.7753 km/s	13.748 km/s	14.865 km/s	2.6633 km/s	10.845 km/s
	1.8941 km/s	3.7753 km/s	13.811 km/s	14.865 km/s	3.9696 km/s	10.845 km/s
	2.8006 km/s	3.7753 km/s	13.947 km/s	14.865 km/s	5.8693 km/s	10.845 km/s
	3.6591 km/s	3.7753 km/s	14.122 km/s	14.865 km/s	7.6686 km/s	10.845 km/s
	5.1747 km/s	3.7753 km/s	14.536 km/s	14.865 km/s	10.845 km/s	10.845 km/s
	6.3378 km/s	3.7753 km/s	14.938 km/s	14.865 km/s	13.282 km/s	10.845 km/s
	7.0689 km/s	3.7753 km/s	15.226 km/s	14.865 km/s	14.815 km/s	10.845 km/s

Although not shown in the preceding analysis, the required for the second vacuum-only maneuver decreases as the spacecraft altitude increases since , the angle required to complete a specified change in orbit inclination and RAAN as defined in Equation 21, varies proportionally with orbit velocity in Equation 20.

For the third vacuum-only maneuver, coplanar phasing rendezvous, the required increases as altitude decreases from 1000 km to 200 km and as the phasing angle between the interceptor and target vehicles increases from 0 to 180 . Phasing angles within the range were not analyzed however because if the interceptor trails the target by an angle greater than 180 , then the angular separation can be interpreted as a situation in which the interceptor leads the target by an angle less than 180 , and vice versa. Illustrated in Figure 43, the required increases at a steep rate until a phasing angle of approximately 50 , after which the required continues to increase but asymptotically and at a slower rate. From an initial altitude of 200 km, the required increases from 5.1492 km/s to 6.4091 km/s at phase angles of 1 and 180 , respectively, while at an altitude of 1000 km, the required increases from 4.8621 km/s to 6.0517 km/s for the same phase angles. Unlike the other vacuum-only maneuvers analyzed, the case of coplanar phasing rendezvous was only evaluated at different values of altitude and not initial orbit inclination since such maneuvers are formulated with the interceptor and target orbiting at the same inclination.

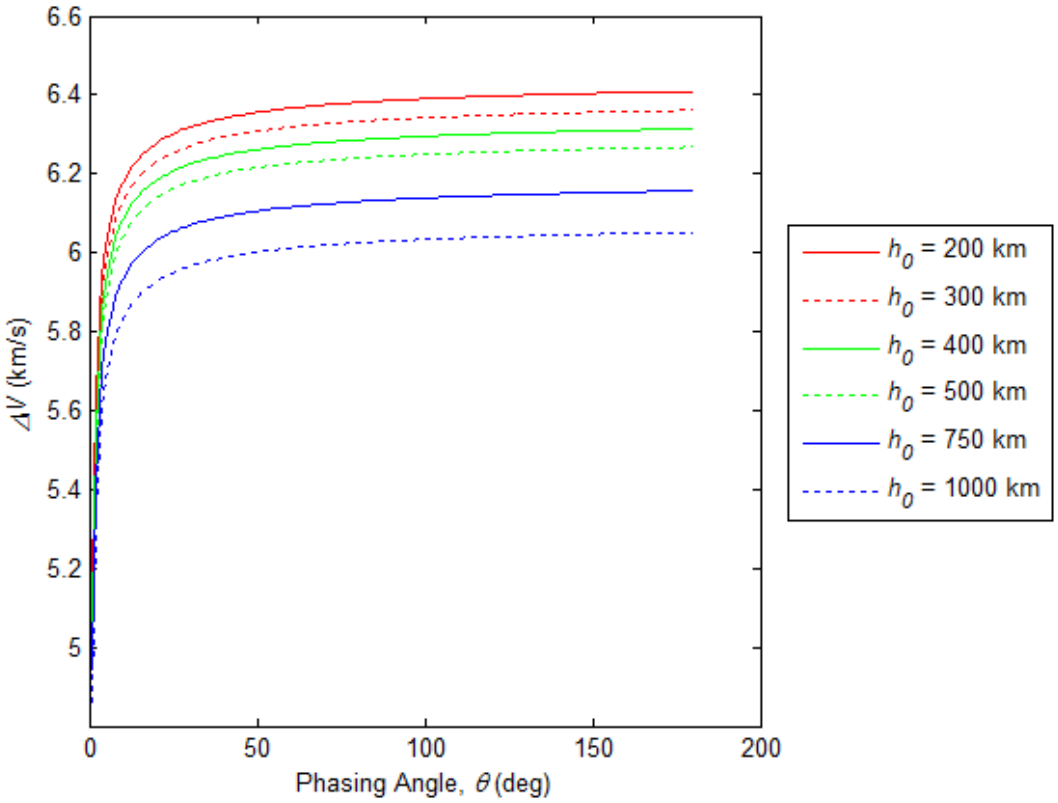

Figure 47. ΔV Required for Coplanar Phasing Rendezvous (i = 28.5°)

The final vacuum-only maneuver, non-coplanar phasing rendezvous, produced the greatest values for required because the interceptor and target do not reside within the same orbital plane. Based on the assumption that the rendezvous was completed at an altitude of 400 km between an interceptor and target at a circular inclined and a circular equatorial orbit, respectively, the required for the non-coplanar rendezvous was first calculated for an interceptor at an initial orbit inclination of with varying values for argument of latitude from 5 to 60 . As depicted in Figure 44, the required increased from 15.473 km/s for to 30.338 km/s for at , and from 38.454 km/s for to 53.320 km/s for at . For the

second case, the required was calculated over the same varying values of argument of latitude for the interceptor, but from an initial orbit inclination of 90 . Shown in Figure 45, the required increased from 12.771 km/s for to 23.616 km/s for at , and from 20.835 km/s for to 31.681 km/s for at .

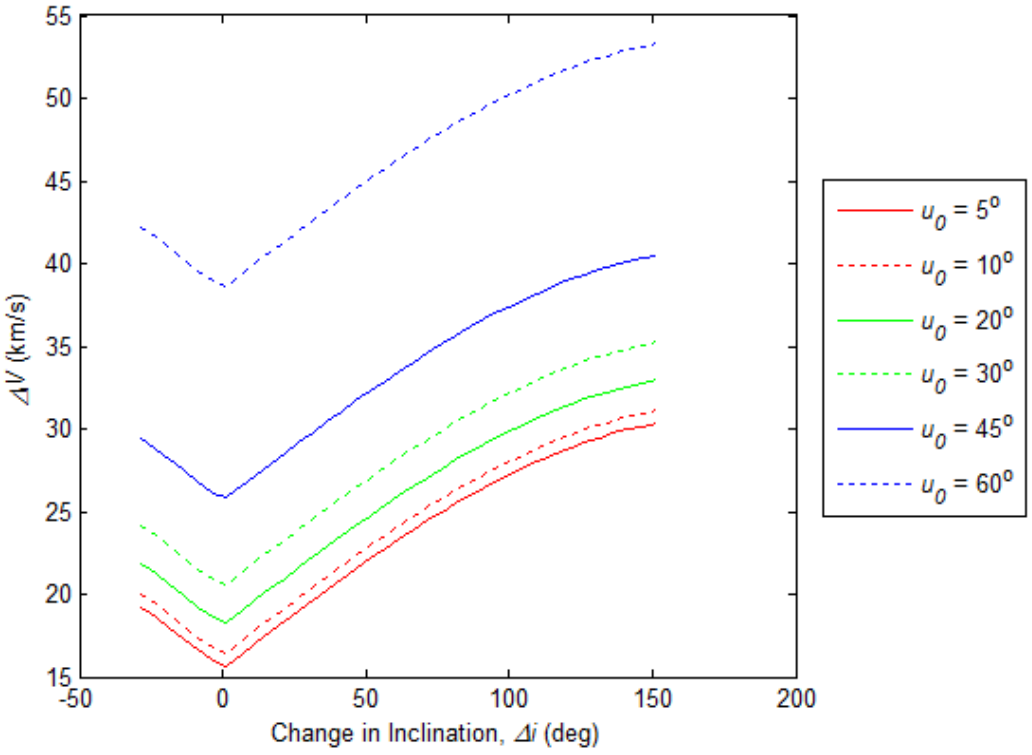

Figure 48. ΔV Required for Non-Coplanar Phasing Rendezvous (i = 28.5°)

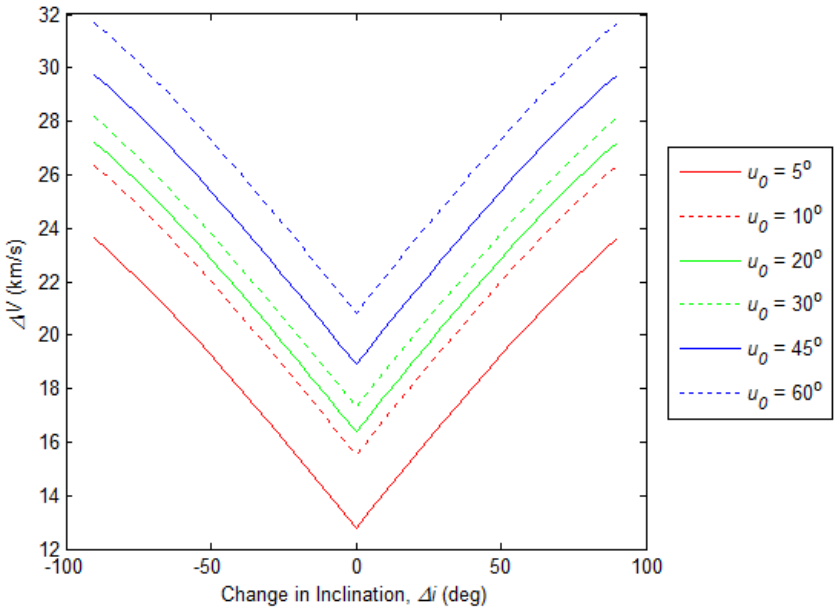

Figure 49. ΔV Required for Non-Coplanar Phasing Rendezvous (i = 90°)

When compared with the maximum capability of 3 km/s, the preceding analysis illustrates the inability of the X-37B and the notional satellite to perform coplanar and non-coplanar phasing rendezvous maneuvers within the LEO altitude regime. In terms of the coplanar phasing rendezvous case, the required surpasses the maximum capability by 74.64% for a maneuver at 200 km for a phasing angle of 1 , and by 62.07% for a maneuver at the same phasing angle and an altitude of 1000 km. For the non-coplanar phasing rendezvous case at an altitude of 400 km with an initial interceptor orbit inclination of 28.5 , the maximum capability is surpassed by 415.77% for and , and by 1181.80% for and . With the case of an initial interceptor altitude of 400 km and an orbit inclination of 90 , the maximum capability is surpassed by 325.70% for and , and by 594.50% for and .

Besides the maneuver cases of coplanar and non-coplanar phasing rendezvous, the X-37B and the notional satellite do possess the capability of performing combined changes to orbit inclination and RAAN and simple plane changes. Such maneuvers however maintain angle restrictions which are dependent upon orbit altitude. For an altitude of 400 km and an initial orbit inclination of 28.5 , spacecraft – specifically the X-37B and the notional satellite – are only capable of performing a maximum inclination change of with from the cases simulated. When the altitude is increased to 1000 km, the maximum inclination change increases to with . At an altitude of 400 km and an initial orbit inclination of however, the maximum inclination change decreases from to with , and from to with at an altitude of 1000 km. For the case of the simple plane change maneuver, the maximum inclination change capable of being performed is and from initial altitudes of 200 km and 1000 km, respectively.

Orbit Inclination-Change Analysis

As a means of directly comparing skip entry and vacuum-only maneuver performance, the required to complete a desired change in orbit inclination was calculated for the two maneuver types. With respect to skip entry maneuvers, a change in inclination can occur by altering either the entry vehicle's heading angle , bank angle , or a combination thereof. Since the current trajectory simulation only accounts for an alteration of the heading angle at the initiation of the skip entry maneuver, then any changes in inclination are analogous to those obtained by a simple plane change

maneuver. Consequently, this research will only analyze changes in inclination incurred by altering the bank angle of the X-37B and notional satellite for varying cases of entry altitude, flight-path angle, latitude, and longitude. An extension of the present analysis to encompass the impact of heading angle and combined changes to both heading and bank angle on changes in inclination is outlined in the following chapter as a recommended action for future research.

For the X-37B, the relationship between heading angle and change in inclination is shown below for skip entry from an altitude of 200 km, with latitude and longitude both equal to 0 , and the flight-path angle either -10 or -30 . While parametric studies were conducted for an entry altitude of 120 km at the preceding flight-path angles, only the results for the 200 km altitude case are presented since the change in inclination achieved for a given bank angle was the same for both cases. In addition, the results for the notional satellite simulations are also omitted since they depict zero deviation from the X-37B results illustrated in the following figures.

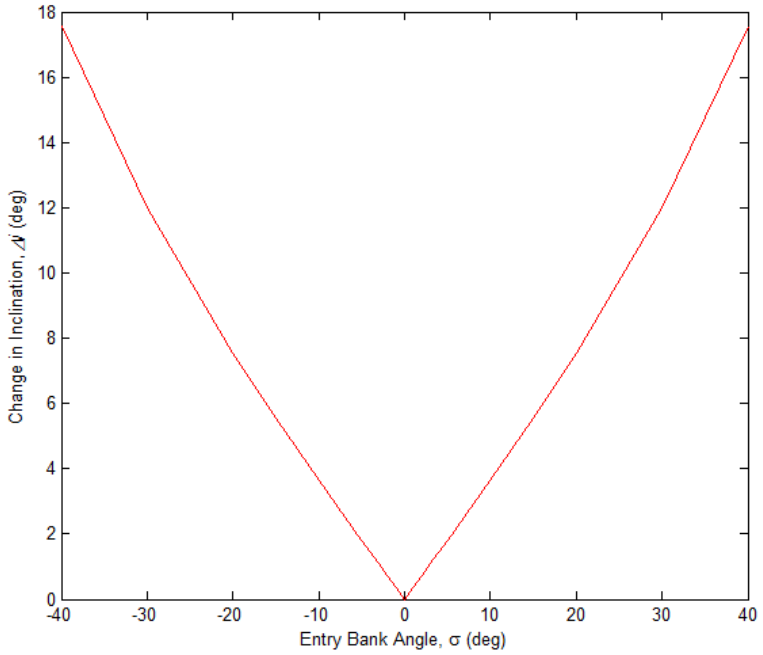

Figure 50. Change in Inclination for X-37B with Variable Bank Angle
(h = 200 km, γ = -10°, $\varphi = \theta$ = 0°)

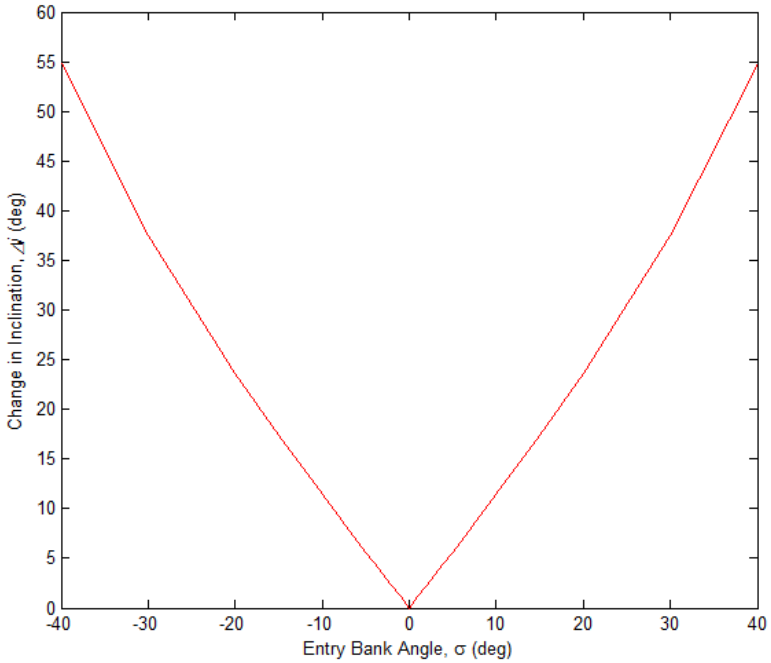

Figure 51. Change in Inclination for X-37B with Variable Bank Angle
(h = 200 km, γ = -30°, $\varphi = \theta$ = 0°)

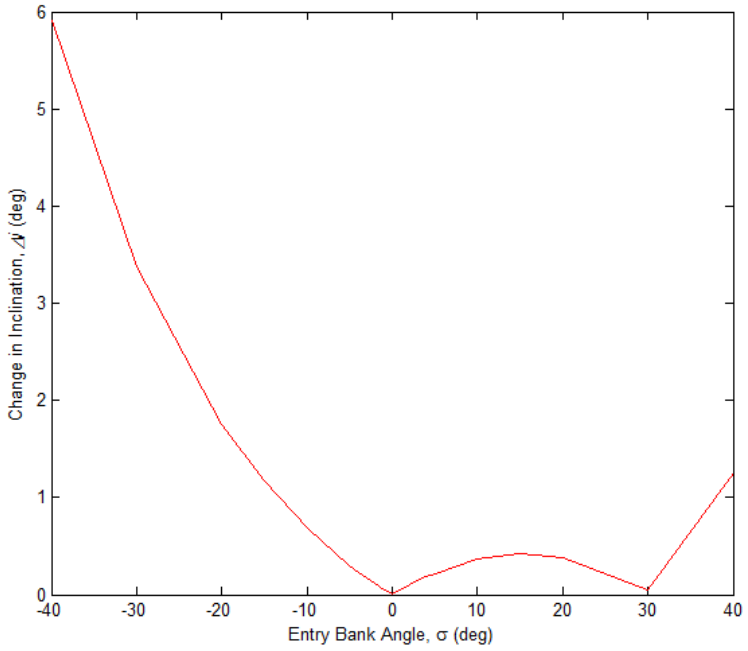

Figure 52. Change in Inclination for X-37B with Variable Bank Angle
(h = 200 km, γ = -10°, ,)

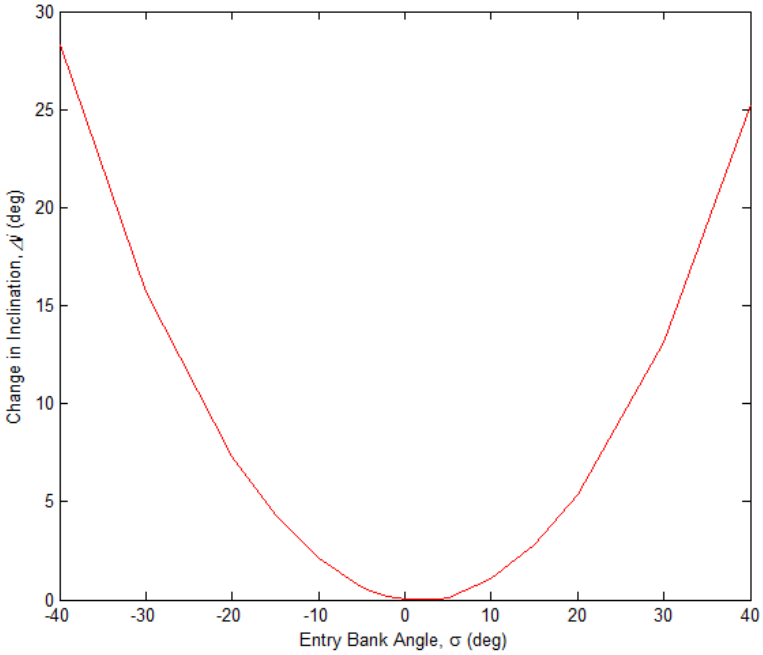

Figure 53. Change in Inclination for X-37B with Variable Bank Angle
(h = 200 km, γ = -30°, ,)

From the figures above it is seen that for a given altitude, such as 200 km, the change in inclination increases as the flight-path increases in magnitude, with the maximum change in inclination for a bank angle of increasing from approximately 17 to 55 for the X-37B and notional satellite at . For the same increase in flight-path angle magnitude, but with skip entry over Kirtland AFB, NM instead of the equator, the maximum change in inclination for the example entry vehicles increases from approximately 5.9 to 28 for , and from approximately 1.2 to 25 for . Overall, it can be concluded that changes in inclination are directly proportional to changes in flight-path angle, with an increase in flight-path magnitude yielding an increase in the change in inclination achieved at a given altitude.

In terms of propellant consumption and maneuver efficiency, the current simulation calculates the required complete a desired change in inclination as only a function of the impulse associated with altering flight-path angle and not vehicle bank angle. The absence of the latter is based on the assumption that the required to alter bank angle is negligible in magnitude compared with that to change flight-path angle. With this assumption as a basis for the calculations, a cursory comparison of maneuver performance can be made between the X-37B and notional satellite for example orbit altitudes of 120 km and 200 km with . Outlined in the following tables, the required for a skip entry and vacuum-only maneuver, specifically the simple plane change, to complete a desired change in inclination is illustrated for varying values of flight-path angle and orbit altitude:

Table 32. Comparison of ΔV Required to Change Inclination for X-37B

Orbit Altitude	Flight-Path Angle	Change in Inclination	Skip Entry (km/s)	Vacuum-Only (km/s)
120 km	-10	5	4.3606	0.6833
		10	4.4109	1.3652
		30	5.2314	4.0542
		60	6.7538	7.8320
	-30	5	10.440	0.6833
		10	10.432	1.3652
		30	10.203	4.0542
		60	10.616	7.8320
200 km	-10	5	4.0464	0.6791
		10	4.1805	1.3569
		30	5.1995	4.0294
		60	6.6602	7.7843
	-30	5	9.9440	0.6791
		10	9.9598	1.3569
		30	10.120	4.0294
		60	10.534	7.7843

As shown in the table above, the given for the skip entry maneuver represents the required to alter the entry vehicle flight-path angle in order to commence the skip entry, as well as the required to re-circularize the orbit at the end of the trajectory. Based on this definition, the skip entry maneuver for both the X-37B and notional satellite is more expensive in terms of than the simple plane change vacuum-only maneuver for small changes in inclination angle with large flight-path angles. For both example entry vehicles at altitudes of 120 km and 200 km, the required to complete a skip entry maneuver at a flight-path angle of -10 becomes less than that for a simple plane change when .

Table 33. Comparison of ΔV Required to Change Inclination for Notional Satellite

Orbit Altitude	Flight-Path Angle	Change in Inclination	Skip Entry (km/s)	Vacuum-Only (km/s)
120 km	-10	5	4.5460	0.6833
		10	4.6346	1.3652
		30	5.3220	4.0542
		60	6.7710	7.8320
	-30	5	10.701	0.6833
		10	10.701	1.3652
		30	10.700	4.0542
		60	10.623	7.8320
200 km	-10	5	4.0758	0.6791
		10	4.2100	1.3569
		30	5.2279	4.0294
		60	6.6828	7.7843
	-30	5	9.9530	0.6791
		10	9.9687	1.3569
		30	10.129	4.0294
		460	10.541	7.7843

Based on the maximum capability of 3 km/s for the X-37B and notional satellite, a change in inclination produced by a skip entry maneuver can only be considered for flight-path angles shallower than -10 . Even though a shallower flight-path angle leads to a higher minimum altitude reached during skip entry, Table 23 indicates that at a flight-path angle of -5 for lift-to-drag ratios of 1.0, 1.5, and 2.0, the trajectory of the X-37B will still penetrate to an altitude lower than 80 km and temporarily exit the ionosphere. For the notional satellite however, Table 24 shows that at the same flight-path angle and lift-to-drag cases, the trajectory will remain within the ionosphere and not penetrate to an altitude lower than 80 km. From this it can be asserted that only spacecraft which maintain similar aerodynamic and mass characteristics to the X-37B can execute a

skip entry maneuver in order to not only alter inclination angle, but also temporarily operate at an altitude lower than 80 km.

Investigative Questions Answered

As previously outlined in Chapter 1, the investigative questions underpinning this thesis and their associated answers derived through parametric studies of both skip and vacuum-only maneuvers are as follows:

- *What is the impact of flight-path angle and entry vehicle aerodynamics, specifically coefficients of drag and lift, on skip entry trajectory dynamical parameters such as drag and lift force, deceleration, stagnation heat flux, and entry vehicle velocity?*

  Overall, the skip entry parametric studies were divided in two categories: (1) Variable coefficient of lift and constant flight-path angle, and (2) constant coefficient of lift and variable flight-path angle. With the first category, increases in coefficient of lift produce an increase in lift force and a decrease in drag force experienced by the entry vehicle. With penetration depth into the atmosphere decreasing as the coefficient of lift increases, the deceleration and stagnation heat flux both decrease, and the entry vehicle velocity increases. For the second category, increases in flight-path angle lead to a decrease in the lift and drag force, an increase in deceleration and stagnation heat flux, and a decrease in entry vehicle velocity.

- *What is the relationship between entry altitude and the minimum altitude that can be reached for a skip entry maneuver? Also, what is the relationship between the*

coefficient of lift and flight-path angle of an entry vehicle and the minimum skip entry trajectory altitude?

As identified by the parametric studies, the minimum skip entry trajectory altitude decreases in magnitude as the entry altitude also decreases. In addition, deeper penetration into the atmosphere can also be achieved as the entry vehicle coefficient of lift decreases and the flight-path angle increases in magnitude.

- *What is the relationship between entry altitude and the required to complete a single skip entry maneuver?*

  The required to complete a single skip entry maneuver decreases as entry altitude increases since the orbital velocity is inversely related to altitude and decreases in magnitude as orbit altitude increases.

- *What is the required to complete two successive skip entry maneuvers?*

  The required to complete two successive skip entry maneuvers is a function of the altitude, flight-path angle, and aerodynamics of the entry vehicle. With this, the required decreases as the flight-path angle decreases in magnitude and as either the altitude or entry vehicle lift-to-drag ratio increase.

- *What is the required to complete a user-specified change in orbit inclination angle for a skip entry maneuver compared with that of a vacuum-only maneuver?*

  In terms of vacuum-only maneuvers, such as the simple plane change, the required to complete a user-specified change in inclination decreases as the orbit altitude increases. For skip entry maneuvers, the required decreases as the magnitude of the flight-path angle decreases. In comparison with the simple plane

change, the skip entry maneuver becomes less expensive in terms of as the desired change in inclination increases for shallow flight-path angles.

Summary

As demonstrated by the parametric studies, skip entry maneuvers are dependent on not only the orbit altitude and flight-path orientation, but also the aerodynamics of a given entry vehicle. In terms of vacuum-only maneuvers, it was identified that due to the maximum capability of the X-37B and notional satellite, the simple plane change and the combined change to inclination and RAAN represent the only permissible exo-atmospheric maneuvers. From the orbit inclination analysis of the skip entry and simple plane maneuvers, it was discerned that for shallow flight-path angles and large changes in inclination the skip entry requires less than the vacuum-only alternative.

V. Conclusions and Recommendations

Chapter Overview

The purpose of this chapter is to outline the conclusions formulated upon review of the skip entry and vacuum-only maneuver parametric studies and associated simulation analyses. In addition, the significance of this thesis and associated skip entry maneuver analysis will be assessed in relation to the relevant literature reviewed in Chapter 2. Finally, recommendations for action and future research will be identified in order to both improve and expand upon the preceding maneuver analysis.

Conclusions of Research

Through parametric study and trajectory simulation, the research indicates that skip entry maneuvers maintain the potential of being employed as a responsive maneuver to fulfill various demand-taskings. Specifically, the ability a skip entry trajectory to penetrate to an altitude below the ionosphere as well as the viability of skip entry maneuver to complete a desired change in orbit inclination was demonstrated. Compared with the simple plane change maneuver, it was determined that the skip entry maneuver requires less than the vacuum-only alternative with shallow flight-path angles and large changes in inclination, with and . Due to restrictions in maximum capability for the example entry vehicles, it was identified that only skip entry maneuvers with a flight-path angle less than -10 in magnitude are permitted since is required to enter a skip entry trajectory as well as to re-circularize the orbit at the end of the trajectory.

Significance of Research

The research which comprises this thesis is significant to the engineering community because it expands upon existing literature to convey the relationship between the aerodynamics, initial altitude, and flight-path orientation of an entry vehicle on the skip entry trajectory, as well as the cases in which skip entry maneuvers require less ΔV than simple plane change maneuvers to execute a change in orbit inclination. In terms of the U.S. Air Force, the research is significant for it illustrates the viability of skip entry maneuvers as both a responsive maneuver and an alternative to vacuum-only maneuvers as a means to alter a spacecraft's orbital elements. In addition, the research alludes to the potential of nullifying foreign orbit estimation efforts by changing inclination angle within the upper atmosphere.

Recommendations for Action

Although the research objectives were met and the investigative questions answered by the preceding analysis, several improvements can be made within the trajectory and maneuver simulations and the following outlines the various recommendations for action required to achieve increased solution realism and accuracy within the parametric studies:

- Employ an ordinary differential equation system solver rather than a first-order numerical integration method to solve the kinematic and force equations of motion for atmospheric re-entry. An example of such an equation solver is the *ode45* function within *Matlab*.

- Conduct all skip entry maneuver parametric studies with the inclusion of the planetary rotation rate.
- Assess the impact of variable heading and bank angle on skip entry trajectory parameters.
- Assess the impact of entry altitude, flight-path angle, and entry vehicle aerodynamics on total skip entry trajectory time-of-flight as well as the time-of-flight below particular threshold altitudes, such as 80 km.
- Determine the required to alter the vehicle heading angle and/or bank angle in order to accurately assess the required for a skip entry maneuver to change orbit inclination angle when compared with the simple plane change vacuum-only maneuver.
- Determine the required to complete a vacuum-only, non-coplanar rendezvous between spacecraft in two non-equatorial circular orbits.

Recommendations for Future Research

The following outlines various recommendations for future research discerned from the preceding analysis and parametric studies:

- Determine the required to achieve a desired change in orbit inclination for the X-37B and notional satellite if either the vehicle heading angle or both the heading and bank angle are changed during rather than at the initiation of a skip entry maneuver.

- Assess the impact of variable coefficients of lift and drag on the minimum trajectory altitude, exit flight-path angle, and the required to commence multiple skip entry maneuvers.
- Analytically calculate the coefficients of lift and drag for the geometry of the example entry vehicles for a given flow environment rather than relying on estimated values, such as a coefficient of drag of 0.5 for a lifting entry vehicle, or 2.2 for a cube-shaped satellite.
- Investigate the effect of reducing entry vehicle mass during a skip entry maneuver on the trajectory profile.

Summary

A type of responsive maneuvers which operate within Earth's upper atmosphere, skip entry maneuvers provide the user with a new environment within which orbital elements, particularly inclination angle, can be altered aerodynamically rather than by purely propulsive means. In addition, skip entry maneuvers allow the pursuance of missions and demand-taskings which require payload operations at altitudes, such as those below the ionosphere, not achievable by conventional low-Earth orbits. Despite these advantages however, skip entry maneuvers also proffer a new set of challenges arising the requirement to design trans-atmospheric trajectories which account for not only aerodynamic force and deceleration, but also re-entry heating experienced by the entry vehicle.

Appendix A: Skip Entry Maneuver *Matlab* Code

The following *Matlab* files (m-files) comprise the code employed to conduct the preceding skip entry maneuver trade studies:

Table A.1. Skip Entry Maneuver *Matlab* Code Classification

m-File Name	Type of File
Maneuver_Sim.m	Script
Maneuver_Sim_Cases.m	Script
ManeuverSimFunc.m	Function

```
%%%%%%%%%%%%%%%%%%%%%%%%%%%%%%%%%%%%%%%%%%%%%%%%%%%%%%%%%%%%%%%%%%%%%%%%%%%%%%%
%
% Use: Maneuver_Sim.m
%
% This script calculates and plots the maneuver profile for a user-defined
% entry vehicle. The script can either simulate constant thrust maneuvers,
% skip entry profile, or a combined continuous thrust and skip entry
% maneuver. In addition, the simulation will indicate to the user if
% altitude, velocity, deceleration, or heat flux constraints are surpassed.
%
% Author/Date: Bettinger, Robert AFIT/ENY                        Spring 2011
%
% Baseline Simulation Inputs:
%   deltaT       - Simulation propagation time-step (sec)
%   Sim_Time_max - Maximum user-defined simulation run-time (sec)
%   h            - Mission orbit altitude (km)
%
% Vehicle Model Inputs:
%   Cd           - Coefficient of drag
%   Cl           - Coefficient of lift
%   m            - Mass of vehicle (kg)
%   S_m2         - Planform area (m^2)
%   T_max        - Magnitude of maximum thrust (N)
%   throttle     - Throttle percentage for vehicle engine
%   eps_T        - Angle between thrust and velocity vectors (deg)
%   zeta_T       - Angle between thrust and velocity vectors (deg)
%   deltaV_max   - Maximum vehicle delta-V capability (km/s)
%   Vf_max       - Maximum vehicle final velocity (km/s)
%   ag_max       - Maximum value of vehicle deceleration
%   qs_max       - Maximum value of vehicle stagnation heat flux
%
% Maneuver Profile Inputs:
%   gamma_e      - Flight-path angle (deg)
%   theta_e      - Longitude (deg)
%   phi_e        - Latitude (deg)
%   psi_e        - Vehicle heading angle (deg)
%   sigma_e      - Vehicle bank angle (deg)
```

```
%
% Outputs:
%   r                       - Position vector of maneuver (km)
%   V                       - Velocity vector of maneuver (km/s)
%   T_total                 - Total time of maneuver (s)
%   ag_decel_mag            - Magnitude of vehicle deceleration
%   qdot_s                  - Vehicle stagnation heat flux
%   qdot_w                  - Vehicle wall (average) heat flux
%   Threshold_Entry_Time    - Time below threshold altitude (h<=80 km) (s)
%   Th_first_min            - First altitude minimum in trajectory (km)
%   Th_first_max            - First altitude maximum in trajectory (km)
%   Skip_DeltaV             - Delta-V required for initial skip entry
%                             maneuver (km)
%   Maneuver_DeltaV         - Delta-V required for subsequent skip entry
%                             maneuver (km/s)
%
% Globals:  None
% Constants:
%   r0            - Earth planetary radius (km)
%   MU            - Earth gravitational parameter (km^3/s^2)
%   g0            - Gravitational acceleration at planetary surface (km/s^2)
%   omega_e       - Planetary rotational velocity (rad/s)
%   beta          - Atmospheric scale height (km^-1)
%   rho0          - Atmospheric density at planetary surface (kg/km^3)
%
% Coupling: None
%
% References: Hicks, Kerry D. Introduction to Astrodynamic Reentry.
%             Wright-Patterson AFB: AF Institute of Technology, 2003.
%
%             Vallado, David A. Fundamentals of Astrodynamics and
%             Applications. Boston: Microcosm Press, 2001.
%
%%%%%%%%%%%%%%%%%%%%%%%%%%%%%%%%%%%%%%%%%%%%%%%%%%%%%%%%%%%%%%%%%%%%%%%%%%%%%%%

clear all; clc; close all
format long

%%%%%%%%%%%%%%%%%%%%%%%%%%%%%%%%%%%%%%%%%%%%%%%%%%%%%%%%%%%%%%%%%%%%%%%%%%%%%%%
%% User-Defined Simulation Initial Conditions
deltaT = 0.1; %Simulation propagation time-step (sec)
Sim_Time_Max = 10000; %Maximum user-defined simulation run-time (sec)

h = 200; %Mission/entry orbit altitude (km)
h_max = 500; %Max. altitude for continuous-thrusting orbit-raising (km)

Vehicle_Choice = 1; %1 = X-37B (m = 4989.5 kg, Cd = 0.5)
                    %2 = ESPA SPL Notional Satellite (m = 200 kg, Cd = 2.2)
                    %3 = Notional Satellite (m = 1000 kg, Cd = 2.2)

Scenario_Choice = 1; %1 = Single skip entry scenario
                     %2 = Continuous-thrust orbit-raising OR
                     %    Multiple skip entry scenario
```

```
gamma_e = -10; %Entry flight-path angle (deg) (*Negative for skip entry*)
theta_e = 0; %110; %Initial simulation longitude (deg)
phi_e = 0; %35.05; %Initial simulation latitude (deg)
psi_e = 28.5; %Vehicle heading angle (deg)
sigma_e = 0; %Vehicle bank angle (deg)

%%%%%%%%%%%%%%%%%%%%%%%%%%%%%%%%%%%%%%%%%%%%%%%%%%%%%%%%%%%%%%%%%%%%%%%%%%%%%%%
%% Gravity Model
r0 = 6378.137; %Earth planetary radius (km)
r = r0 + h; %Mission/entry orbit radius (km)
r_max = r0+ h_max; %Max. radius for continuous-thrusting orbit-raising (km)
MU = 398600.5; %Earth gravitational parameter (km^3/s^2)
g0 = 0.00981; %Gravitational acceleration at planetary surface (km/s^2)
g_r = g0*(r0/r)^2; %Gravitational acceleration at given radius (km/s^2)

%%%%%%%%%%%%%%%%%%%%%%%%%%%%%%%%%%%%%%%%%%%%%%%%%%%%%%%%%%%%%%%%%%%%%%%%%%%%%%%
%% Atmosphere/Planet Model
omega_e = 0; %7.292115e-5; %Planetary rotational velocity (rad/s) (Vallado 138)
beta = 0.14; %Atmospheric scale height (km^-1)
rho0 = 1.225 * (1000)^3; %Atmospheric density at planetary surface (kg/km^3)
rho_r = rho0*exp(-beta*(r - r0)); %Atmospheric density at given radius (kg/km^3)

%%%%%%%%%%%%%%%%%%%%%%%%%%%%%%%%%%%%%%%%%%%%%%%%%%%%%%%%%%%%%%%%%%%%%%%%%%%%%%%
%% Orbit Model
e = 0.0; %Entry orbit eccentricity
a = r/(1-e); %Entry orbit semi-major axis (km)
n = sqrt(MU/(a^3)); %Entry orbit mean motion (rad/s)
SMA = -MU/(2*a); %Entry orbit specific mechanical energy (km^2/s^2)
V = sqrt(MU*((2/r) - (1/a))); %Entry orbit velocity (km/s)

%%%%%%%%%%%%%%%%%%%%%%%%%%%%%%%%%%%%%%%%%%%%%%%%%%%%%%%%%%%%%%%%%%%%%%%%%%%%%%%
%% Vehicle Model
if Vehicle_Choice == 1
    m = 4989.5; %Wet mass; X-37B (kg)
    Cd = 0.5; %Approx. coefficient of drag for lifting entry vehicles

elseif Vehicle_Choice == 2
    m = 200; %Wet mass; ESPA SPL notional satellite (kg)
    Cd = 2.2; %Approx. coefficient of drag for satellites

elseif Vehicle_Choice == 3
    m = 1000; %Wet mass; Primary payload notional satellite (kg)
    Cd = 2.2; %Approx. coefficient of drag for satellites
end

%Engine Parameters
%Thrust Options: 14679 N (Impulsive thrusting; H2O2/JP-8; X-37B)
%                13345 N (Impulsive thrusting; H2O2/JP-10; X-37B)
%                 9901 N (Impulsive thrusting; H2O2; X-37B)
%               300E-3 N (Continuous thrusting; notional satellite)
%               500E-3 N (Continuous thrusting; notional satellite)
T_max = 0; %Maximum thrust (N)
Throttle = 50; %Throttle (percentage)
T = T_max * (Throttle/100); %Magnitude of thrust (N)
```

```
eps_T = deg2rad(0.0); %Angle between thrust and velocity vectors (rad)
zeta_T = deg2rad(0.0); %Angle between thrust and velocity vectors (rad)

%Vehicle Maneuver Constraints
deltaV_max = 5.00; %Maximum vehicle delta-V capability (km/s)
Vf_max = 15.0; %Maximum vehicle final velocity (km/s)
ag_max = 100; %Maximum value of vehicle deceleration
qs_max = 0.25; %Maximum value of vehicle stagnation heat flux

%%%%%%%%%%%%%%%%%%%%%%%%%%%%%%%%%%%%%%%%%%%%%%%%%%%%%%%%%%%%%%%%%%%%%%%%%%%%%%%
%% Vehicle Aerodynamics
%Planform Area
S_m2 = 18.63; %(m^2)
S = S_m2 / (1000)^2; %(km^2)

L2D = linspace(0.8,2.0,25); %Lift-to-drag ratio
%Lift-to-drag ratio vector:
%L2D = [0.80,0.85,0.90,0.95,1.00,
%       1.05,1.10,1.15,1.20,1.25,
%       1.30,1.35,1.40,1.45,1.50,
%       1.55,1.60,1.65,1.70,1.75,
%       1.80,1.85,1.90,1.95,2.00]

Cl_vec = L2D.*Cd; %Coefficient of lift vector
Cl = Cl_vec(5); %User-specified coefficient of lift

D = 0.5*rho_r*Cd*S*V^2; %Drag force (N)
L = 0.5*rho_r*Cl*S*V^2; %Lift force (N)

%%%%%%%%%%%%%%%%%%%%%%%%%%%%%%%%%%%%%%%%%%%%%%%%%%%%%%%%%%%%%%%%%%%%%%%%%%%%%%%
%% Equations of Motion
%Maneuver Profile Angles
gamma_e(1) = deg2rad(gamma_e); %Flight-path angle (rad)
theta_e(1) = deg2rad(theta_e); %Longitude (rad)
phi_e(1) = deg2rad(phi_e); %Latitude (rad)
psi_e(1) = deg2rad(psi_e); %Vehicle heading angle (rad)
sigma_e(1) = deg2rad(sigma_e); %Vehicle bank angle (rad)

%%%%%%%%%%%%%%%%%%%%%%%%%%%%%%%%%%%%%%%%%%%%%%%%%%%%%%%%%%%%%%%%%%%%%%%%%%%%%%%
%% Numerical Integration of Equations of Motion
r(1) = r; V(1) = V; %Initial conditions for vehicle dynamics
g_r(1) = g_r; rho_r(1) = rho_r; %Initial conditions for entry environment
D(1) = D; L(1) = L; %Initial conditions for vehicle aerodynamics

%Loop end state for vehicle orbit radius
if Scenario_Choice == 1
    r_choice = r(1);
elseif Scenario_Choice == 2
    r_choice = r_max;
end

%Initial vehicle deceleration
a_decel_v(1) = (D(1)/m) + g_r(1)*sin(gamma_e(1));
```

```
a_decel_L(1) = (-L(1)/m) - (((V(1)^2)/r(1)) - g_r(1))*cos(gamma_e(1));
a_decel_mag(1) = sqrt((a_decel_v(1))^2 + (a_decel_L(1))^2);
ag_decel_mag(1) = a_decel_mag(1)/g_r(1);

%Initial vehicle stagnation and wall heat flux
qdot_s(1) = sqrt((rho_r(1)*S*Cd)/(2*m*beta))*((V(1)^2)/(2*g_r(1)*r(1)))^(3/2);
qdot_w(1) = ((rho_r(1)*S*Cd)/(2*m*beta))*((V(1)^2)/(2*g_r(1)*r(1)))^(3/2);

T_total(1) = 0; %Initial condition for total mission time

i = 1; %Initializes iteration counter at one
Sim_Time_ctr = 1; %Initializes simulation time counter at one

while (r <= r_choice) & (r > r0) & ...
      (V <= Vf_max) & (ag_decel_mag <= ag_max) & ...
      (qdot_s <= qs_max) & (Sim_Time_ctr < Sim_Time_Max);

    %Vehicle position (r) differential equation
    r_dot = V(i)*sin(gamma_e(i));

    %Vehicle velocity (V) differential equation
    V_dot = ((T/m)*(cos(zeta_T)*cos(eps_T))) - (D(i)/m) - ...
            (g_r(i)*sin(gamma_e(i))) + ...
            (r(i)*(omega_e^2)*cos(phi_e(i))*(cos(phi_e(i))*sin(gamma_e(i)) - ...
             sin(phi_e(i))*sin(psi_e(i))*cos(gamma_e(i))));

    %Vehicle flight-path angle (gamma) differential equation
    Vgamma_dot = ((T/m)*(sin(zeta_T)*sin(sigma_e(i)) + ...
                  cos(zeta_T)*sin(eps_T)*cos(sigma_e(i)))) + ...
                 ((L(i)/m)*cos(sigma_e(i))) - (g_r(i)*cos(gamma_e(i))) + ...
                 ((V(i)^2)/r(i))*cos(gamma_e(i)) + ...
                 (2*V(i)*omega_e*cos(phi_e(i))*cos(psi_e(i))) + ...
                 (r(i)*(omega_e^2)*cos(phi_e(i))*(cos(phi_e(i))*cos(gamma_e(i)) + ...
                  sin(phi_e(i))*sin(psi_e(i))*sin(gamma_e(i))));

    %Vehicle longitude (theta) differential equation
    theta_dot = ((V(i)*cos(gamma_e(i))*cos(psi_e(i)))/(r(i)*cos(phi_e(i))));

    %Vehicle latitude (phi) differential equation
    phi_dot = (1/r(i))*(V(i)*cos(gamma_e(i))*sin(psi_e(i)));

    %Vehicle heading angle (psi) differential equation
    Vpsi_dot = (1/(m*cos(gamma_e(i))))*(T*(cos(zeta_T)*sin(eps_T)*sin(sigma_e(i)) -
...
        sin(zeta_T)*cos(sigma_e(i))) + L(i)*sin(sigma_e(i))) - ...
        ((V(i)^2)/r(i))*cos(gamma_e(i))*cos(psi_e(i))*tan(phi_e(i)) + ...
        2*V(i)*omega_e*(sin(psi_e(i))*cos(phi_e(i))*tan(gamma_e(i)) - ...
        sin(phi_e(i))) - ((r(i)*omega_e^2)/cos(gamma_e(i)))* ...
        sin(phi_e(i))*cos(phi_e(i))*cos(psi_e(i));

    %Updates to Vehicle Dynamics
    r(i+1) = r(i) + r_dot*deltaT; %Vehicle position
    V(i+1) = V(i) + V_dot*deltaT; %Vehicle velocity
```

```
    gamma_e(i+1) = gamma_e(i) + (Vgamma_dot/V(i))*deltaT; %Flight-path angle

    %Updates to Maneuver Profile Angles
    theta_e(i+1) = theta_e(i) + theta_dot*deltaT;
    phi_e(i+1) = phi_e(i) + phi_dot*deltaT;
    psi_e(i+1) = psi_e(i) + (Vpsi_dot/V(i))*deltaT;
    sigma_e(i+1) = sigma_e(i);

    %Updates to Simulation Environment
    g_r(i+1) = g0*(r0/r(i+1))^2; %Gravitational acceleration
    rho_r(i+1) = rho0*exp(-beta*(r(i+1) - r0)); %Atmospheric density
    D(i+1) = 0.5*rho_r(i+1)*Cd*S*V(i+1)^2; %Drag force
    L(i+1) = 0.5*rho_r(i+1)*Cl*S*V(i+1)^2; %Lift force

    %Update to Vehicle Deceleration
    a_decel_v(i+1) = -V_dot/g_r(i+1);
    a_decel_L(i+1) = -Vgamma_dot/g_r(i+1);
    ag_decel_mag(i+1) = sqrt((a_decel_v(i+1))^2 + (a_decel_L(i+1))^2);

    %Update to Vehicle Stagnation and Wall Heat Flux
    qdot_s(i+1) =
sqrt((rho_r(i+1)*S*Cd)/(2*m*beta))*((V(i+1)^2)/(2*g_r(i+1)*r(i+1)))^(3/2);
    qdot_w(i+1) =
((rho_r(i+1)*S*Cd)/(2*m*beta))*((V(i+1)^2)/(2*g_r(i+1)*r(i+1)))^(3/2);

    T_total(i+1) = T_total(i) + deltaT; %Update to total skip entry time

    i = i + 1; %Update to iteration counter
    Sim_Time_ctr = Sim_Time_ctr + 1; %Update to simulation time counter

end

%Error messages for surpassing user-defined simulation constraints
if (r(end) < r0)
    disp('Simulation Abort - Vehicle has impacted planet (r < r0)')
elseif(V > Vf_max)
    disp('Simulation Abort - Vehicle has exceeded maximum velocity constraint')
elseif (ag_decel_mag > ag_max)
    disp('Simulation Abort - Vehicle has exceeded maximum deceleration constraint')
elseif (qdot_s > qs_max)
    disp('Simulation Abort - Vehicle has exceeded maximum stagnation heat flux
constraint')
elseif (Sim_Time_ctr == Sim_Time_Max);
    disp('Simulation Abort - Maximum user-defined simulation run-time has been
reached')
end

%%%%%%%%%%%%%%%%%%%%%%%%%%%%%%%%%%%%%%%%%%%%%%%%%%%%%%%%%%%%%%%%%%%%%%%%%%%%%%%
%Extraction of altitude and time values that occur at (h<=80 km) threshold
k = 0; %Initializes counter at zero
m = 0; %Initializes vector concatenation counter at zero
```

```
%Initializes position and time vectors of flight below (h<=80 km) threshold
%to zero
r_threshold(1) = 0;
T_threshold(1) = 0;

for k = 1:length(r)
    if r(k) <= (6458.137)
        m = m + 1;
        r_threshold(m) = r(k);
        T_threshold(m) = T_total(k);
    end
end

%Entry time below threshold altitude (h<=80 km)
Threshold_Entry_Time = T_threshold(end) - T_threshold(1)

%%%%%%%%%%%%%%%%%%%%%%%%%%%%%%%%%%%%%%%%%%%%%%%%%%%%%%%%%%%%%%%%%%%%%%%%%%%%%%%
%% Determination of First Local Altitude Minimum in Trajectory
for ctr_min = 2:length(r)
    if r(ctr_min) < r(ctr_min - 1)
        ctr_min = ctr_min + 1;
    else
        r_first_min = r(ctr_min - 1); %First local radius minimum (km)
        %Time and radial position of first local minimum
        Tr_first_min = [T_total(ctr_min - 1),r_first_min];
        ctr_min = ctr_min - 1; %Counter value for first local minimum
        break
    end
end

Th_first_min = Tr_first_min - [0,r0]; %Conversion from radius to altitude

%%%%%%%%%%%%%%%%%%%%%%%%%%%%%%%%%%%%%%%%%%%%%%%%%%%%%%%%%%%%%%%%%%%%%%%%%%%%%%%
%% Determination of First Local Altitude Maximum in Trajectory
for ctr_max = (ctr_min + 1):length(r)
    if r(ctr_max) > r(ctr_max - 1) && ctr_max < length(r)
        ctr_max = ctr_max + 1;
    else
        r_first_max = r(ctr_max); %First local radius minimum (km)
        %Time and radial position of first local maximum
        Tr_first_max = [T_total(ctr_max),r_first_max];
        ctr_max = ctr_max; %Counter value for first local maximum
        break
    end
end

Th_first_max = Tr_first_max - [0,r0]; %Conversion from radius to altitude

%%%%%%%%%%%%%%%%%%%%%%%%%%%%%%%%%%%%%%%%%%%%%%%%%%%%%%%%%%%%%%%%%%%%%%%%%%%%%%%
%% Delta-V Required for Initial Skip Entry Maneuver
V_entry1 = V(1);

%Delta-V required to alter vehicle flight-path angle in order to enter into
%skip entry trajectory while maintaining orbital velocity
```

```
Skip_DeltaV = sqrt((V_entry1^2) + (V_entry1^2) - ...
    (2*V_entry1*V_entry1*cos(gamma_e(1))))

%%%%%%%%%%%%%%%%%%%%%%%%%%%%%%%%%%%%%%%%%%%%%%%%%%%%%%%%%%%%%%%%%%%%%%%%%%%%
%% Delta-V Required for Subsequent Skip Entry Maneuver
Boost_DeltaV = abs(V(ctr_max) - V(1));

if V(ctr_max) < sqrt(MU/r(1))
    V_exit = V(ctr_max); %Exit velocity of skip (i)
    V_entry = V(ctr_max) + Boost_DeltaV; %Entry velocity of skip (i+1)
else
    V_exit = V(ctr_max); %Exit velocity of skip (i)
    V_entry = V(ctr_max); %Entry velocity of skip (i+1)
end

Delta_Gamma = abs(gamma_e(ctr_max)-gamma_e(1));%Change in flight-path angle

%Delta-V required to alter vehicle flight-path angle and velocity such that
%Vf = Vi for subsequent skip entry maneuver
Maneuver_DeltaV = sqrt((V_exit^2) + (V_entry^2) - ...
    (2*V_exit*V_entry*cos(Delta_Gamma)))
dV_sum = Skip_DeltaV + Maneuver_DeltaV

%%%%%%%%%%%%%%%%%%%%%%%%%%%%%%%%%%%%%%%%%%%%%%%%%%%%%%%%%%%%%%%%%%%%%%%%%%%%
%% Calculation of Inclination at Skip Exit
%Trajectory parameters at Skip Exit
r_end = r(ctr_max); %Radius (km)
V_end = V(ctr_max); %Velocity (km)
gamma_end = gamma_e(ctr_max); %Flight-path angle (rad)
theta_end = theta_e(ctr_max); %Longitude (rad)
phi_end = phi_e(ctr_max); %Latitude (rad)
psi_end = psi_e(ctr_max); %Vehicle heading angle (rad)
omega_dt = omega_e*deltaT; %Planetary rotational velocity * Time Step (rad)

r_X2 = r_end*[1;0;0]; %Radius in Vehicle-Pointing frame

V_X2 = [V_end*sin(gamma_end); ...
        V_end*cos(gamma_end)*cos(psi_end); ...
        V_end*cos(gamma_end)*sin(psi_end)]; %Velocity in Vehicle-Pointing frame

%3-3-2 rotation matrix from Inertial to Vehicle-Pointing frame
RI_X2 = [cos(-phi_end) 0 -sin(-phi_end); 0 1 0; sin(-phi_end) 0 cos(-phi_end)]*...
        [cos(theta_end) sin(theta_end) 0; -sin(theta_end) cos(theta_end) 0; 0 0
1]*...
        [cos(omega_dt) sin(omega_dt) 0; -sin(omega_dt) cos(omega_dt) 0; 0 0 1];

r_I = inv(RI_X2)*r_X2; %Radius in Inertial frame
V_I = inv(RI_X2)*V_X2; %Velocity in Inertial frame

h_bar = cross(r_I,V_I); %Angular momentum in Inertial frame
incl_rad = acos(dot(h_bar,[0;0;1])/norm(h_bar)); %Inclination (rad)
incl_deg = rad2deg(incl_rad) %Inclination (deg)
```

```
%%%%%%%%%%%%%%%%%%%%%%%%%%%%%%%%%%%%%%%%%%%%%%%%%%%%%%%%%%%%%%%%%%%%%%%%%%%%
%% Plotting of Vehicle States (km | km/s) vs. Time (sec)
subplot(2,3,1), [yy_states] = plotyy(T_total,(r - r0),T_total,V,'plot'); grid off;
title('Vehicle States');
xlabel('Time, \itt\rm (sec)');
set(get(yy_states(1),'Ylabel'),'String','Altitude, \ith\rm (km)');
set(get(yy_states(2),'Ylabel'),'String','Velocity, \it^RV\rm (km/s)');

%% Plotting of Flight-Path Angle (deg) vs. Time (sec)
subplot(2,3,2), plot(T_total,gamma_e*(180/pi)); grid on;
title('Vehicle Flight-Path Angle (\gamma) Profile');
xlabel('Time, \itt\rm (sec)'); ylabel('Flight-Path Angle, \gamma (deg)');

%% Plotting of Heat Flux vs. Time (sec)
subplot(2,3,3), [yy_flux] = plotyy(T_total,qdot_s,T_total,qdot_w,'plot'); grid off;
title('Vehicle Heat Flux Profile');
xlabel('Time, \itt\rm (sec)');
set(get(yy_flux(1),'Ylabel'),'String','Stagnation Heat Flux, \itq_s\rm');
set(get(yy_flux(2),'Ylabel'),'String',{'Wall (Average)';'Heat Flux, \itq_w\rm'});

%% Plotting of Lift Force (N) vs. Time (sec)
subplot(2,3,4), plot(T_total,L); grid off;
title('Vehicle Lift Force Profile');
xlabel('Time, \itt\rm (sec)'); ylabel('Lift, \itL\rm (N)');

%% Plotting of Drag Force (N) vs. Time (sec)
subplot(2,3,5), plot(T_total,D); grid off;
title('Vehicle Drag Force Profile');
xlabel('Time, \itt\rm (sec)'); ylabel('Drag, \itD\rm (N)');

%% Plotting of Vehicle Deceleration vs. Time (sec)
subplot(2,3,6),
plot(T_total,ag_decel_mag,'b',T_total,a_decel_v,'r:',T_total,a_decel_L,'g:');
grid off;
legend('Magnitude','Tangential','Normal','Location','Northeast');
title('Vehicle Deceleration (a/g_0) Profile');
xlabel('Time, \itt\rm (sec)'); ylabel('Vehicle Deceleration, (a/g_0)');

%% Plotting of Altitude (km) vs. Longitude (deg)
figure
subplot(2,2,1), plot(theta_e*(180/pi),r-r0); grid on;
title('Vehicle Altitude (\ith\rm) Profile');
xlabel('Longitude, \theta (deg)'); ylabel('Altitude, \ith\rm (km)');

%% Plotting of Velocity (km/s) vs. Longitude (deg)
subplot(2,2,2), plot(theta_e*(180/pi),V); grid on;
title('Vehicle Velocity (\it^RV\rm) Profile');
xlabel('Longitude, \theta (deg)'); ylabel('Velocity, \it^RV\rm (km/s)');

%% Plotting of Flight-Path Angle (deg) vs. Longitude (deg)
subplot(2,1,2), plot(theta_e*(180/pi),gamma_e*(180/pi)); grid on;
title('Vehicle Flight-Path Angle (\gamma) Profile');
xlabel('Longitude, \theta (deg)'); ylabel('Flight-Path Angle, \gamma (deg)');
```

```
%%%%%%%%%%%%%%%%%%%%%%%%%%%%%%%%%%%%%%%%%%%%%%%%%%%%%%%%%%%%%%%%%%%%%%%%%%%%
%
% Use: Maneuver_Sim_Cases.m
%
% This script calculates and plots the maneuver profile from one of four
% simulation cases for a user-defined entry vehicle. The simulation cases
% are as follows:
% (1) Variable coefficient of lift
% (2) Variable flight-path angle
% (3) Variable altitude and flight-path angle
% (4) Variable vehicle heading angle
% (5) Variable vehicle bank angle
%
% Author/Date: Bettinger, Robert AFIT/ENY                        Spring 2011
%
% Baseline Simulation Inputs:
%   Sim_Choice      - User-defined simulation case as defined above
%   Vehicle_Choice  - User-defined entry vehicle
%
% Simulation Case Inputs:
%   h             - Entry orbit altitude (km)
%   gamma_e       - Flight-path angle (deg)
%   theta_e       - Longitude (deg)
%   phi_e         - Latitude (deg)
%   psi_e         - Vehicle heading angle (deg)
%   sigma_e       - Vehicle bank angle (deg)
%
% Simulation Case Graphical Outputs:
% (1) Variable coefficient of lift / (2) Variable flight-path angle
%   - Vehicle Position (km) vs. Time (sec)
%   - Vehicle Velocity (km/s) vs. Time (sec)
%   - Stagnation Heat Flux vs. Time (sec)
%   - Lift Force (N) vs. Time (sec)
%   - Drag Force (N) vs. Time (sec)
%   - Vehicle Deceleration vs. Time (sec)
%
% (3) Variable altitude and flight-path angle
%   - Min. Altitude of Trajectory (km) vs. Flight-Path Angle (deg)
%   - Delta-V (km/s) for Second Skip Entry vs. Flight-Path Angle (deg)
%   - Total Delta-V (km/s) vs. Flight-Path Angle (deg)
%   - Delta-Flight-Path Angle (deg) vs. Flight-Path Angle (deg)
%
% (4) Variable vehicle heading angle
%   - Exit Latitude (deg) vs. Entry Heading Angle (deg)
%   - Inclination (deg) vs. Entry Heading Angle (deg)
%   - Change in Inclination (deg) vs. Entry Heading Angle (deg)
%
% (5) Variable vehicle bank angle
%   - Inclination (deg) vs. Entry Bank Angle (deg)
%   - Change in Inclination (deg) vs. Entry Bank Angle (deg)
%
% Globals:  None
% Constants:
%   r0            - Earth planetary radius (km)
```

```
%   MU            - Earth gravitational parameter (km^3/s^2)
%   g0            - Gravitational acceleration at planetary surface (km/s^2)
%
% Coupling:
%  ManeuverSimFunc.m    - Inputs: Entry vehicle mass; coefficients of drag
%                         and lift; planform area; entry flight-path angle;
%                         initial longitude and latitude; vehicle heading
%                         angle; vehicle bank angle;altitude; orbital velocity
%                       - Outputs: Entry vehicle position and velocity;
%                         flight-path angle; latitude; deceleration
%                         magnitude; lift and drag force; stagnation heat
%                         flux
%
% References: Hicks, Kerry D. Introduction to Astrodynamic Reentry.
%             Wright-Patterson AFB: AF Institute of Technology, 2003.
%
%             Vallado, David A. Fundamentals of Astrodynamics and
%             Applications. Boston: Microcosm Press, 2001.
%
%%%%%%%%%%%%%%%%%%%%%%%%%%%%%%%%%%%%%%%%%%%%%%%%%%%%%%%%%%%%%%%%%%%%%%%%%%%%

clear all; clc; close all

%%%%%%%%%%%%%%%%%%%%%%%%%%%%%%%%%%%%%%%%%%%%%%%%%%%%%%%%%%%%%%%%%%%%%%%%%%%%
%% User-Defined Simulation Initial Conditions
%Simulation Options: 1 = Variable coefficient of lift
%                    2 = Variable flight-path angle
%                    3 = Variable altitude and flight-path angle
%                    4 = Variable vehicle heading angle
%                    5 = Variable vehicle bank angle
Sim_Choice = 5;

%Vehicle Options: 1 = X-37B (m = 4989.5 kg, Cd = 0.5)
%                 2 = ESPA SPL Notional Satellite (m = 200 kg, Cd = 2.2)
%                 3 = Notional Satellite (m = 1000 kg, Cd = 2.2)
Vehicle_Choice = 1;

h_max = 500; %Max. altitude for continuous-thrusting orbit-raising (km)


if Sim_Choice == 1
    h = 400; %Entry orbit altitude (km)
    gamma_e = -10.0; %Flight-path angle (deg)

    theta_e = 110; %Initial simulation longitude (deg)
    phi_e = 35.05; %Initial simulation latitude (deg)
    psi_e = 0.0; %Vehicle heading angle (deg)
    sigma_e = 0.0; %Vehicle bank angle (deg)

elseif Sim_Choice == 2
    h = 400; %Entry orbit altitude (km)
    gamma_e = [-10.0,-15.0,-20.0,-25.0]; %Flight-path angle vector (deg)

    theta_e = 110; %Initial simulation longitude (deg)
```

```
    phi_e = 35.05; %Initial simulation latitude (deg)
    psi_e = 0.0; %Vehicle heading angle (deg)
    sigma_e = 0.0; %Vehicle bank angle (deg)

elseif Sim_Choice == 3
    h_vec = [100,120,140,150,160,180,200,400]; %Entry orbit altitude (km)
    gamma_e = linspace(-5,-30);

    theta_e = 110; %Initial simulation longitude (deg)
    phi_e = 35.05; %Initial simulation latitude (deg)
    psi_e = 0.0; %Vehicle heading angle (deg)
    sigma_e = 0.0; %Vehicle bank angle (deg)

elseif Sim_Choice == 4
    psi_e = linspace(-80,80); %Heading angle vector (deg)
    psi_e = psi_e';
    gamma_e = -10.0; %Flight-path angle (deg)

    h = 120; %Entry orbit altitude (km)
    theta_e = 0; %Initial simulation longitude (deg)
    phi_e = 0; %Initial simulation latitude (deg)
    sigma_e = 0; %Vehicle bank angle (deg)

elseif Sim_Choice == 5
    sigma_e = [-40,-30,-20,-15,-10,-5,-4,-3,-2,-1,0,...
               1,2,3,4,5,10,15,20,30,40]; %Vehicle bank angle vector (deg)
    sigma_e = sigma_e';
    gamma_e = -10.0; %Flight-path angle (deg)

    h = 200; %Entry orbit altitude (km)
    theta_e = 0; %Initial simulation longitude (deg)
    phi_e = 0; %Initial simulation latitude (deg)
    psi_e = 0; %Vehicle heading angle (deg)
end

%%%%%%%%%%%%%%%%%%%%%%%%%%%%%%%%%%%%%%%%%%%%%%%%%%%%%%%%%%%%%%%%%%%%%%%%%%%%
%% Vehicle Model
if Vehicle_Choice == 1
    m = 4989.5; %Wet mass; X-37B (kg)
    Cd = 0.5; %Approx. coefficient of drag for lifting entry vehicles

elseif Vehicle_Choice == 2
    m = 200; %Wet mass; ESPA SPL notional satellite (kg)
    Cd = 2.2; %Approx. coefficient of drag for satellites

elseif Vehicle_Choice == 3
    m = 1000; %Wet mass; Primary payload notional satellite (kg)
    Cd = 2.2; %Approx. coefficient of drag for satellites
end

%%%%%%%%%%%%%%%%%%%%%%%%%%%%%%%%%%%%%%%%%%%%%%%%%%%%%%%%%%%%%%%%%%%%%%%%%%%%
%% Gravity Model
r0 = 6378.137; %Earth planetary radius (km)
```

```
r_max = r0+ h_max; %Max. radius for continuous-thrusting orbit-raising (km)
MU = 398600.5; %Earth gravitational parameter (km^3/s^2)
g0 = 0.00981; %Gravitational acceleration at planetary surface (km/s^2)

%%%%%%%%%%%%%%%%%%%%%%%%%%%%%%%%%%%%%%%%%%%%%%%%%%%%%%%%%%%%%%%%%%%%%%%%%%%%%%%
%% Vehicle Aerodynamics
S_m2 = 18.63; %Planform Area (m^2)

L2D = linspace(0.8,2.0,25); %Lift-to-drag ratio
%Lift-to-drag ratio vector:
%L2D = [0.80,0.85,0.90,0.95,1.00,
%       1.05,1.10,1.15,1.20,1.25,
%       1.30,1.35,1.40,1.45,1.50,
%       1.55,1.60,1.65,1.70,1.75,
%       1.80,1.85,1.90,1.95,2.00]

Cl_vec = L2D.*Cd; %Coefficient of lift vector

%%%%%%%%%%%%%%%%%%%%%%%%%%%%%%%%%%%%%%%%%%%%%%%%%%%%%%%%%%%%%%%%%%%%%%%%%%%%%%%
if Sim_Choice == 1

%% Test Case Set #1: Variable Coefficient of Lift
r = r0 + h; %Mission/entry orbit radius (km)
V = sqrt(MU/r); %Initial vehicle velocity (km/s)
g_r = g0*(r0/r)^2; %Gravitational acceleration at given radius (km/s^2)

[r1,V1,T_total1,gamma_e1,theta_e1,phi_e1,incl_deg1,...
 ag_decel_mag1,L1,D1,qdot_s1,Skip_DeltaV1,...
 Maneuver_DeltaV1,Delta_Gamma1,Th_First_min1] = ...
 ManeuverSimFunc(m,Cd,Cl_vec(3),S_m2,gamma_e,theta_e,phi_e,psi_e,sigma_e,h,h_max,V);

[r2,V2,T_total2,gamma_e2,theta_e2,phi_e2,incl_deg2,...
 ag_decel_mag2,L2,D2,qdot_s2,Skip_DeltaV2,...
 Maneuver_DeltaV2,Delta_Gamma2,Th_First_min2] = ...
 ManeuverSimFunc(m,Cd,Cl_vec(5),S_m2,gamma_e,theta_e,phi_e,psi_e,sigma_e,h,h_max,V);

[r3,V3,T_total3,gamma_e3,theta_e3,phi_e3,incl_deg3,...
 ag_decel_mag3,L3,D3,qdot_s3,Skip_DeltaV3,...
 Maneuver_DeltaV3,Delta_Gamma3,Th_First_min3] = ...
 ManeuverSimFunc(m,Cd,Cl_vec(15),S_m2,gamma_e,theta_e,phi_e,psi_e,sigma_e,h,h_max,V);

[r4,V4,T_total4,gamma_e4,theta_e4,phi_e4,incl_deg4,...
 ag_decel_mag4,L4,D4,qdot_s4,Skip_DeltaV4,...
 Maneuver_DeltaV4,Delta_Gamma4,Th_First_min4] = ...
 ManeuverSimFunc(m,Cd,Cl_vec(25),S_m2,gamma_e,theta_e,phi_e,psi_e,sigma_e,h,h_max,V);

%% Plotting of Vehicle Position (km) vs. Time (sec)
subplot(2,3,1), plot(T_total1,r1-r0,T_total2,r2-r0,...
                     T_total3,r3-r0,T_total4,r4-r0); grid off;
legend('\itL/D\rm =0.9','\itL/D\rm =1.0',...
       '\itL/D\rm =1.5','\itL/D\rm =2.0','Location','Southeast');
title('Skip Entry Vehicle Position');
xlabel('Time, \itt\rm (sec)'); ylabel('Altitude, \ith\rm (km)');
```

```
%% Plotting of Vehicle Velocity (km/s) vs. Time (sec)
subplot(2,3,2), plot(T_total1,V1,T_total2,V2,...
                     T_total3,V3,T_total4,V4); grid off;
legend('\itL/D\rm =0.9','\itL/D\rm =1.0',...
       '\itL/D\rm =1.5','\itL/D\rm =2.0','Location','Southeast');
title('Skip Entry Vehicle Velocity');
xlabel('Time, \itt\rm (sec)'); ylabel('Velocity, \it^RV\rm (km/s)');

%% Plotting of Stagnation Heat Flux vs. Time (sec)
subplot(2,3,3), plot(T_total1,qdot_s1,T_total2,qdot_s2,...
                     T_total3,qdot_s3,T_total4,qdot_s4); grid off;
legend('\itL/D\rm =0.9','\itL/D\rm =1.0',...
       '\itL/D\rm =1.5','\itL/D\rm =2.0','Location','Southeast');
title('Vehicle Stagnation Heat Flux Profile');
xlabel('Time, \itt\rm (sec)'); ylabel('Stagnation Heat Flux, \itq_s\rm');

%% Plotting of Lift Force (N) vs. Time (sec)
subplot(2,3,4), plot(T_total1,L1,T_total2,L2,T_total3,L3,T_total4,L4); grid off;
legend('\itL/D\rm =0.9','\itL/D\rm =1.0',...
       '\itL/D\rm =1.5','\itL/D\rm =2.0','Location','Northeast');
title('Vehicle Lift Force Profile');
xlabel('Time, \itt\rm (sec)'); ylabel('Lift, \itL\rm (N)');

%% Plotting of Drag Force (N) vs. Time (sec)
subplot(2,3,5), plot(T_total1,D1,T_total2,D2,T_total3,D3,T_total4,D4); grid off;
legend('\itL/D\rm =0.9','\itL/D\rm =1.0',...
       '\itL/D\rm =1.5','\itL/D\rm =2.0','Location','Northeast');
title('Vehicle Drag Force Profile');
xlabel('Time, \itt\rm (sec)'); ylabel('Drag, \itD\rm (N)');

%% Plotting of Vehicle Deceleration vs. Time (sec)
subplot(2,3,6), plot(T_total1,ag_decel_mag1,...
                     T_total2,ag_decel_mag2,...
                     T_total3,ag_decel_mag3,...
                     T_total4,ag_decel_mag4); grid off;
legend('\itL/D\rm =0.9','\itL/D\rm =1.0',...
       '\itL/D\rm =1.5','\itL/D\rm =2.0','Location','Northeast');
title('Skip Entry Deceleration (a/g_0) Profile');
xlabel('Time, \itt\rm (sec)'); ylabel('Vehicle Deceleration, (a/g_0)');

%%%%%%%%%%%%%%%%%%%%%%%%%%%%%%%%%%%%%%%%%%%%%%%%%%%%%%%%%%%%%%%%%%%%%%%%%%%%
elseif Sim_Choice == 2

%% Test Case Set #2: Variable Flight-Path Angle
r = r0 + h; %Mission/entry orbit radius (km)
V = sqrt(MU/r); %Initial vehicle velocity (km/s)
g_r = g0*(r0/r)^2; %Gravitational acceleration at given radius (km/s^2)

[r1,V1,T_total1,gamma_e1,theta_e1,phi_e1,incl_deg1,...
 ag_decel_mag1,L1,D1,qdot_s1,Skip_DeltaV1,...
 Maneuver_DeltaV1,Delta_Gamma1,Th_First_min1] = ...
 ManeuverSimFunc(m,Cd,Cl_vec(5),S_m2,gamma_e(1),theta_e,...
                 phi_e,psi_e,sigma_e,h,h_max,V);
```

```
[r2,V2,T_total2,gamma_e2,theta_e2,phi_e2,incl_deg2,...
 ag_decel_mag2,L2,D2,qdot_s2,Skip_DeltaV2,...
 Maneuver_DeltaV2,Delta_Gamma2,Th_First_min2] = ...
 ManeuverSimFunc(m,Cd,Cl_vec(5),S_m2,gamma_e(2),theta_e,...
                 phi_e,psi_e,sigma_e,h,h_max,V);

[r3,V3,T_total3,gamma_e3,theta_e3,phi_e3,incl_deg3,...
 ag_decel_mag3,L3,D3,qdot_s3,Skip_DeltaV3,...
 Maneuver_DeltaV3,Delta_Gamma3,Th_First_min3] = ...
 ManeuverSimFunc(m,Cd,Cl_vec(5),S_m2,gamma_e(3),theta_e,...
                 phi_e,psi_e,sigma_e,h,h_max,V);

[r4,V4,T_total4,gamma_e4,theta_e4,phi_e4,incl_deg4,...
 ag_decel_mag4,L4,D4,qdot_s4,Skip_DeltaV4,...
 Maneuver_DeltaV4,Delta_Gamma4,Th_First_min4] = ...
 ManeuverSimFunc(m,Cd,Cl_vec(5),S_m2,gamma_e(4),theta_e,...
                 phi_e,psi_e,sigma_e,h,h_max,V);

%% Plotting of Vehicle Position (km) vs. Time (sec)
subplot(2,3,1), plot(T_total1,r1-r0,T_total2,r2-r0,...
                     T_total3,r3-r0,T_total4,r4-r0); grid off;
legend('\gamma_e=-10.0^o','\gamma_e=-15.0^o',...
       '\gamma_e=-20.0^o','\gamma_e=-25.0^o','Location','Southeast');
title('Skip Entry Vehicle Position');
xlabel('Time, \itt\rm (sec)'); ylabel('Altitude, \ith\rm (km)');

%% Plotting of Vehicle Velocity (km/s) vs. Time (sec)
subplot(2,3,2), plot(T_total1,V1,T_total2,V2,...
                     T_total3,V3,T_total4,V4); grid off;
legend('\gamma_e=-10.0^o','\gamma_e=-15.0^o',...
       '\gamma_e=-20.0^o','\gamma_e=-25.0^o','Location','Southeast');
title('Skip Entry Vehicle Velocity');
xlabel('Time, \itt\rm (sec)'); ylabel('Velocity, \it^RV\rm (km/s)');

%% Plotting of Stagnation Heat Flux vs. Time (sec)
subplot(2,3,3), plot(T_total1,qdot_s1,T_total2,qdot_s2,...
                     T_total3,qdot_s3,T_total4,qdot_s4); grid off;
legend('\gamma_e=-10.0^o','\gamma_e=-15.0^o',...
       '\gamma_e=-20.0^o','\gamma_e=-25.0^o','Location','Northeast');
title('Vehicle Stagnation Heat Flux Profile');
xlabel('Time, \itt\rm (sec)'); ylabel('Stagnation Heat Flux, \itq_s\rm');

%% Plotting of Lift Force (N) vs. Time (sec)
subplot(2,3,4), plot(T_total1,L1,T_total2,L2,...
                     T_total3,L3,T_total4,L4); grid off;
legend('\gamma_e=-10.0^o','\gamma_e=-15.0^o',...
       '\gamma_e=-20.0^o','\gamma_e=-25.0^o','Location','Northeast');
title('Vehicle Lift Force Profile');
xlabel('Time, \itt\rm (sec)'); ylabel('Lift, \itL\rm (N)');

%% Plotting of Drag Force (N) vs. Time (sec)
subplot(2,3,5), plot(T_total1,D1,T_total2,D2,...
                     T_total3,D3,T_total4,D4); grid off;
```

```
legend('\gamma_e=-10.0^o','\gamma_e=-15.0^o',...
       '\gamma_e=-20.0^o','\gamma_e=-25.0^o','Location','Northeast');
title('Vehicle Drag Force Profile');
xlabel('Time, \itt\rm (sec)'); ylabel('Drag, \itD\rm (N)');

%% Plotting of Vehicle Deceleration vs. Time (sec)
subplot(2,3,6), plot(T_total1,ag_decel_mag1,...
                     T_total2,ag_decel_mag2,...
                     T_total3,ag_decel_mag3,...
                     T_total4,ag_decel_mag4); grid off;
legend('\gamma_e=-10.0^o','\gamma_e=-15.0^o',...
       '\gamma_e=-20.0^o','\gamma_e=-25.0^o','Location','Northeast');
title('Skip Entry Deceleration (a/g_0) Profile');
xlabel('Time, \itt\rm (sec)'); ylabel('Vehicle Deceleration, (a/g_0)');

%%%%%%%%%%%%%%%%%%%%%%%%%%%%%%%%%%%%%%%%%%%%%%%%%%%%%%%%%%%%%%%%%%%%%%%%%%%%%%%
elseif Sim_Choice == 3

%% Test Case Set #3: Variable Altitude and Flight-Path Angle
%Altitude Cases: [100,120,140,150,160,180,200,400] (km)
alt_case = 8; %User input: 1 = 100 km, 8 = 400 km
h = h_vec(alt_case); r = r0 + h; %Mission/entry orbit alt./radius (km)
V = sqrt(MU/r); %Initial vehicle velocity (km/s)
g_r = g0*(r0/r)^2; %Gravitational acceleration at given radius (km/s^2)

for ctr_gamma = 1:length(gamma_e)
    [r1,V1,T_total1,...
     gamma_e1,theta_e1,phi_e1,incl_deg1,...
     ag_decel_mag1,L1,D1,qdot_s1,...
     Skip_DeltaV1,Maneuver_DeltaV1,Delta_Gamma1,Th_first1] = ...
     ManeuverSimFunc(m,Cd,Cl_vec(5),S_m2,gamma_e(ctr_gamma),...
                     theta_e,phi_e,psi_e,sigma_e,h,h_max,V);

    Skip_dV_vec1(ctr_gamma,:) = Skip_DeltaV1;
    Maneuver_dV_vec1(ctr_gamma,:) = Maneuver_DeltaV1;
    Delta_Gamma_vec1(ctr_gamma,:) = rad2deg(Delta_Gamma1);
    Th_first_vec1(ctr_gamma,:) = Th_first1;

    [r2,V2,T_total2,...
     gamma_e2,theta_e2,phi_e2,incl_deg2,...
     ag_decel_mag2,L2,D2,qdot_s2,...
     Skip_DeltaV2,Maneuver_DeltaV2,Delta_Gamma2,Th_first2] = ...
     ManeuverSimFunc(m,Cd,Cl_vec(15),S_m2,gamma_e(ctr_gamma),...
                     theta_e,phi_e,psi_e,sigma_e,h,h_max,V);

    Skip_dV_vec2(ctr_gamma,:) = Skip_DeltaV2;
    Maneuver_dV_vec2(ctr_gamma,:) = Maneuver_DeltaV2;
    Delta_Gamma_vec2(ctr_gamma,:) = rad2deg(Delta_Gamma2);
    Th_first_vec2(ctr_gamma,:) = Th_first2;

    [r3,V3,T_total3,...
     gamma_e3,theta_e3,phi_e3,incl_deg3,...
     ag_decel_mag3,L3,D3,qdot_s3,...
     Skip_DeltaV3,Maneuver_DeltaV3,Delta_Gamma3,Th_first3] = ...
```

```
     ManeuverSimFunc(m,Cd,Cl_vec(25),S_m2,gamma_e(ctr_gamma),...
                     theta_e,phi_e,psi_e,sigma_e,h,h_max,V);

    Skip_dV_vec3(ctr_gamma,:) = Skip_DeltaV3;
    Maneuver_dV_vec3(ctr_gamma,:) = Maneuver_DeltaV3;
    Delta_Gamma_vec3(ctr_gamma,:) = rad2deg(Delta_Gamma3);
    Th_first_vec3(ctr_gamma,:) = Th_first3;

    Max_dV_vec(ctr_gamma,:) = [3]; %Maximum delta-V capability of entry vehicle

    %Total Delta-V required to complete two skip entry maneuvers at the
    %same entry flight-path angle
    Total_dV_vec1 = Skip_dV_vec1 + Maneuver_dV_vec1;
    Total_dV_vec2 = Skip_dV_vec2 + Maneuver_dV_vec2;
    Total_dV_vec3 = Skip_dV_vec3 + Maneuver_dV_vec3;

    %Delta-V remaining following two skip entry maneuvers
    Residual_dV_vec1 = Total_dV_vec1 - Max_dV_vec;
    Residual_dV_vec2 = Total_dV_vec2 - Max_dV_vec;
    Residual_dV_vec3 = Total_dV_vec3 - Max_dV_vec;
end

%% Plotting of Min. Altitude of Trajectory (km) vs. Flight-Path Angle (deg)
plot(gamma_e,Th_first_vec1(:,2),gamma_e,Th_first_vec2(:,2),gamma_e,Th_first_vec3(:,2)
)
set(gca,'XDir','reverse')
legend('\itL/D\rm =1.0','\itL/D\rm =1.5','\itL/D\rm =2.0','Location','Southwest');
title('Minimum Altitude of Skip Entry Trajectory');
xlabel('Flight-Path Angle, \gamma (deg)'); ylabel('Altitude, \ith\rm (km)');

figure
%% Plotting of Delta-V (km/s) for First Skip Entry vs. Flight-Path Angle (deg)
subplot(1,2,1), plot(gamma_e,Skip_dV_vec1,gamma_e,Skip_dV_vec2,gamma_e,Skip_dV_vec3)
set(gca,'XDir','reverse')
legend('\itL/D\rm =1.0','\itL/D\rm =1.5','\itL/D\rm =2.0','Location','Southeast');
title({'\it\DeltaV\rm Required for','First Skip Entry Trajectory'});
xlabel('Flight-Path Angle, \gamma (deg)'); ylabel('\it\DeltaV\rm (km/s)');

%% Plotting of Delta-V (km/s) for Second Skip Entry vs. Flight-Path Angle (deg)
subplot(1,2,2),
plot(gamma_e,Maneuver_dV_vec1,gamma_e,Maneuver_dV_vec2,gamma_e,Maneuver_dV_vec3)
set(gca,'XDir','reverse')
legend('\itL/D\rm =1.0','\itL/D\rm =1.5','\itL/D\rm =2.0','Location','Southeast');
title({'\it\DeltaV\rm Required for','Second Skip Entry Trajectory'});
xlabel('Flight-Path Angle, \gamma (deg)'); ylabel('\it\DeltaV\rm (km/s)');

figure
%% Plotting of Total Delta-V (km/s) vs. Flight-Path Angle (deg)
subplot(1,2,1),
plot(gamma_e,Total_dV_vec1,gamma_e,Total_dV_vec2,gamma_e,Total_dV_vec3)
set(gca,'XDir','reverse')
hold on; plot(gamma_e,Max_dV_vec,'--r')
legend('\itL/D\rm =1.0','\itL/D\rm =1.5','\itL/D\rm =2.0','Location','Northwest');
title('\it\DeltaV\rm Required for Initiation of Two Skip Entry Maneuvers');
```

```
xlabel('Flight-Path Angle, \gamma (deg)'); ylabel('\it\DeltaV\rm (km/s)');


%% Plotting of Total Delta-V (km/s) vs. Flight-Path Angle (deg)
subplot(1,2,2),
plot(gamma_e,Total_dV_vec1,gamma_e,Total_dV_vec2,gamma_e,Total_dV_vec3)
xlim([-10 -5]); ylim([1 4]); set(gca,'XDir','reverse');
hold on; plot(gamma_e,Max_dV_vec,'--r')
legend('\itL/D\rm =1.0','\itL/D\rm =1.5','\itL/D\rm =2.0','Location','Southeast');
xlabel('Flight-Path Angle, \gamma (deg)'); ylabel('\it\DeltaV\rm (km/s)');

figure
%% Plotting of Delta-Flight-Path Angle (deg) vs. Flight-Path Angle (deg)
plot(gamma_e,Delta_Gamma_vec1,gamma_e,Delta_Gamma_vec2,gamma_e,Delta_Gamma_vec3)
set(gca,'XDir','reverse')
legend('\itL/D\rm =1.0','\itL/D\rm =1.5','\itL/D\rm =2.0','Location','Southeast');
title({'Difference between Exit and Entry Flight-Path Angle',...
       'for a Single Skip Entry Trajectory'});
xlabel('Flight-Path Angle, \gamma (deg)'); ylabel('\Delta\gamma (deg)');

%%%%%%%%%%%%%%%%%%%%%%%%%%%%%%%%%%%%%%%%%%%%%%%%%%%%%%%%%%%%%%%%%%%%%%%%%%%%%%%
elseif Sim_Choice == 4

%% Test Case Set #4: Variable Heading Angle
r = r0 + h; %Mission/entry orbit radius (km)
V = sqrt(MU/r); %Initial vehicle velocity (km/s)
g_r = g0*(r0/r)^2; %Gravitational acceleration at given radius (km/s^2)

for ctr_psi = 1:length(psi_e)
    [r1,V1,T_total1,...
     gamma_e1,theta_e1,phi_e1,incl_deg1,...
     ag_decel_mag1,L1,D1,qdot_s1,...
     Skip_DeltaV1,Maneuver_DeltaV1,Th_first1] = ...
     ManeuverSimFunc(m,Cd,Cl_vec(5),S_m2,gamma_e,theta_e,...
                     phi_e,psi_e(ctr_psi),sigma_e,h,h_max,V);

    phi_e_vec1(ctr_psi,:) = rad2deg(phi_e1(end));
    incl_deg_vec1(ctr_psi,:) = incl_deg1;
    delta_i_vec1(ctr_psi,:) = abs(incl_deg_vec1(ctr_psi,:) - phi_e);
    Skip_dV_vec1(ctr_psi,:) = Skip_DeltaV1;

    [r2,V2,T_total2,...
     gamma_e2,theta_e2,phi_e2,incl_deg2,...
     ag_decel_mag2,L2,D2,qdot_s2,...
     Skip_DeltaV2,Maneuver_DeltaV2,Th_first2] = ...
     ManeuverSimFunc(m,Cd,Cl_vec(15),S_m2,gamma_e,theta_e,...
                     phi_e,psi_e(ctr_psi),sigma_e,h,h_max,V);

    phi_e_vec2(ctr_psi,:) = rad2deg(phi_e2(end));
    incl_deg_vec2(ctr_psi,:) = incl_deg2;
    delta_i_vec2(ctr_psi,:) = abs(incl_deg_vec2(ctr_psi,:) - phi_e);
    Skip_dV_vec2(ctr_psi,:) = Skip_DeltaV2;
```

```
    [r3,V3,T_total3,...
     gamma_e3,theta_e3,phi_e3,incl_deg3,...
     ag_decel_mag3,L3,D3,qdot_s3,...
     Skip_DeltaV3,Maneuver_DeltaV3,Th_first3] = ...
     ManeuverSimFunc(m,Cd,Cl_vec(25),S_m2,gamma_e,theta_e,...
                     phi_e,psi_e(ctr_psi),sigma_e,h,h_max,V);

    phi_e_vec3(ctr_psi,:) = rad2deg(phi_e3(end));
    incl_deg_vec3(ctr_psi,:) = incl_deg3;
    delta_i_vec3(ctr_psi,:) = abs(incl_deg_vec3(ctr_psi,:) - phi_e);
    Skip_dV_vec3(ctr_psi,:) = Skip_DeltaV3;

end

%% Plotting of Exit Latitude (deg) vs. Entry Heading Angle (deg)
plot(psi_e,phi_e_vec1,psi_e,phi_e_vec2,psi_e,phi_e_vec3)
% legend('\itL/D\rm =1.0','\itL/D\rm =1.5','\itL/D\rm =2.0','Location','Southeast');
xlabel('Entry Heading Angle, \psi (deg)'); ylabel('Exit Latitude, \phi (deg)');

figure
%% Plotting of Exit Latitude (deg) vs. Inclination Angle (deg)
plot(psi_e,incl_deg_vec1,psi_e,incl_deg_vec2,psi_e,incl_deg_vec3)
% legend('\itL/D\rm =1.0','\itL/D\rm =1.5','\itL/D\rm =2.0','Location','Southeast');
xlabel('Entry Heading Angle, \psi (deg)'); ylabel('Inclination, \iti\rm (deg)');

%% Plotting of Change in Inclination (deg) vs. Entry Heading Angle (deg)
figure; plot(psi_e,delta_i_vec1,psi_e,delta_i_vec2,psi_e,delta_i_vec3)
% legend('\itL/D\rm =1.0','\itL/D\rm =1.5','\itL/D\rm =2.0','Location','Southeast');
xlabel('Entry Heading Angle, \psi (deg)');
ylabel('Change in Inclination, \it\Deltai\rm (deg)');

%%%%%%%%%%%%%%%%%%%%%%%%%%%%%%%%%%%%%%%%%%%%%%%%%%%%%%%%%%%%%%%%%%%%%%%%%%%%
elseif Sim_Choice == 5

%% Test Case Set #5: Variable Bank Angle
r = r0 + h; %Mission/entry orbit radius (km)
V = sqrt(MU/r); %Initial vehicle velocity (km/s)
g_r = g0*(r0/r)^2; %Gravitational acceleration at given radius (km/s^2)

for ctr_sigma = 1:length(sigma_e)
    [r1,V1,T_total1,...
     gamma_e1,theta_e1,phi_e1,incl_deg1,...
     ag_decel_mag1,L1,D1,qdot_s1,...
     Skip_DeltaV1,Maneuver_DeltaV1,Th_first1] = ...
     ManeuverSimFunc(m,Cd,Cl_vec(5),S_m2,gamma_e,theta_e,...
                     phi_e,psi_e,sigma_e(ctr_sigma),h,h_max,V);

    incl_deg_vec1(ctr_sigma,:) = incl_deg1;
    delta_i_vec1(ctr_sigma,:) = abs(incl_deg_vec1(ctr_sigma,:) - phi_e);
    Skip_dV_vec1(ctr_sigma,:) = Skip_DeltaV1;

    [r2,V2,T_total2,...
     gamma_e2,theta_e2,phi_e2,incl_deg2,...
```

```
     ag_decel_mag2,L2,D2,qdot_s2,...
     Skip_DeltaV2,Maneuver_DeltaV2,Th_first2] = ...
     ManeuverSimFunc(m,Cd,Cl_vec(5),S_m2,gamma_e,theta_e,...
                     phi_e,psi_e,sigma_e(ctr_sigma),h,h_max,V);

    incl_deg_vec2(ctr_sigma,:) = incl_deg2;
    delta_i_vec2(ctr_sigma,:) = abs(incl_deg_vec2(ctr_sigma,:) - phi_e);
    Skip_dV_vec2(ctr_sigma,:) = Skip_DeltaV2;

    [r3,V3,T_total3,...
     gamma_e3,theta_e3,phi_e3,incl_deg3,...
     ag_decel_mag3,L3,D3,qdot_s3,...
     Skip_DeltaV3,Maneuver_DeltaV3,Th_first3] = ...
     ManeuverSimFunc(m,Cd,Cl_vec(5),S_m2,gamma_e,theta_e,...
                     phi_e,psi_e,sigma_e(ctr_sigma),h,h_max,V);

    incl_deg_vec3(ctr_sigma,:) = incl_deg3;
    delta_i_vec3(ctr_sigma,:) = abs(incl_deg_vec3(ctr_sigma,:) - phi_e);
    Skip_dV_vec3(ctr_sigma,:) = Skip_DeltaV3;

end

%% Plotting of Inclination (deg) vs. Entry Bank Angle (deg)
plot(sigma_e,incl_deg_vec1,sigma_e,incl_deg_vec2,sigma_e,incl_deg_vec3)
% legend('\itL/D\rm =1.0','\itL/D\rm =1.5','\itL/D\rm =2.0','Location','Southeast');
xlabel('Entry Bank Angle, \sigma (deg)'); ylabel('Inclination, \iti\rm (deg)');

figure
%% Plotting of Change in Inclination (deg) vs. Entry Bank Angle (deg)
plot(sigma_e,delta_i_vec1,sigma_e,delta_i_vec2,sigma_e,delta_i_vec3)
% legend('\itL/D\rm =1.0','\itL/D\rm =1.5','\itL/D\rm =2.0','Location','Southeast');
xlabel('Entry Bank Angle, \sigma (deg)');
ylabel('Change in Inclination, \it\Deltai\rm (deg)');

end
```

```
function [r,V,T_total,gamma_e,theta_e,phi_e,incl_deg...
          ag_decel_mag,L,D,qdot_s,...
          Skip_DeltaV,Maneuver_DeltaV,Delta_Gamma,Th_first_min] = ...
          ManeuverSimFunc(m,Cd,Cl,S_m2,gamma_e,theta_e,phi_e,psi_e,sigma_e,h,h_max,V)

%%%%%%%%%%%%%%%%%%%%%%%%%%%%%%%%%%%%%%%%%%%%%%%%%%%%%%%%%%%%%%%%%%%%%%%%%%%%
%
% Use: [r,V,T_total,gamma_e,theta_e,phi_e,incl_deg...
%       ag_decel_mag,L,D,qdot_s,...
%       Skip_DeltaV,Maneuver_DeltaV,Delta_Gamma,Th_first_min] = ...
%       ManeuverSimFunc(m,Cd,Cl,S_m2,gamma_e,theta_e,phi_e,psi_e,sigma_e,h,h_max,V)
%
% This function calculates the skip entry maneuver profile for a
% user-defined entry vehicle and initial orbit conditions.
%
% Author/Date: Bettinger, Robert AFIT/ENY                      Spring 2011
%
% Inputs:
%   m             - Mass of vehicle (kg)
%   Cd            - Coefficient of drag
%   Cl            - Coefficient of lift
%   S_m2          - Planform area (m^2)
%   gamma_e       - Flight-path angle (deg)
%   theta_e       - Longitude (deg)
%   phi_e         - Latitude (deg)
%   psi_e         - Vehicle heading angle (deg)
%   sigma_e       - Vehicle bank angle (deg)
%   h             - Mission orbit altitude (km)
%   h_max         - Max. altitude for continuous-thrusting orbit-raising (km)
%   V             - Entry orbit velocity (km/s)
%
% Outputs:
%   r                     - Position vector of maneuver (km)
%   V                     - Velocity vector of maneuver (km/s)
%   T_total               - Total time of maneuver (s)
%   theta_e               - Longitude (rad)
%   phi_e                 - Latitude (rad)
%   incl_deg              - Inclinaton (deg)
%   ag_decel_mag          - Magnitude of vehicle deceleration
%   L                     - Lift force (N)
%   D                     - Drag force (N)
%   qdot_s                - Vehicle stagnation heat flux
%   Skip_DeltaV           - Delta-V required for initial skip entry
%                           maneuver (km)
%   Maneuver_DeltaV       - Delta-V required for subsequent skip entry
%                           maneuver (km/s)
%   Delta_Gamma           - Change in flight-path angle (rad)
%   Th_first_min          - First altitude minimum in trajectory (km)
%
% Globals:  None
% Constants:
%   r0            - Earth planetary radius (km)
%   MU            - Earth gravitational parameter (km^3/s^2)
%   g0            - Gravitational acceleration at planetary surface (km/s^2)
%   omega_e       - Planetary rotational velocity (rad/s)
```

```
%   beta         - Atmospheric scale height (km^-1)
%   rho0         - Atmospheric density at planetary surface (kg/km^3)
%
% Coupling: None
%
% References: Hicks, Kerry D. Introduction to Astrodynamic Reentry.
%             Wright-Patterson AFB: AF Institute of Technology, 2003.
%
%             Vallado, David A. Fundamentals of Astrodynamics and
%             Applications. Boston: Microcosm Press, 2001.
%
%%%%%%%%%%%%%%%%%%%%%%%%%%%%%%%%%%%%%%%%%%%%%%%%%%%%%%%%%%%%%%%%%%%%%%%%%%%%%%%

format long

%% User-Defined Simulation Initial Conditions
deltaT = 0.1; %Simulation propagation time-step (sec)
Scenario_Choice = 1; %1 = Single skip entry scenario
                     %2 = Continuous-thrusting orbit-raising OR
                     %    Multiple skip entry scenario

%% Gravity Model
r0 = 6378.137; %Earth planetary radius (km)
r = r0 + h; %Mission/entry orbit radius (km)
r_max = r0+ h_max; %Max. radius for continuous-thrusting orbit-raising (km)
MU = 398600.5; %Earth gravitational parameter (km^3/s^2)
g0 = 0.00981; %Gravitational acceleration at planetary surface (km/s^2)
g_r = g0*(r0/r)^2; %Gravitational acceleration at given radius (km/s^2)

%% Atmosphere/Planet Model
omega_e = 0; %7.292115e-5; %Planetary rotational velocity (rad/s) (Vallado 138)
beta = 0.14; %Atmospheric scale height (km^-1)
rho0 = 1.225 * (1000)^3; %Atmospheric density at planetary surface (kg/km^3)
rho_r = rho0*exp(-beta*(r - r0)); %Atmospheric density at given radius (kg/km^3)

%% Orbit Model
e = 0.0; %Entry orbit eccentricity
a = r/(1-e); %Entry orbit semi-major axis (km)
n = sqrt(MU/(a^3)); %Entry orbit mean motion (rad/s)
SMA = -MU/(2*a); %Entry orbit specific mechanical energy (km^2/s^2)

%% Vehicle Model
%Engine Parameters
%Thrust Options: 14679 N (Impulsive thrusting; H2O2/JP-8; X-37B)
%                13345 N (Impulsive thrusting; H2O2/JP-10; X-37B)
%                 9901 N (Impulsive thrusting; H2O2; X-37B)
%               300E-3 N (Continuous thrusting; notional satellite)
%               500E-3 N (Continuous thrusting; notional satellite)
T_max = 0; %Maximum thrust (N)
Throttle = 50; %Throttle (percentage)
T = T_max * (Throttle/100); %Magnitude of thrust (N)
eps_T = deg2rad(0.0); %Angle between thrust and velocity vectors (rad)
zeta_T = deg2rad(0.0); %Angle between thrust and velocity vectors (rad)
```

```
%Vehicle Maneuver Constraints
deltaV_max = 5.00; %Maximum vehicle delta-V capability (km/s)
Vf_max = 15.0; %Maximum vehicle final velocity (km/s)
ag_max = 100; %Maximum value of vehicle deceleration
qs_max = 0.25; %Maximum value of vehicle stagnation heat flux

%Vehicle Aerodynamics
S = S_m2 / (1000)^2; %Planform Area (km^2)
D = 0.5*rho_r*Cd*S*V^2; %Drag force (N)
L = 0.5*rho_r*Cl*S*V^2; %Lift force (N)

%% Equations of Motion
%Maneuver Profile Angles
gamma_e(1) = deg2rad(gamma_e); %Flight-path angle (rad)
theta_e(1) = deg2rad(theta_e); %Longitude (rad)
phi_e(1) = deg2rad(phi_e); %Latitude (rad)
psi_e(1) = deg2rad(psi_e); %Vehicle heading angle (rad)
sigma_e(1) = deg2rad(sigma_e); %Vehicle bank angle (rad)

%%%%%%%%%%%%%%%%%%%%%%%%%%%%%%%%%%%%%%%%%%%%%%%%%%%%%%%%%%%%%%%%%%%%%%%%%%%%
%% Numerical Integration of Equations of Motion
r(1) = r; V(1) = V; %Initial conditions for vehicle dynamics
g_r(1) = g_r; rho_r(1) = rho_r; %Initial conditions for entry environment
D(1) = D; L(1) = L; %Initial conditions for vehicle aerodynamics

%Loop end state for vehicle orbit radius
if Scenario_Choice == 1
    r_choice = r(1);
elseif Scenario_Choice == 2
    r_choice = r_max;
end

%Initial vehicle deceleration
a_decel_v(1) = (D(1)/m) + g_r(1)*sin(gamma_e(1)); %Equation (3.31)
a_decel_L(1) = (-L(1)/m) - (((V(1)^2)/r(1)) - g_r(1))*cos(gamma_e(1)); %Equation
(3.32)
a_decel_mag(1) = sqrt((a_decel_v(1))^2 + (a_decel_L(1))^2);
ag_decel_mag(1) = a_decel_mag(1)/g_r(1);

%Initial vehicle stagnation and wall heat flux
qdot_s(1) = sqrt((rho_r(1)*S*Cd)/(2*m*beta))*((V(1)^2)/(2*g_r(1)*r(1)))^(3/2);
qdot_w(1) = ((rho_r(1)*S*Cd)/(2*m*beta))*((V(1)^2)/(2*g_r(1)*r(1)))^(3/2);

T_total(1) = 0; %Initial condition for total mission time

i = 1; %Initializes iteration counter at one
Sim_Time_ctr = 1; %Initializes simulation time counter at one
Sim_Time_Max = 10000; %Maximum user-defined simulation run-time

while (r <= r_choice) & (r > r0) & ...
      (V <= Vf_max) & (ag_decel_mag <= ag_max) & ...
      (qdot_s <= qs_max) & (Sim_Time_ctr < Sim_Time_Max);
```

```
%Vehicle position (r) differential equation
   r_dot = V(i)*sin(gamma_e(i));

   %Vehicle velocity (V) differential equation
   V_dot = ((T/m)*(cos(zeta_T)*cos(eps_T))) - (D(i)/m) - ...
           (g_r(i)*sin(gamma_e(i))) + ...
           (r(i)*(omega_e^2)*cos(phi_e(i))*(cos(phi_e(i))*sin(gamma_e(i)) - ...
            sin(phi_e(i))*sin(psi_e(i))*cos(gamma_e(i))));

   %Vehicle flight-path angle (gamma) differential equation
   Vgamma_dot = ((T/m)*(sin(zeta_T)*sin(sigma_e(i)) + ...
                 cos(zeta_T)*sin(eps_T)*cos(sigma_e(i)))) + ...
                ((L(i)/m)*cos(sigma_e(i))) - (g_r(i)*cos(gamma_e(i))) + ...
                ((V(i)^2)/r(i))*cos(gamma_e(i)) + ...
                (2*V(i)*omega_e*cos(phi_e(i))*cos(psi_e(i))) + ...
                (r(i)*(omega_e^2)*cos(phi_e(i))*(cos(phi_e(i))*cos(gamma_e(i)) + ...
                 sin(phi_e(i))*sin(psi_e(i))*sin(gamma_e(i))));

   %Vehicle longitude (theta) differential equation
   theta_dot = ((V(i)*cos(gamma_e(i))*cos(psi_e(i)))/(r(i)*cos(phi_e(i))));

   %Vehicle latitude (phi) differential equation
   phi_dot = (1/r(i))*(V(i)*cos(gamma_e(i))*sin(psi_e(i)));

   %Vehicle heading angle (psi) differential equation
   Vpsi_dot = (1/(m*cos(gamma_e(i))))*(T*(cos(zeta_T)*sin(eps_T)*sin(sigma_e(i)) -
...
       sin(zeta_T)*cos(sigma_e(i))) + L(i)*sin(sigma_e(i))) - ...
       ((V(i)^2)/r(i))*cos(gamma_e(i))*cos(psi_e(i))*tan(phi_e(i)) + ...
       2*V(i)*omega_e*(sin(psi_e(i))*cos(phi_e(i))*tan(gamma_e(i)) - ...
       sin(phi_e(i))) - ((r(i)*omega_e^2)/cos(gamma_e(i)))* ...
       sin(phi_e(i))*cos(phi_e(i))*cos(psi_e(i));

   %Updates to Vehicle Dynamics
   r(i+1) = r(i) + r_dot*deltaT; %Vehicle position
   V(i+1) = V(i) + V_dot*deltaT; %Vehicle velocity
   gamma_e(i+1) = gamma_e(i) + (Vgamma_dot/V(i))*deltaT; %Flight-path angle

   %Updates to Maneuver Profile Angles
   theta_e(i+1) = theta_e(i) + theta_dot*deltaT;
   phi_e(i+1) = phi_e(i) + phi_dot*deltaT;
   psi_e(i+1) = psi_e(i) + (Vpsi_dot/V(i))*deltaT;
   sigma_e(i+1) = sigma_e(i);

   %Updates to Simulation Environment
   g_r(i+1) = g0*(r0/r(i+1))^2; %Gravitational acceleration
   rho_r(i+1) = rho0*exp(-beta*(r(i+1) - r0)); %Atmospheric density
   D(i+1) = 0.5*rho_r(i+1)*Cd*S*V(i+1)^2; %Drag force
   L(i+1) = 0.5*rho_r(i+1)*Cl*S*V(i+1)^2; %Lift force

   %Update to Vehicle Deceleration
   a_decel_v(i+1) = -V_dot/g_r(i+1);
   a_decel_L(i+1) = -Vgamma_dot/g_r(i+1);
```

```
    ag_decel_mag(i+1) = sqrt((a_decel_v(i+1))^2 + (a_decel_L(i+1))^2);

    %Update to Vehicle Stagnation and Wall Heat Flux
    qdot_s(i+1) = sqrt((rho_r(i+1)*S*Cd)/(2*m*beta))*...
                  ((V(i+1)^2)/(2*g_r(i+1)*r(i+1)))^(3/2);
    qdot_w(i+1) = ((rho_r(i+1)*S*Cd)/(2*m*beta))*...
                  ((V(i+1)^2)/(2*g_r(i+1)*r(i+1)))^(3/2);

    T_total(i+1) = T_total(i) + deltaT; %Update to total skip entry time

    i = i + 1; %Update to iteration counter
    Sim_Time_ctr = Sim_Time_ctr + 1; %Update to simulation time counter

end

%%%%%%%%%%%%%%%%%%%%%%%%%%%%%%%%%%%%%%%%%%%%%%%%%%%%%%%%%%%%%%%%%%%%%%%%%%%%%%%
%% Determination of First Local Altitude Minimum in Trajectory
for ctr_min = 2:length(r)
    if r(ctr_min) < r(ctr_min - 1)
        ctr_min = ctr_min + 1;
    else
        r_first_min = r(ctr_min - 1); %First local radius minimum (km)
        %Time and radius of first local minimum
        Tr_first_min = [T_total(ctr_min - 1),r_first_min];
        ctr_min = ctr_min - 1; %Counter value for first local minimum
        break
    end
end

Th_first_min = Tr_first_min - [0,r0]; %Conversion from radius to altitude

%%%%%%%%%%%%%%%%%%%%%%%%%%%%%%%%%%%%%%%%%%%%%%%%%%%%%%%%%%%%%%%%%%%%%%%%%%%%%%%
%% Determination of First Local Altitude Maximum in Trajectory
for ctr_max = (ctr_min + 1):length(r)
    if r(ctr_max) > r(ctr_max - 1) && ctr_max < length(r)
        ctr_max = ctr_max + 1;
    else
        r_first_max = r(ctr_max); %First local radius minimum (km)
        %Time and radius of first local maximum
        Tr_first_max = [T_total(ctr_max),r_first_max];
        ctr_max = ctr_max; %Counter value for first local maximum
        break
    end
end

Th_first_max = Tr_first_max - [0,r0]; %Conversion from radius to altitude

%%%%%%%%%%%%%%%%%%%%%%%%%%%%%%%%%%%%%%%%%%%%%%%%%%%%%%%%%%%%%%%%%%%%%%%%%%%%%%%
%% Delta-V Required for Initial Skip Entry Maneuver
V_entry1 = V(1);

%Delta-V required to alter vehicle flight-path angle in order to enter into
%skip entry trajectory while maintaining orbital velocity
```

```
Skip_DeltaV = sqrt((V_entry1^2) + (V_entry1^2) - ...
    (2*V_entry1*V_entry1*cos(gamma_e(1))));

%%%%%%%%%%%%%%%%%%%%%%%%%%%%%%%%%%%%%%%%%%%%%%%%%%%%%%%%%%%%%%%%%%%%%%%%%%%%%%%
%% Delta-V Required for Subsequent Skip Entry Maneuver
Boost_DeltaV = abs(V(ctr_max) - V(1));

if V(ctr_max) < sqrt(MU/r(1))
    V_exit = V(ctr_max); %Exit velocity of skip (i)
    V_entry = V(ctr_max) + Boost_DeltaV; %Entry velocity of skip (i+1)
else
    V_exit = V(ctr_max); %Exit velocity of skip (i)
    V_entry = V(ctr_max); %Entry velocity of skip (i+1)
end

Delta_Gamma = abs(gamma_e(ctr_max)-gamma_e(1));%Change in flight-path angle



%Delta-V required to alter vehicle flight-path angle and velocity such that
%Vf = Vi for subsequent skip entry maneuver
Maneuver_DeltaV = sqrt((V_exit^2) + (V_entry^2) - ...
    (2*V_exit*V_entry*cos(Delta_Gamma)));

%%%%%%%%%%%%%%%%%%%%%%%%%%%%%%%%%%%%%%%%%%%%%%%%%%%%%%%%%%%%%%%%%%%%%%%%%%%%%%%
%% Calculation of Inclination at Skip Exit
%Trajectory parameters at Skip Exit
r_end = r(ctr_max); %Radius (km)
V_end = V(ctr_max); %Velocity (km)
gamma_end = gamma_e(ctr_max); %Flight-path angle (rad)
theta_end = theta_e(ctr_max); %Longitude (rad)
phi_end = phi_e(ctr_max); %Latitude (rad)
psi_end = psi_e(ctr_max); %Vehicle heading angle (rad)
omega_dt = omega_e*deltaT; %Planetary rotational velocity * Time Step (rad)

r_X2 = r_end*[1;0;0]; %Radius in Vehicle-Pointing frame

V_X2 = [V_end*sin(gamma_end); ...
        V_end*cos(gamma_end)*cos(psi_end); ...
        V_end*cos(gamma_end)*sin(psi_end)]; %Velocity in Vehicle-Pointing frame

%3-3-2 rotation matrix from Inertial to Vehicle-Pointing frame
RI_X2 = [cos(-phi_end) 0 -sin(-phi_end); 0 1 0; sin(-phi_end) 0 cos(-phi_end)]*...
        [cos(theta_end) sin(theta_end) 0; -sin(theta_end) cos(theta_end) 0; 0 0
1]*...
        [cos(omega_dt) sin(omega_dt) 0; -sin(omega_dt) cos(omega_dt) 0; 0 0 1];

r_I = inv(RI_X2)*r_X2; %Radius in Inertial frame
V_I = inv(RI_X2)*V_X2; %Velocity in Inertial frame

h_bar = cross(r_I,V_I); %Angular momentum in Inertial frame
incl_rad = acos(dot(h_bar,[0;0;1])/norm(h_bar)); %Inclination (rad)
incl_deg = rad2deg(incl_rad); %Inclination (deg)
```

Appendix B: Vacuum-Only Maneuver *Matlab* Code

The following *Matlab* files (m-files) comprise the code employed to conduct the preceding skip entry maneuver trade studies:

Table B.1. Vacuum-Only Maneuver *Matlab* Code Classification

m-File Name	Type of File
Vacuum_Cases.m	Script
deltaV_simple.m	Function
raanincl_change.m	Function
co_phasing.m	Function
nonco_phasing.m	Function

```
%%%%%%%%%%%%%%%%%%%%%%%%%%%%%%%%%%%%%%%%%%%%%%%%%%%%%%%%%%%%%%%%%%%%%%%%%%%%%%%
%
% Use: Vacuum_Cases.m
%
% This script calculates and plots the delta-V required to execute the
% following vacuum-only maneuvers: simple plane change, combined change to
% inclination and RAAN, and a coplanar and non-coplanar phasing rendezvous.
%
% Author/Date: Bettinger, Robert AFIT/ENY                        Spring 2011
%
% Baseline Simulation Input:
%   h                - Mission orbit altitude (km)
%
% Maneuver Inputs:
%   i1_deg           - Initial inclination (deg)
%   i2_deg           - Final inclination (deg)
%   delta_raan_deg   - Change in right ascension of the ascending node
%                      (RAAN) angle (deg)
%
% Outputs:
%   Graphs depicting delta-V required to execute vacuum-only maneuvers
%
% Globals:  None
% Constants:
%   MU           - Earth gravitational parameter (km^3/s^2)
%   r0           - Earth planetary radius (km)
%
% Coupling:
%  deltaV_simple.m      - Inputs: Orbit radius; initial and final
%                         inclination angle
%                       - Outputs: Change in inclination angle; Delta-V
%                         required for simple plane change
%  raanincl_change.m    - Inputs: Orbit radius; initial and final
%                         inclination angle; change in RAAN angle
```

```
%                       - Outputs: Change in RAAN angle; Delta-V required
%                         to conduct RAAN change
%  co_phasing.m         - Inputs: Semi-major axis of orbit; initial phasing
%                         angle of target/interceptor; number of phasing
%                         orbits for target/interceptor
%                       - Outputs: Delta-V required to conduct rendezvous;
%                         time-of-flight of maneuver
%  nonco_phasing.m      - Inputs: Semi-major axis of target/interceptor;
%                         number of phasing orbits for target/interceptor;
%                         initial argument of latitude for interceptor;
%                         initial RAAN for interceptor; initial inclination
%                         for target/interceptor; initial true longitude
%                         for target; required inclination change between
%                         target/interceptor
%                       - Outputs: Delta-V required to conduct rendezvous;
%                         time-of-flight of maneuver
%
% References: Vallado, David A. Fundamentals of Astrodynamics and
%             Applications. Boston: Microcosm Press, 2001.
%
%%%%%%%%%%%%%%%%%%%%%%%%%%%%%%%%%%%%%%%%%%%%%%%%%%%%%%%%%%%%%%%%%%%%%%%%%%%%

clc; clear all; close all;
format long

%% User-Defined Orbit Initial Conditions
MU = 398600.5; %Earth gravitational parameter (km^3/s^2)
r0 = 6378.137; %Radius of Earth (km)
h = 400; %Altitude (km)
r = r0 + h; %Circular orbital radius (km)

%% User-Defined Orbital Angles
i1_deg = 28.5; %Initial inclination (deg)
i2_deg = [0:1:180]; %Final inclination (deg)
delta_i_deg = i2_deg - i1_deg; %Change in inclination (deg)

%Values for change in RAAN
delta_raan_deg1 = 10; delta_raan_deg2 = 20;
delta_raan_deg3 = 30; delta_raan_deg4 = 45;
delta_raan_deg5 = 60; delta_raan_deg6 = 90;
delta_raan_deg7 = 120; delta_raan_deg8 = 150;

%% Simple Plane Change (Circular)
[delta_i_deg_simp1,deltaV_simp1] = deltaV_simple(r0+200,i1_deg,i2_deg,MU);
[delta_i_deg_simp2,deltaV_simp2] = deltaV_simple(r0+300,i1_deg,i2_deg,MU);
[delta_i_deg_simp3,deltaV_simp3] = deltaV_simple(r0+400,i1_deg,i2_deg,MU);
[delta_i_deg_simp4,deltaV_simp4] = deltaV_simple(r0+500,i1_deg,i2_deg,MU);
[delta_i_deg_simp5,deltaV_simp5] = deltaV_simple(r0+750,i1_deg,i2_deg,MU);
[delta_i_deg_simp6,deltaV_simp6] = deltaV_simple(r0+1000,i1_deg,i2_deg,MU);

figure; grid off;
plot(delta_i_deg_simp1,deltaV_simp1,'r',delta_i_deg_simp2,deltaV_simp2,'r:',...
     delta_i_deg_simp3,deltaV_simp3,'g',delta_i_deg_simp4,deltaV_simp4,'g:',...
     delta_i_deg_simp5,deltaV_simp5,'b',delta_i_deg_simp6,deltaV_simp6,'b:');
```

```
legend('\ith_0\rm = 200 km','\ith_0\rm = 300 km',...
       '\ith_0\rm = 400 km','\ith_0\rm = 500 km',...
       '\ith_0\rm = 750 km','\ith_0\rm = 1000 km','Location','EastOutside')
title({'\it\DeltaV\rm Required for Simple Plane Change',...
       '(\iti_0\rm = 28.5^o)'});
xlabel('Change in Inclination, \it\Deltai\rm (deg)'); ylabel('\it\DeltaV\rm (km/s)');

%% Combined Changes to Inclination and RAAN (Circular)
[delta_raan_deg1,deltaV_i_raan1] =
raanincl_change(r,MU,i1_deg,i2_deg,delta_raan_deg1);
[delta_raan_deg2,deltaV_i_raan2] =
raanincl_change(r,MU,i1_deg,i2_deg,delta_raan_deg2);
[delta_raan_deg3,deltaV_i_raan3] =
raanincl_change(r,MU,i1_deg,i2_deg,delta_raan_deg3);
[delta_raan_deg4,deltaV_i_raan4] =
raanincl_change(r,MU,i1_deg,i2_deg,delta_raan_deg4);
[delta_raan_deg5,deltaV_i_raan5] =
raanincl_change(r,MU,i1_deg,i2_deg,delta_raan_deg5);
[delta_raan_deg6,deltaV_i_raan6] =
raanincl_change(r,MU,i1_deg,i2_deg,delta_raan_deg6);
[delta_raan_deg7,deltaV_i_raan7] =
raanincl_change(r,MU,i1_deg,i2_deg,delta_raan_deg7);
[delta_raan_deg8,deltaV_i_raan8] =
raanincl_change(r,MU,i1_deg,i2_deg,delta_raan_deg8);

figure; grid off;
plot(delta_i_deg,deltaV_i_raan1,'r',delta_i_deg,deltaV_i_raan2,'r:',...
     delta_i_deg,deltaV_i_raan3,'g',delta_i_deg,deltaV_i_raan4,'g:',...
     delta_i_deg,deltaV_i_raan5,'b',delta_i_deg,deltaV_i_raan6,'b:',...
     delta_i_deg,deltaV_i_raan7,'m',delta_i_deg,deltaV_i_raan8,'m:');
legend('\it\Delta\Omega\rm = 10^o','\it\Delta\Omega\rm = 20^o',...
       '\it\Delta\Omega\rm = 30^o','\it\Delta\Omega\rm = 45^o',...
       '\it\Delta\Omega\rm = 60^o','\it\Delta\Omega\rm = 90^o',...
       '\it\Delta\Omega\rm = 120^o','\it\Delta\Omega\rm = 150^o',...
       'Location','EastOutside')
title({'\it\DeltaV\rm Required for Combined Change to Inclination and RAAN',...
       '(\iti_0\rm = 28.5^o)'});
xlabel('Change in Inclination, \it\Deltai\rm (deg)'); ylabel('\it\DeltaV\rm (km/s)');

%% Coplanar Phasing Rendezvous (Circular)
k_int = 1; k_tgt = 0; %Number of desired phasing orbits
phi_initial = [0:1:180]; %Phase angle between interceptor & target(deg)

[deltaV_cophase1,TOF_cophase1,TOF_cophase_min1] =
co_phasing(r0+200,MU,phi_initial,k_tgt,k_int);
[deltaV_cophase2,TOF_cophase2,TOF_cophase_min2] =
co_phasing(r0+300,MU,phi_initial,k_tgt,k_int);
[deltaV_cophase3,TOF_cophase3,TOF_cophase_min3] =
co_phasing(r0+400,MU,phi_initial,k_tgt,k_int);
[deltaV_cophase4,TOF_cophase4,TOF_cophase_min4] =
co_phasing(r0+500,MU,phi_initial,k_tgt,k_int);
[deltaV_cophase5,TOF_cophase5,TOF_cophase_min5] =
co_phasing(r0+750,MU,phi_initial,k_tgt,k_int);
```

```
[deltaV_cophase6,TOF_cophase6,TOF_cophase_min6] =
co_phasing(r0+1000,MU,phi_initial,k_tgt,k_int);

figure; grid off;
plot(phi_initial,deltaV_cophase1,'r',phi_initial,deltaV_cophase2,'r:',...
     phi_initial,deltaV_cophase3,'g',phi_initial,deltaV_cophase4,'g:',...
     phi_initial,deltaV_cophase5,'b',phi_initial,deltaV_cophase6,'b:');
legend('\ith_0\rm = 200 km','\ith_0\rm = 300 km',...
       '\ith_0\rm = 400 km','\ith_0\rm = 500 km',...
       '\ith_0\rm = 750 km','\ith_0\rm = 1000 km','Location','EastOutside')
title({'\it\DeltaV\rm Required for Coplanar Phasing Rendezvous';...
       '(\iti_0\rm = 28.5^o)'});
xlabel('Phasing Angle, \it\theta\rm (deg)'); ylabel('\it\DeltaV\rm (km/s)');

%% Non-Coplanar Phasing Rendezvous (Circular)
k_int = 1; k_tgt = 0; %Number of desired phasing orbits
u_int_deg1 = 5;  u_int_deg2 = 10;
u_int_deg3 = 20; u_int_deg4 = 30;
u_int_deg5 = 45; u_int_deg6 = 60;
raan_int_deg = 45; %Additional interceptor orbit parameters
lambda_true_tgt0 = 0; %Additional target orbit parameter

[deltaV_non_co1] = nonco_phasing(r,r,...
                           k_int,k_tgt,u_int_deg1,raan_int_deg,...
                           i1_deg,i2_deg,lambda_true_tgt0,delta_i_deg);
[deltaV_non_co2] = nonco_phasing(r,r,...
                           k_int,k_tgt,u_int_deg2,raan_int_deg,...
                           i1_deg,i2_deg,lambda_true_tgt0,delta_i_deg);
[deltaV_non_co3] = nonco_phasing(r,r,...
                           k_int,k_tgt,u_int_deg3,raan_int_deg,...
                           i1_deg,i2_deg,lambda_true_tgt0,delta_i_deg);
[deltaV_non_co4] = nonco_phasing(r,r,...
                           k_int,k_tgt,u_int_deg4,raan_int_deg,...
                           i1_deg,i2_deg,lambda_true_tgt0,delta_i_deg);
[deltaV_non_co5] = nonco_phasing(r,r,...
                           k_int,k_tgt,u_int_deg5,raan_int_deg,...
                           i1_deg,i2_deg,lambda_true_tgt0,delta_i_deg);
[deltaV_non_co6] = nonco_phasing(r,r,...
                           k_int,k_tgt,u_int_deg6,raan_int_deg,...
                           i1_deg,i2_deg,lambda_true_tgt0,delta_i_deg);

figure; grid off;
plot(delta_i_deg,deltaV_non_co1,'r',delta_i_deg,deltaV_non_co2,'r:',...
     delta_i_deg,deltaV_non_co3,'g',delta_i_deg,deltaV_non_co4,'g:',...
     delta_i_deg,deltaV_non_co5,'b',delta_i_deg,deltaV_non_co6,'b:');
legend('\itu_0\rm = 5^o','\itu_0\rm = 10^o',...
       '\itu_0\rm = 20^o','\itu_0\rm = 30^o',...
       '\itu_0\rm = 45^o','\itu_0\rm = 60^o','Location','EastOutside')
title({'\it\DeltaV\rm Required for Non-Coplanar Phasing Rendezvous';...
       '(\iti_0\rm = 28.5^o)'});
xlabel('Change in Inclination, \it\Deltai\rm (deg)'); ylabel('\it\DeltaV\rm (km/s)');
```

```
function [delta_i_deg, deltaV_simp] = deltaV_simple(r,i1_deg,i2_deg,MU)

%%%%%%%%%%%%%%%%%%%%%%%%%%%%%%%%%%%%%%%%%%%%%%%%%%%%%%%%%%%%%%%%%%%%%%%%%%%%
%
% Use: [delta_i_deg, deltaV_simp] = deltaV_simple(r,i1_deg,i2_deg,MU)
%
% This program calculates the parameters associated with a simple plane
% change, where only the inclination angle is changed and the semi-major
% axis and right-ascension of the ascending node (RAAN) remain constant.
%
% Author/Date: Bettinger, Robert AFIT/ENY                       Spring 2011
%
% Inputs:
%   r               - Radius of orbit (circular orbit)
%   i1_deg          - Initial inclination (deg)
%   i2_deg          - Final inclination (deg)
%   MU              - Gravitational parameter (km^3/s^2)
%
% Outputs:
%   delta_i_deg     - Change in inclination angle between orbits (deg)
%   deltaV_simp     - Delta-V required for simple plane change (km/s)
%
% Globals:  None
% Constants: None
% Coupling: None
%
% References: Vallado , David A. Fundamentals of Astrodynamics and
%             Applications. Boston: Microcosm Press, 2001.
%
%%%%%%%%%%%%%%%%%%%%%%%%%%%%%%%%%%%%%%%%%%%%%%%%%%%%%%%%%%%%%%%%%%%%%%%%%%%%

%Calculation of orbital velocity
Vc = sqrt(MU/r);

%Calculation of inclination-change angle parameters
i1_rad = deg2rad(i1_deg); i2_rad = deg2rad(i2_deg);
delta_i_rad = i2_rad - i1_rad;
delta_i_deg = rad2deg(delta_i_rad);

%Total delta-V required for simple plane change
deltaV_simp = 2*Vc*sin((delta_i_rad)/2);
deltaV_simp = abs(deltaV_simp);
```

```
function [delta_raan_deg, deltaV_i_raan] = ...
          raanincl_change(r,MU,i1_deg,i2_deg,delta_raan_deg)

%%%%%%%%%%%%%%%%%%%%%%%%%%%%%%%%%%%%%%%%%%%%%%%%%%%%%%%%%%%%%%%%%%%%%%%%%%%%
%
% Use: [delta_raan_deg, deltaV_i_raan] =
%       raanincl_change(r,MU,i1_deg,i2_deg,delta_raan_deg)
%
% This program calculates the total delta-V required to change both
% inclination and right ascension of the ascending node (RAAN). Note that
% this program can be also be utilized to calculated delta-V requirements
% for changes only to raan by having the initial and final values for
% inclination be equal.
%
% Author/Date: Bettinger, Robert AFIT/ENY                        Spring 2011
%
% Inputs:
%   r               - Radius of orbit (circular orbit)
%   MU              - Gravitational parameter (km^3/s^2)
%   i1_deg          - Inclination of first orbit (deg)
%   i2_deg          - Inclination of second orbit (deg)
%   delta_raan_deg  - Change in RAAN angle between orbits (deg)
%
% Outputs:
%   delta_raan_deg  - Change in RAAN angle between orbits (deg)
%   deltaV_i_raan   - Delta-V required to conduct RAAN change (km/s)
%
% Globals:  None
% Constants: None
% Coupling: None
%
% References: Vallado , David A. Fundamentals of Astrodynamics and
%             Applications. Boston: Microcosm Press, 2001.
%
%%%%%%%%%%%%%%%%%%%%%%%%%%%%%%%%%%%%%%%%%%%%%%%%%%%%%%%%%%%%%%%%%%%%%%%%%%%%

%Calculation of orbital velocity
Vc = sqrt(MU/r);

%Calculation of orbital angle parameters
i1_rad = deg2rad(i1_deg);
i2_rad = deg2rad(i2_deg);
delta_raan_deg = delta_raan_deg;
delta_raan = deg2rad(delta_raan_deg);

%Calculation of the angle between the velocity vectors of the initial and
%final orbits
theta = acos((cos(i1_rad)*cos(i2_rad))+(sin(i1_rad)*sin(i2_rad)*cos(delta_raan)));

%Total delta-V required for change in inclination and RAAN
deltaV_i_raan = 2*Vc*sin(theta/2);
```

```
function [deltaV_cophase,TOF_cophase,TOF_cophase_min] = ...
          co_phasing(a,MU,phi_initial_deg,k_tgt,k_int)

%%%%%%%%%%%%%%%%%%%%%%%%%%%%%%%%%%%%%%%%%%%%%%%%%%%%%%%%%%%%%%%%%%%%%%%%%%%%
%
% Use: [deltaV_cophase,TOF_cophase,TOF_cophase_min] =
%       co_phasing(a,MU,phi_initial_deg,k_tgt,k_int)
%
% This program calculates the parameters associated with a coplanar
% rendezvous between a target and interceptor.
%
% Author/Date: Bettinger, Robert AFIT/ENY                      Spring 2011
%
% Inputs:
%   a                - Semi-major axis of orbit (circular orbit)
%   MU               - Gravitational parameter (km^3/s^2)
%   phi_initial_deg  - Initial phasing angle of target/interceptor (deg)
%   k_tgt            - Number of phasing orbits for target
%   k_int            - Number of phasing orbits for interceptor
%
% Outputs:
%   deltaV_cophase   - Delta-V required to conduct rendezvous (km/s)
%   TOF_cophase      - Time-of-flight of maneuver (sec)
%   TOF_cophase_min  - Time-of-flight of maneuver (min)
%
% Globals:  None
% Constants: None
% Coupling: None
%
% References: Vallado , David A. Fundamentals of Astrodynamics and
%             Applications. Boston: Microcosm Press, 2001.
%
%%%%%%%%%%%%%%%%%%%%%%%%%%%%%%%%%%%%%%%%%%%%%%%%%%%%%%%%%%%%%%%%%%%%%%%%%%%%

%Calculation of target's orbital angular velocity
w_tgt = sqrt(MU/a^3);

%Calculation of time-of-flight for phasing orbit
TOF_cophase = ((2*pi*k_tgt) + rad2deg(phi_initial_deg))./w_tgt;
TOF_cophase_min = TOF_cophase.*(1/60);
a_cophase = (MU.*(TOF_cophase./(2*pi*k_int)).^2).^(1/3);

if a_cophase < 6378.137
    k_int = k_int + 1;
    a_cophase = (MU.*(TOF_cophase./(2*pi*k_int)).^2).^(1/3);
end

%Total delta-V required for coplanar phasing rendezvous
deltaV_cophase = 2*abs(sqrt(((2*MU)/a) - (MU./a_cophase)) - sqrt(MU/a));
```

```
function [deltaV_non_co,TOF_non_co,TOF_non_co_min] = ...
          nonco_phasing(a_int,a_tgt,k_int,k_tgt,u_int_deg,raan_int_deg,...
                        i_int_deg,i_tgt_deg,lambda_true_tgt0,delta_i_deg)

%%%%%%%%%%%%%%%%%%%%%%%%%%%%%%%%%%%%%%%%%%%%%%%%%%%%%%%%%%%%%%%%%%%%%%%%%%%%
%
% Use: [deltaV_non_co,TOF_non_co,TOF_non_co_min] = ...
%       nonco_phasing(a_int,a_tgt,k_int,k_tgt,u_int_deg,raan_int_deg,...
%                     i_int_deg,i_tgt_deg,lamda_true_tgt0,delta_i_deg)
%
% This program calculates the parameters associated with non-coplanar
% rendezvous between a target and interceptor.
%
% Author/Date: Bettinger, Robert AFIT/ENY                       Spring 2011
%
% Inputs:
%   a_int             - Semi-major axis of interceptor (circular orbit)
%   a_tgt             - Semi-major axis of target (circular orbit)
%   k_int             - Number of interceptor phasing orbit revolutions
%   k_tgt             - Number of target phasing orbit revolutions
%   u_int_deg         - Initial argument of latitude for interceptor (deg)
%   raan_int_deg      - Initial raan for interceptor (deg)
%   i_int_deg         - Initial inclination for interceptor (deg)
%   i_tgt_deg         - Initial inclination for target (deg)
%   lambda_true_tgt0  - Initial true longitude for target (deg)
%   delta_i_deg       - Required inclination change between interceptor and
%                       target orbital planes (deg)
%
% Outputs:
%   deltaV_non_co     - Delta-V required for non-coplanar rendezvous (km/s)
%   TOF_non_co        - Time-of-flight of maneuver (sec)
%   TOF_non_co_min    - TIme-of-flight of maneuver (min)
%
% Globals:  None
% Constants:
%   MU                - Earth gravitational parameter (km^3/s^2)
% Coupling: None
%
% References: Vallado , David A. Fundamentals of Astrodynamics and
%             Applications. Boston: Microcosm Press, 2001.
%
%%%%%%%%%%%%%%%%%%%%%%%%%%%%%%%%%%%%%%%%%%%%%%%%%%%%%%%%%%%%%%%%%%%%%%%%%%%%

MU = 398600.5; %Earth gravitational parameter (km^3/s^2)

%% Velocity parameters for interceptor and target
w_int = sqrt(MU/a_int^3); w_tgt = sqrt(MU/a_tgt^3); %Angular velocity
v_int = sqrt(MU/a_int); v_tgt = sqrt(MU/a_tgt); %Orbital velocity (km/s)

%% Transfer orbit parameters
a_t = (a_int + a_tgt)/2; %Semi-major axis (km)
TOF_t = pi*sqrt((a_t^3)/MU); %Time-of-flight (sec)
alpha_lead = w_tgt*TOF_t; %Initial target lead angle (rad)
```

```
%% Lead and phasing angle update
%Conversion of orbital elements from degrees to radians
u_int = deg2rad(u_int_deg);
raan_int = deg2rad(raan_int_deg);
i_int = deg2rad(i_int_deg);
i_tgt = deg2rad(i_tgt_deg);
delta_i = deg2rad(delta_i_deg);

%Quadrant check for calculation of phasing angle between interceptor
%initial angular position and the nearest node
if u_int > 0 && u_int < pi
    delta_theta_int = pi - u_int;
elseif u_int > pi && u_int < 2*pi
    delta_theta_int = 2*pi - u_int;
end

%Calculation of the time required for the interceptor to reach nearest node
t_node = (delta_theta_int/w_int);

%Update of target's true longitude based on interceptor nodal transfer time
lambda_true_tgt1 = deg2rad(lambda_true_tgt0) + (w_tgt*t_node);

%Calculation of new phasing angle between target and interceptor
lambda_u = atan(cos(i_int)*tan(u_int));
lambda_true_int1 = raan_int + lambda_u;
theta_new = lambda_true_int1 - lambda_true_tgt1;

%Calculation of new lead angle between target and interceptor
alpha_new = pi + theta_new;

%% Phasing orbit parameters
phase_period = (alpha_new - alpha_lead + (2*pi*k_tgt))/w_tgt; %Orbit period (sec)
a_phase = (MU*(phase_period/(2*pi*k_int))^2)^(1/3); %Semi-major axis (km)
TOF_phase = 2*pi*sqrt((a_phase^3)/MU); %Time-of-flight (sec)

%% Maneuver velocity and delta-V parameters
%Calculation of velocity required for phasing and transfer orbits
v_phase = sqrt(((2*MU)/a_int) - (MU/a_phase));
v_t1 = sqrt(((2*MU)/a_int) - (MU/a_t));
v_t2 = sqrt(((2*MU)/a_tgt) - (MU/a_t));

%Delta-V required for the phasing and transfer orbit burn segments of
%non-coplanar rendezvous
deltaV_phase = abs(v_phase - v_int);
deltaV_t1 = abs(v_t1 - v_phase);
deltaV_t2 = sqrt((v_t2^2) + (v_tgt^2) - (2*v_t2*v_tgt*cos(delta_i)));

%Total delta-V and time-of-flight required for non-coplanar rendezvous
deltaV_non_co = deltaV_phase + deltaV_t1 + deltaV_t2;
TOF_non_co = TOF_phase + TOF_t + t_node;
TOF_non_co_min = TOF_non_co * (1/60);
```

Bibliography

Anderson Jr., John D. *Hypersonic and High-Temperature Gas Dynamics* (Second Edition). Reston: American Institute of Aeronautics and Astronautics, Inc., 2006.

Andrews Space & Technology. "X-37 – Specs." Available from http://www.spaceandtech.com/spacedata/rlvs/x37_specs.shtml. Internet; Accessed 31 December 2010.

Bedford, Anthony and Wallace Fowler. *Engineering Mechanics: Dynamics* (Fourth Edition). Upper Saddle River: Pearson Prentice Hall, 2005.

Bertin, John J. *Aerodynamics for Engineers* (Fourth Edition). Upper Saddle River: Prentice Hall, Inc., 2002.

Bilbey, Charles A. *Investigation of the Performance Characteristics of Re-Entry Vehicles*. MS thesis, AFIT/GSS/ENY/05-S01. School of Engineering and Management, Air Force Institute of Technology (AU), Wright-Patterson AFB OH, September 2005 (ADA440191).

Boeing. "X-37B Orbital Test Vehicle: Overview." Available from http://www.boeing.com/defensespace/ic/sis/x37b_otv.html. Internet; Accessed 30 July 2010.

Brown, Charles D. *Spacecraft Mission Design* (Second Edition). Reston: American Institute of Aeronautics and Astronautics, Inc., 1998.

Covault, Craig. "Wings Into Space: Air Force X-37B," *AIAA: Aerospace America*, 11: 34-39 (November 2010).

Darby, Christopher L. and Anil V. Rao. "Minimum-Fuel Low-Earth Orbit Aeroassisted Orbital Transfer of Small Spacecraft." Paper presented at the 20th AAS/AIAA Space Flight Mechanics Meeting, San Diego, California, 14-17 February 2010.

Erbland, Peter J. "Current and Near-Term RLV/Hypersonic Vehicle Programs: Appendix 1 – X-37." Paper presented at the RTO AVT Lecture Series on "Critical Technologies for Hypersonic Vehicle Development," Rhode-St-Genèse, Belgium, 10-14 May 2004.

Gargasz, Michael L. *Optimal Spacecraft Attitude Control using Aerodynamic Torques*. MS thesis, AFIT/GA/ENY/o7-M08. School of Engineering and Management, Air Force Institute of Technology (AU), Wright-Patterson AFB OH, March 2007 (ADA469919).

Guettler, David B. *Satellite Attitude Control using Atmospheric Drag*. MS thesis, AFIT/GA/ENY/07-M10. School of Engineering and Management, Air Force

Institute of Technology (AU), Wright-Patterson AFB OH, March 2007 (ADA469265).

Hajovsky, Blake B. *Satellite Formation Control using Atmospheric Drag*. MS thesis, AFIT/GA/ENY/07-M11. School of Engineering and Management, Air Force Institute of Technology (AU), Wright-Patterson AFB OH, March 2007 (ADA469289).

Hall, Timothy S. *Orbit Maneuver for Responsive Coverage using Electric Propulsion*. MS thesis, AFIT/GSS/ENY/10-M04. School of Engineering and Management, Air Force Institute of Technology (AU), Wright-Patterson AFB OH, March 2010 (ADA516854).

Hicks, Kerry D. *Introduction to Astrodynamic Reentry*. Wright-Patterson AFB: Air Force Institute of Technology, 2009.

Humble, Ronald W., et al. *Space Propulsion Analysis and Design*, (New York: The McGraw-Hill Companies, Inc., 1995), 188.

Johnson, Richard E. *Effects of Thrust Vector Control on the Performance of the Aerobang Orbital Plane Change Maneuver*. MS thesis; Department of Aeronautical and Astronautical Engineering, Naval Postgraduate School, Monterey, CA, June 1993 (ADA272532).

Larson, Wiley J. and James R. Wertz. *Space Mission Analysis and Design* (Third Edition). El Segundo: Microcosm Press, 2003.

Maly, Joseph R., et al. "Adapter Ring for Small Satellites on Responsive Launch Vehicles." Paper presented at the 7th Responsive Space Conference, Los Angeles, California, 27-30 April 2009.

McNabb, Dennis J., Vann M. Stavast, Gregory E. Stanford, and Michael E. Evert. *Investigation of Atmospheric Re-Entry for the Space Maneuver Vehicle*. MS thesis, AFIT/GA/ENY/04-M03. School of Engineering and Management, Air Force Institute of Technology (AU), Wright-Patterson AFB OH, March 2004 (ADA424074).

Newberry, Robert D. "Powered Spaceflight for Responsive Space Systems." *High Frontier*, 1: 46-49 (October-December 2005).

Nicholson, John C. *Numerical Optimization of Synergistic Maneuvers*. MS thesis; Department of Aeronautical and Astronautical Engineering, Naval Postgraduate School, Monterey, CA, June 1994 (ADA283398).

Office of the Secretary of the Air Force (Public Affairs). "U.S. Air Force Fact Sheet: X-37B Orbital Test Vehicle." Available from http://www.af.mil/information/factsheets/factsheet_print.asp?fsID=16639&page=1. Internet; Accessed 30 July 2010.

Parish II, Michael S. *Optimality of Aeroassisted Orbital Plane Changes*. MS thesis; Department of Aeronautical and Astronautical Engineering, Naval Postgraduate School, Monterey, CA, December 1995 (ADA306573).

Powell, R.W., J.C. Naftel, and M.J. Cunningham. "Performance Evaluation of an Entry Research Vehicle." *Journal of Spacecraft and Rockets*, 24: 489-495 (November-December 1987).

Rao, Anil V. and Arthur E. Scherich. "A Concept for Operationally Responsive Space Mission Planning Using Aeroassisted Orbital Transfer." Paper presented at the 6th Responsive Space Conference, Los Angeles, California, 28 April – 1 May 2008.

Space.com. "X-37B Launch in April 2010." Available from http://www.space.com/common/forums/viewtopic.php?t=20686. Internet; Accessed 7 November 2010.

Spaceflight Mission Design Division, SMC Det 12/STX. *DoD Space Test Program: Secondary Payload Planner's Guide for use on the EELV Secondary Payload Adapter*. Kirtland AFB: DoD Space Test Program, 2006.

Strom, Steven R. "Jurassic Technology: The History of the Dynasoar." Crosslink. 2004. Available from http://www.aero.org/publications/crosslink/winter2004/01.html. Internet; Accessed 1 August 2010.

Tascione, Thomas F. *Introduction to the Space Environment* (Second Edition). Malabar: Krieger Publishing Company, 1994.

U.S. Department of Defense. "Mr. Gary Payton, Under Secretary of the Air Force for Space Programs, Media Teleconference Transcript: X-37B Launch." Available from http://www.defense.gov/Blog_files/Blog_assets/PaytonX-37.pdf. Internet; Accessed 31 December 2010.

Vallado, David A. *Fundamentals of Astrodynamics and Applications* (Second Edition). Boston: Microcosm Press, 2001.

Vinh, Nguyen X. *Optimal Trajectories in Atmospheric Flight*. Amsterdam: Elsevier Scientific Publishing Company, 1981.

Young, James C. and Jimmy M. Underwood. "The Aerodynamic Challenges of the Design and Development of the Space Shuttle Orbiter," *Space Shuttle Technical Conference: Part 1*. 209-263. Houston: Lyndon B. Johnson Space Center, 1985.

Vita

Captain Robert A. Bettinger graduated from Niagara-Wheatfield Central High School in Wheatfield, New York in June 2003. He attained a nomination to and entered the United States Air Force Academy in Colorado Springs, Colorado where he graduated with a Bachelor of Science in Astronautical Engineering, was recognized as a Distinguished Graduate, and received a Regular Commission in May 2007.

As his first assignment, Captain Bettinger was sent to Kirtland AFB, New Mexico where he began work as a Research Engineer for Spacecraft Navigation and Guidance in the Air Force Research Laboratory's Space Vehicle Directorate in November 2007. Subsequently, he entered the Graduate School of Engineering and Management, Air Force Institute of Technology in May 2010. Upon graduation, Captain Bettinger will be assigned to the United States Air Force Academy where he will be an instructor within the Department of Astronautics.

REPORT DOCUMENTATION PAGE

Form Approved
OMB No. 074-0188

1. REPORT DATE *(DD-MM-YYYY)*	2. REPORT TYPE	3. DATES COVERED *(From – To)*
16062011	Master's Thesis	July 2010 – June 2011

TITLE AND SUBTITLE

Spacecraft Demand Tasking and
Skip Entry Responsive Maneuvers

5a. CONTRACT NUMBER

5b. GRANT NUMBER

5c. PROGRAM ELEMENT NUMBER

6. AUTHOR(S)

Bettinger, Robert A., Captain, USAF

5d. PROJECT NUMBER

5e. TASK NUMBER

5f. WORK UNIT NUMBER

7. PERFORMING ORGANIZATION NAMES(S) AND ADDRESS(S)
Air Force Institute of Technology
Graduate School of Engineering and Management (AFIT/ENY)
2950 Hobson Way, Building 640
WPAFB OH 45433-8865

8. PERFORMING ORGANIZATION REPORT NUMBER

AFIT/GA/ENY/11-J03

9. SPONSORING/MONITORING AGENCY NAME(S) AND ADDRESS(ES)
Intentionally left blank

10. SPONSOR/MONITOR'S ACRONYM(S) N/A

11. SPONSOR/MONITOR'S REPORT NUMBER(S) N/A

12. DISTRIBUTION/AVAILABILITY STATEMENT
APPROVED FOR PUBLIC RELEASE; DISTRIBUTION UNLIMITED.

13. SUPPLEMENTARY NOTES
This material is declared a work of the U.S. Government and is not subject to copyright protection in the United States.

14. ABSTRACT

The purpose of this research was to parametrically investigate the viability of skip entry maneuvers as an alternative to vacuum-only maneuvers, and to identify whether skip entry maneuvers can extend spacecraft mission lifetime by limiting propellant expenditure through the exploitation of the aerodynamic interaction between the upper atmosphere and an example entry vehicle and remote-sensing orbital platform. Employing the X-37B Orbital Test Vehicle (OTV) and a notional satellite design as the example entry vehicles, the entry profile dynamics of a skip entry maneuver were characterized with varying trajectory initial conditions such as entry altitude, entry flight-path angle, and vehicle aerodynamics. In addition, the requirements of skip entry maneuvers were characterized, specifically the required to complete one or more successive skip entry trajectories as well as to execute a desired change in orbit inclination angle.

15. SUBJECT TERMS
Responsive space; responsive maneuver; skip entry; re-entry; inclination angle; plane change

16. SECURITY CLASSIFICATION OF:			17. LIMITATION OF ABSTRACT	18. NUMBER OF PAGES	19a. NAME OF RESPONSIBLE PERSON
a. REPORT	b. ABSTRACT	c. THIS PAGE			Jonathan T. Black, Ph.D, USAF (ENY)
U	U	U	UU	165	19b. TELEPHONE NUMBER *(Include area code)* (937) 255-6565, ext. 4578 (Jonathan.Black@afit.edu)

Standard Form 298 (Rev. 8-98)
Prescribed by ANSI Std. Z39-18